Prediction of fretting wear in spline couplings

ScuDo

Scuola di Dottorato ~ Doctoral School

WHAT YOU ARE, TAKES YOU FAR

Doctoral Dissertation

Doctoral Program in Mechanical Engineering (29^{th}cycle)

Prediction of Fretting Wear in Spline Couplings

By

Waqar Ahmed Qureshi

******

Supervisor(s):

Prof. Francesca Curá

Doctoral Examination Committee:

Prof. Carlo Gorla

Prof. Giovanni Meneghetti

Politecnico di Torino

2017

Declaration

I hereby declare that, the contents and organization of this dissertation constitute my own original work and does not compromise in any way the rights of third parties, including those relating to the security of personal data.

Waqar Ahmed Qureshi
2017

* This dissertation is presented in partial fulfillment of the requirements for **Ph.D. degree** in the Graduate School of Politecnico di Torino (ScuDo).

I dedicate this thesis to my parents

Acknowledgements

First and foremost, I would like to thank my PhD Advisor Prof. Francesca Curá without whose help, guidance, supervision, trust and motivation, it would not have been possible for me to carry out this research. I would like to especially commend her philosophy of giving intellectual freedom to her students, which helped me grow immensely as a researcher. I have to thank Dr. Andrea Mura, who has been extremely supportive, helpful, accommodating and patient throughout my experimental and theoretical activity. He has been very kind when I would repeatedly bombard him with queries about a new activity or experimental finding. Dr. Vincenzo Cuffaro, currently working at Avio Aero GE, was the one who received and introduced me at Politecnico di Torino to our research theme, experimental facilities and provided me with relevant literature to begin my journey as a PhD candidate. I am really thankful and obliged for their precious help and time.

Next, I would like to thank Politecnico di Torino for providing me with funding and the opportunity to take on this task. The help and support from my departmental coordinator Prof. Luigi Garibaldi, administrative secretary Miss. Maria Grazia and all support staff has been phenomenal. I have to mention my PhD fellows Mahmood, Mona, Andrea, Raffaele, Divyaksh and Rehan for providing such a wonderful and congenial environment to stay in. PhD seemed quite a fun in their company.

Last but not the least, I have to especially thank my wife Aisha; my kids Abdullah, Umar, Ali; siblings Irshad, Mariam, Muntaha, Noor and most importantly my father Imtiaz Qureshi and my mother Robina Qureshi whose love, care and encouragement got me going through all times.

Abstract

The original contribution of this work is modeling of fretting wear in aero-engine spline couplings widely used in aero-industry to transfer power and torque. Their safe operation is very critical with respect to flight safety. They consist of two components namely hub and shaft. As they are of light weight, usually it is difficult to realize a perfect alignment. To allow for misalignment, their teeth are designed to be of crowned shape. The crowing allows a degree of misalignment without concentration of stresses which is otherwise inevitable if a misalignment is introduced in case of straight teeth. However, crowing results in another problem of fretting wear and fretting fatigue owing to kinematic constraints imposed as a result of misalignment. The focus of this work is development of mathematical models for prediction of fretting wear and not fretting fatigue. The spline couplings under consideration are industrial scale and made up of nitrogen hardened 42CrMo4. The aero industry requires a reliable method to model and predict fretting wear to be able to optimize the design of spline coupling and reduce the maintenance costs. Wear tests on crowned spline couplings on a dedicated test bench have been conducted and analyzed.

Empirical, artificial neural network based and analytical models have been developed to analyse, predict and formulate fretting wear in spline couplings. The empirical and artificial neural netwrok based models are specific to the given case of spline couplings and tribological conditions. However, the analytical model developed has been found to be quite general. Incremental fretting wear formulation both in terms of wear volume and wear depth has been realized. Some novel findings regarding effect of roughness parameters in conjunction with applied torque and misalignment angles with respect to fretting wear are also reported. It has been observed that the evolution of wear depth accelerates with increased applied torque or misalignment angle. Changes in roughness parameters are also found to be increasing with torque and misalignment angle in most of the cases. Preliminary tests for frequency effects on fretting wear have also been conducted.

Contents

List of Figures

List of Tables

Chapter 1

Introduction

Aero-engine light weight spline couplings are often used for torque and power transfer in aero industry. They typically consist of two components, namely hub and shaft with internal and external teeth respectively. It becomes very difficult to achieve a perfect alignment between the hub and shaft owing to their light weight, tolerances, vibrations and manufacturing constraints. Classically, spline couplings with straight teeth are used in the industry where weight is not a concern. However, straight teeth in case of aero-engine spline couplings poses a problem of misalignment, which results in concentration of stresses and an early failure. Hence, crowned teeth are frequently used to allow for a misalignment between the hub and the shaft.

This modification addresses the issue of concentration of stresses but poses another problem of wear. In the presence of misalignment, the surfaces of meshing teeth are subjected to very small repeated relative movement. The wear as a result is classified as fretting wear. Fretting wear allows a safe operation for a relatively longer period of time. Nevertheless, fretting wear does affect the lifetime of spline coupling and this needs to be quantified and modeled to be able to predict the safe operating cycles and improve the design. That is the aim of this thesis as well.

It has been reported since long that spline couplings require more frequent maintenance and typically fail earlier than engine driven accessories [9]. Various methods and techniques have been employed to predict fretting damage and design the spline couplings in the past [10, 11]. In the forthcoming sections of this chapter, a review of spline couplings followed by introductory theory of fretting wear and identification of different regimes will be presented.

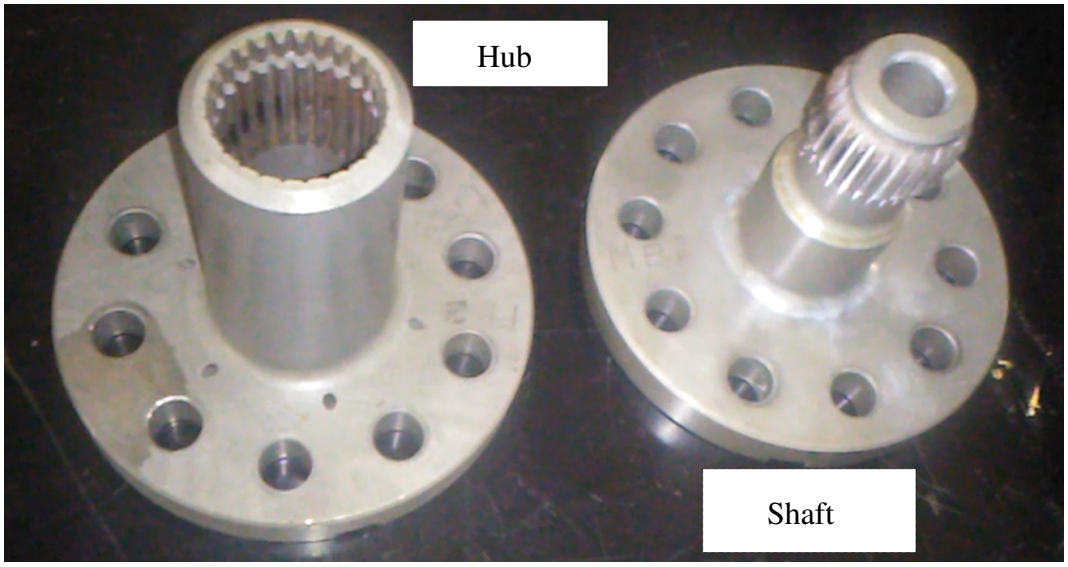

Fig. 1.1 The crowned spline couplings used

1.1 Spline Couplings

Involute spline couplings can be classified into three types based upon their design [12]. A typical spline coupling has been explained in the Figure 1.1

1.1.1 Fixed Splines

Fixed splines do not permit relative surface movement between the hub and the shaft.

1.1.2 Flexible Splines

These allow for a movement between the teeth of hub and shaft. The provision of movement permit axial sliding of teeth under the effect of applied load.

1.1.3 Crowned Splines

In these, sides of the grooves are involute whereas the male teeth are designed in a way to permit angular misalignment between the hub and the shaft. This work focuses on the fretting wear in case of crowned spline couplings in the presence of misalignment.

1.2 Fretting Wear

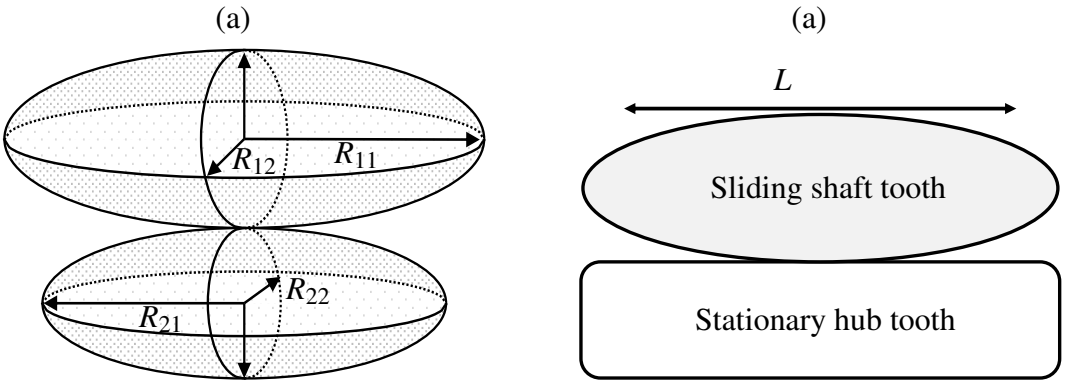

Fig. 1.2 (a) Contact between ellipsoidal teeth [1] (b) Sliding between teeth

Fretting wear is a quasi-static process which appears as a result of repeated relative movement between two surfaces at very small scales. As the process continues, it gives rise to wear of the surfaces in contact. A typical contact between ellipsoidal teeth and the sliding between the teeth has been shown in the Figure 1.2. Fretting wear may further be classified into three regimes.

1.2.1 Stick Regime

In this case, there is no slip between the surfaces, but it may still result in damage in the form of deflections and plastic flow. This situation arises when applied force is less than the force of friction between the surfaces and it typically occurs when the fretting amplitude is extremely small.

1.2.2 Stick-Slip Regime

During reciprocating movement of surfaces, while sliding, they come to a halt and then gain speed. This results in a change in the force of friction. The changes in force of friction are due to the fact that the static coefficient of friction is higher than the kinetic coefficient of friction. Under such a condition, the sliding surfaces briefly stick and then slip, hence the name. This phenomenon may give rise to abrasive wear in the components [13]. Some useful references about stick-slip regime and its modeling for various components have been presented in the literature [14–16].

1.2.3 Gross-Slip Regime

When the amplitude of oscillatory displacement between the surfaces increases more than a certain threshold value, it results in gross slip. In this case, entire contact is subjected to slip and the slip amplitude becomes equal to the fretting amplitude. In gross-slip regime, the fretting amplitudes are larger than the first two cases and applied force is larger than the frictional force between the contacts [17, 18]. A simulation of high resolution gross slip wear of axially symmetrical contacts by the method of dimensionality reduction and finite element method has been presented in [19]. A characterization of wear regimes has been carried out in [20]. Another promising work regarding modeling of fretting wear under gross slip and partial slip conditions by a numerical technique has been given in [21]. The work at hand also focuses on modeling of fretting wear in the gross slip regime in the case of spline couplings.

1.3 Modeling of Fretting Wear

Archard's Model

Classically, Archard's model [22, 23] of wear expresses wear as a function of applied normal load, sliding distance and hardness of the soft contacting surface. Mathematically, it is expressed as:

$$V = K\frac{F_n S}{H} \tag{1.1}$$

where V is the wear volume, K the Archard's wear coefficient, F_n the normal force and H the hardness of the soft material.

Wear Energy Model

A theory for dry wear based upon energy was proposed in [24]. A dry wear model based on energy considerations was developed in [25] which could simulate both the running-in and steady state wear behavior of wear process. More recently, a wear energy description [26] has been the subject of interest in wear and tribology community for modeling of wear. This approach simply relates the wear volume

to the wear work done during the sliding. The biggest advantage of this approach is an explicit representation of coefficient of friction which the classical Archard's model did not address. This approach has been mainly used in the work at hand for the modeling and prediction of fretting wear in spline couplings. Mathematically, it may be expressed as:

$$V = \alpha \mu F_n S \tag{1.2}$$

where α is the wear energy coefficient and μ is the coefficient of friction. The expression $\mu F_n S$ represents the frictional work done throughout the sliding.

This model has been shown to be more representative of the wear phenomenon in various works since then [27, 28]. In another work the energy theories and a molecular mechanics approach increased the range of validity of model [29].

1.4 Wear Regime Identification

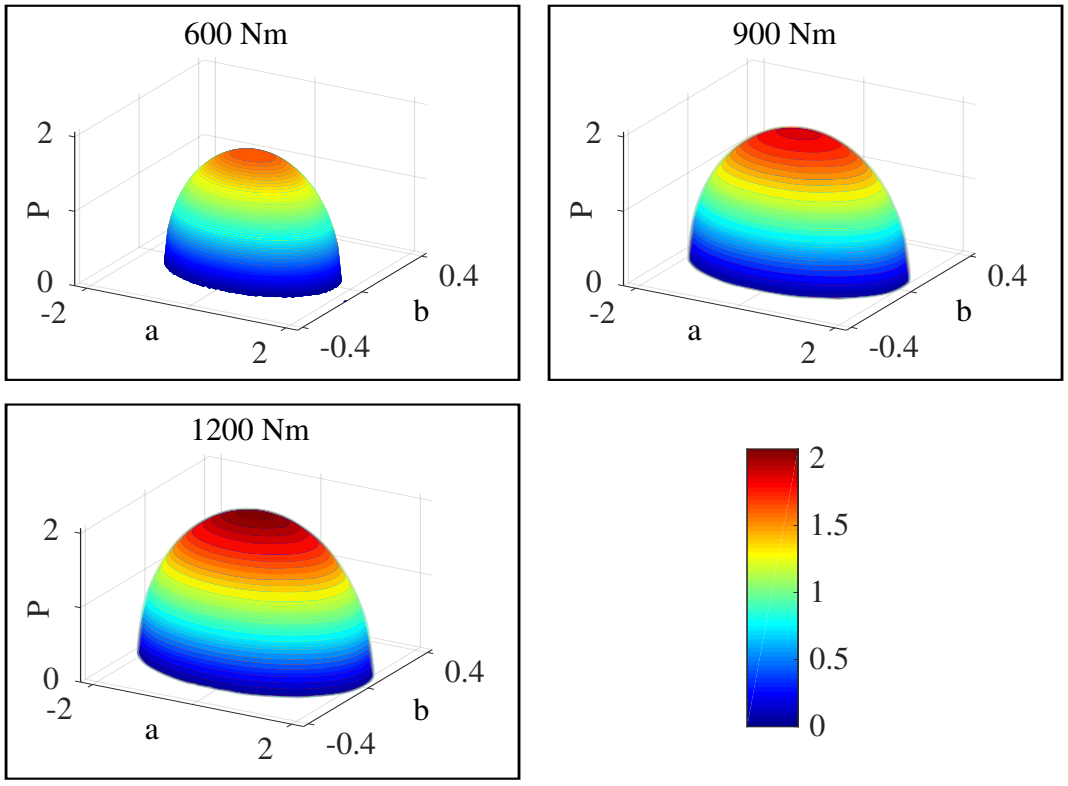

Fig. 1.3 Numerical implementation of Hertz theory. Major and minor contact radii a and b respectively, are in mm. Pressure P is in GPa

Details of Hertz theory have been provided in [30, 31]. This theory has been used for extension of Mindlin's theory [32] to distinguish regimes of fretting wear and design experiments in the desired region. A re-visitation of Cattaneo-Mindlin concept of interfacial slip in tangentially loaded compliant bodies has been provided in [33] which relaxes some assumptions in the initial Mindlin's theory. The extension of Mindlin's theory has been carried out, reported and taken from an already completed work of authors [1].

1.4.1 Review of Hertz Theory

Referring to Hertz theory and the Figure 1.2 (a), the relationships for principal radii of elliptical contact may be derived after assuming ω to be the angle between the major axis of the surfaces in contact.

Body 1

R_{11} = Major radius of contact surface
R_{12} = Minor radius of contact surface
E_1 = Young's modulus
ν_1 = Poisson's ratio
G_1 = Sheer modulus of rigidity

Body 2

R_{21} = Major radius of contact surface
R_{22} = Minor radius of contact surface
E_2 = Young's modulus
ν_2 = Poisson's ratio
G_2 = Sheer modulus of rigidity

Then the following may be derived:

$$\frac{1}{R} = \frac{1}{R_{11}} + \frac{1}{R_{12}} + \frac{1}{R_{21}} + \frac{1}{R_{22}}$$

$$R_1 = \frac{1}{R_{11}} - \frac{1}{R_{12}}$$

$$R_2 = \frac{1}{R_{21}} - \frac{1}{R_{22}}$$

Ω an auxiliary angle is derived as:

$$\Omega = \cos^{-1}\left(R\sqrt{{R_1}^2 + {R_2}^2 + 2R_1R_2\cos(2\omega)}\right)$$

For material properties:

$$\frac{1}{E} = \frac{1-{\nu_1}^2}{E_1} + \frac{1-{\nu_2}^2}{E_2}$$

Major and minor contact radii may be evaluated as:

$$a = f\left[\frac{3FR}{2E}\right]^{1/3} \tag{1.3}$$

$$b = g\left[\frac{3FR}{2E}\right]^{1/3} \tag{1.4}$$

where

$$f = \left[\frac{2I(k)}{\pi\sin^2(\Omega/2)}\right]^{1/3}, g = \left[\frac{2J(k)}{\pi\cos^2(\Omega/2)}\right]^{1/3}$$

The deformation as a result of Hertzian stress may be calculated as:

$$\alpha = \frac{3FH(k)}{2\pi aE}$$

where $H(k)$, $I(k)$ and $J(k)$ are elliptic integrals with $k = b/a$ and given as:

$$H(k) = \int_0^{\pi/2} \frac{d\phi}{\sqrt{1-(1-k^2)\sin^2(\phi)}}$$

$$I(k) = \int_0^{\pi/2} \frac{\cos^2(\phi)d\phi}{\sqrt{1-(1-k^2)\sin^2(\phi)}}$$

$$J(k) = \int_0^{\pi/2} \frac{\cos^2(\phi) d\phi}{\sqrt{1-(1-\frac{1}{k^2})\sin^2(\phi)}}$$

These integrals can be solved for k numerically. And the following transcendental equation is solved for the value of k.

$$\frac{k^3}{\tan^2(\Omega/2)} = \frac{J(k)}{I(k)}$$

The initial guesses to be used by solution of the above equation are:

$0 \leq \Omega \leq 5$, 0.04; $5 < \Omega \leq 73$, 0.56; $73 < \Omega$, 0.85

The source code for the elliptical Hertzian contact in case of spline coupling has been provided in the A.

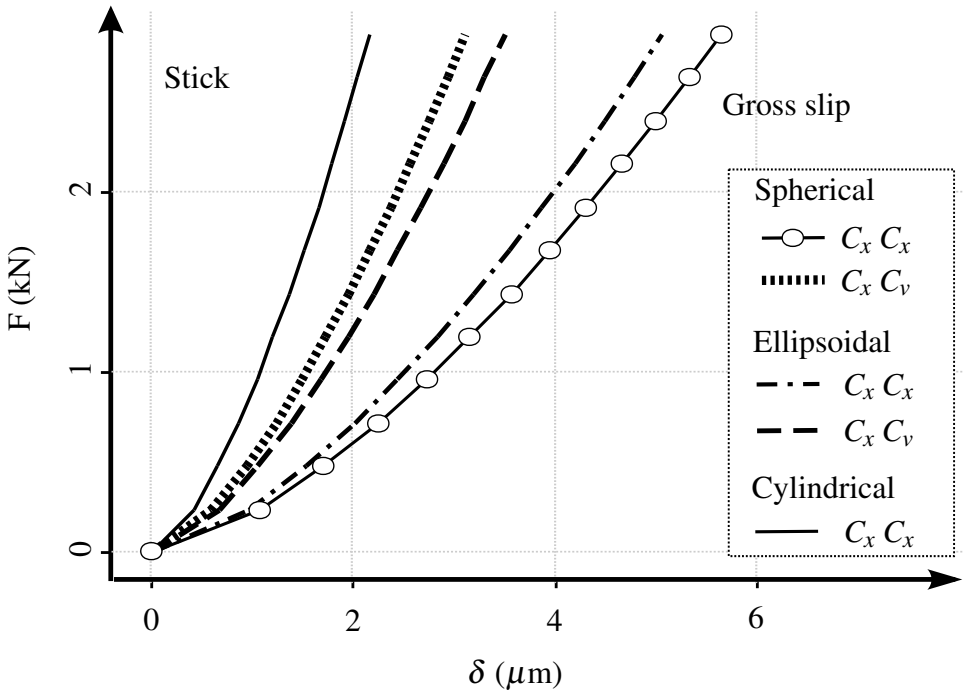

Fig. 1.4 Fretting regimes for different kind of contacts [1]

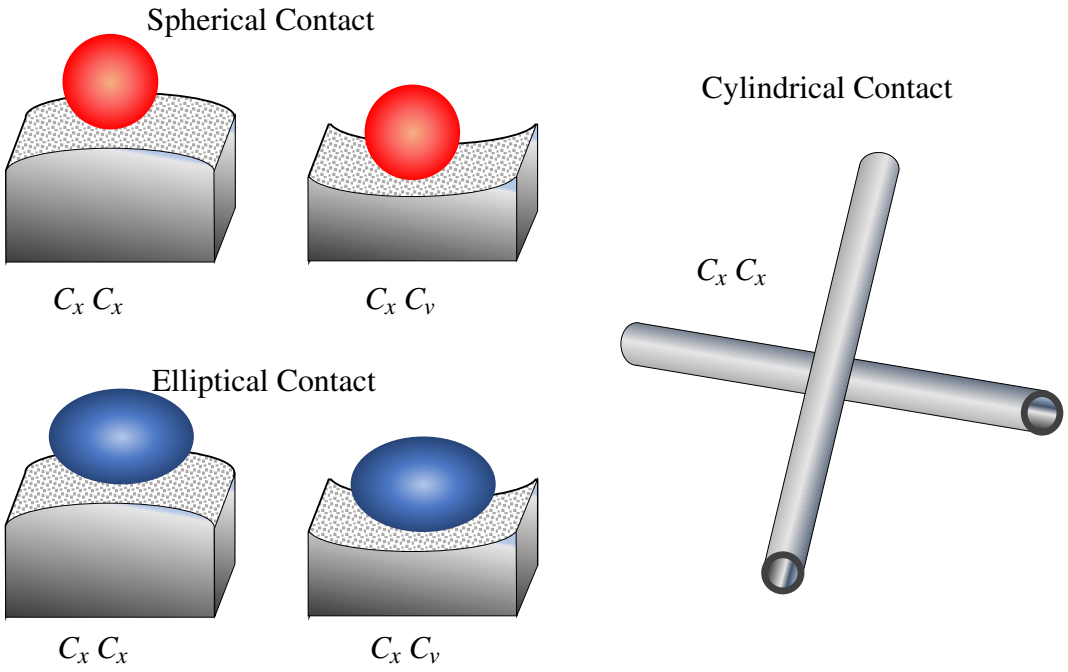

Fig. 1.5 Application of extended Mindlin's theory to various contact problems

1.4.2 Extended Mindlin's Theory

Classically, the Mindlin's theory is used for estimation of wear regimes in case of circular contact. If δ is the sliding amplitude, μ the coefficient of friction and c the equivalent radius of the contact, it has been expressed in the suitable form as:

$$\delta = \frac{\mu k_1 F}{c} \tag{1.5}$$

For an elliptic contact, c may be found as:

$$c = \sqrt{ab} \tag{1.6}$$

The value of K_1 is calculated as:

$$k_1 = \frac{3}{16}\left[\frac{2-\nu_1}{G_1} + \frac{2-\nu_2}{G_2}\right]$$

Finally using the Equation 1.3 and Equation 1.4 and using them in Equation 1.6:

$$c = \left[\frac{3FR}{2E}\right]^{1/3} \sqrt{fg} \tag{1.7}$$

Using c in Equation 1.5:

$$\delta = \frac{\mu k_1}{\sqrt{fg}} \left[\frac{2EF^2}{3R} \right]^{1/3} \tag{1.8}$$

This is the final form of extended Mindlin's formulation which has been used during experimental activity to ensure that the fretting regime stays within gross slip. The variable δ provides the hysteresis which distinguishes the stick and gross slip regions and it itself lies on the partial slip or stick slip region. Finally, the results of various simulations addressing different kind of contacts and geometries have been summarized in the Figure 1.5(a) and the design of experiments for the gross slip region has been shown in the Figure 1.5 (b).

This chapter provided a brief introduction of the background of the problem at hand. It also presented a brief review of Hertz contact theory for elliptical contacts which was subsequently used for an extension in the Mindlin's formulation to design the experiments within the desired wear regimes. It was found that the geometry of contact significantly affects the wear regimes. A crossed cylinder configuration, for example, was found to be the quickest to reach gross-slip regime in terms of sliding amplitude. A spherical contact of the comparable dimensions on the other hand was found to be the last to reach gross slip regime with respect to sliding amplitude for any particular normal force. This work served as the basis for the design and analysis of experimental activity which followed.

1.5 Outline

Rest of the thesis is organized in 8 chapters.

Chapter 2 will present details of experimental setup used along with its statistical validation.

Chapter 3 focuses on modeling of fretting wear by the means of empirical and neural network models.

Chapter 4 explains the dependence of fretting wear on surface roughness parameters.

Chapter 5 develops an analytical model for prediction of fretting wear along with

experimental validation.

Chapter 6 proposes a methodology for development of wear-cycles curves on the analogy of SN curves.

Chapter 7 explains the novel experiments on fretting wear performed with respect to fretting frequency, sliding amplitude and fretting duration.

Chapter 8 contains the conclusions of whole research activity, limitations and future work.

Chapter 2

Experimental Setup and Statistical Validation

Based upon the findings presented in this chapter some work has already been published [2, 34] which aims to interpret experimental data with the help of Principal Component Analysis (PCA). Fretting wear in spline couplings is influenced by many parameters including but not limited to the applied load, sliding distance, surface roughness, tribological conditions, misalignment, angular speed and pressure distribution along the surface of the teeth of hub and shaft. A dedicated test bench has been established to conduct experiments on fretting wear of spline couplings. It was necessary to statistically validate as well as interpret experimental results. PCA was found to be a useful tool to do so in addition to the identification of most significant parameters to simplify the experimental design for future experiments. PCA technique was originally proposed in 1901 [35]. Some of the relevant and useful works are provided in the references [36–41]. Classically and, most commonly, the covariance matrix is used as the criterion for identification of Principal Components. However, a co-median based PCA has been evaluated and compared in conjunction with standard covariance based PCA in this work. It is shown to be more insensitive to outliers, noisy measurements and random errors. Using the framework presented in this work, not only the fretting wear experiments, but any experimental data may be convincingly interpreted even in the presence of outliers thus making it quite generally applicable to a variety of problems. Such a technique also increases the confidence in the experimental setup and gives an opportunity to design experiments with less and only important parameters thus reducing the cost and time.

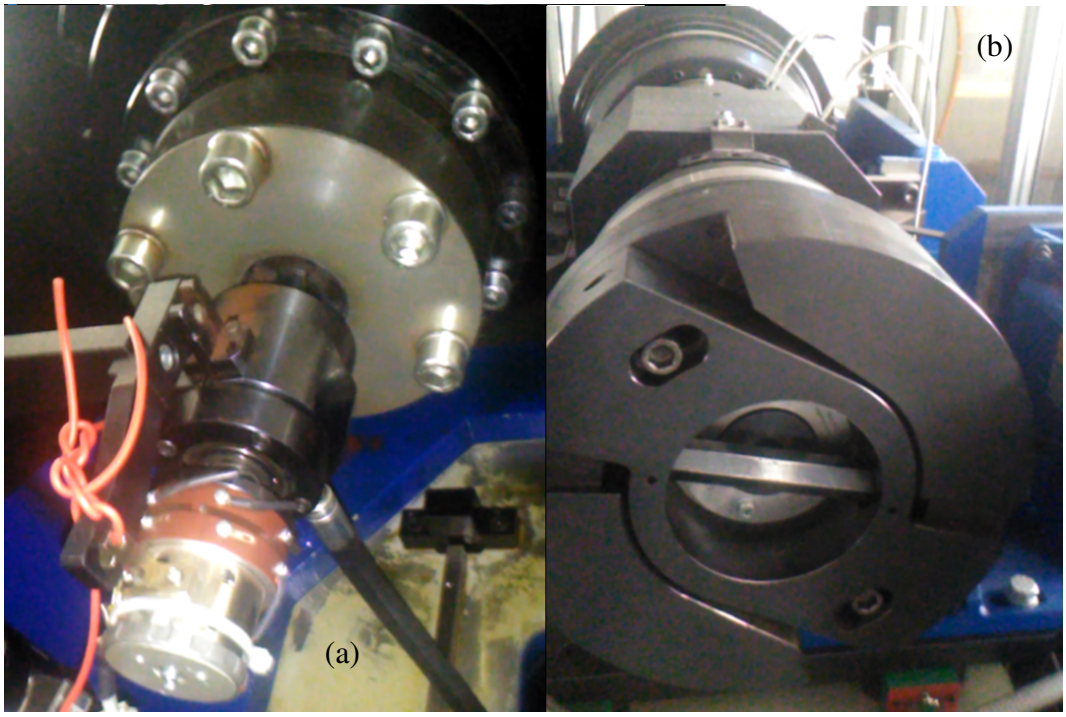

Fig. 2.1 (a) Front end of test bench with data acquisition system for provision of misalignment and measurement of reaction force (b) Rear end of test bench with torque generator

2.1 Experimental Setup

The test bench used during the experiments was capable of running at a maximum torque of 5000Nm, 2000 revolutions per minute (RPM), 60 °C, 1 liter per minute and a misalignment of 10 minutes ($'$) with a resolution $0.5'$ while operating at 6.3kW. There are two coaxial shafts, one inside and the other external both of which are mounted on a torque generator. The torque is applied on the inner shaft which in turn is passed to the outer shaft and then it recirculates to the generator thus saving the required power consumption greatly. The shafts may be rotated by the means of an electric motor. A lever provides provision for misalignment between the hub and the shaft of a spline coupling by the means of a laminated flexible joint. A homokientic joint is used to decouple the hub to find the equilibrium position during the test. The figure of experimental setup has been shown in Figure 2.1.

The accuracy of the applied torque is in the order of $\pm 1\%$. A vectorial engine provides rotation to the shaft. The maximum rotational speed is 2000 rpm. However,

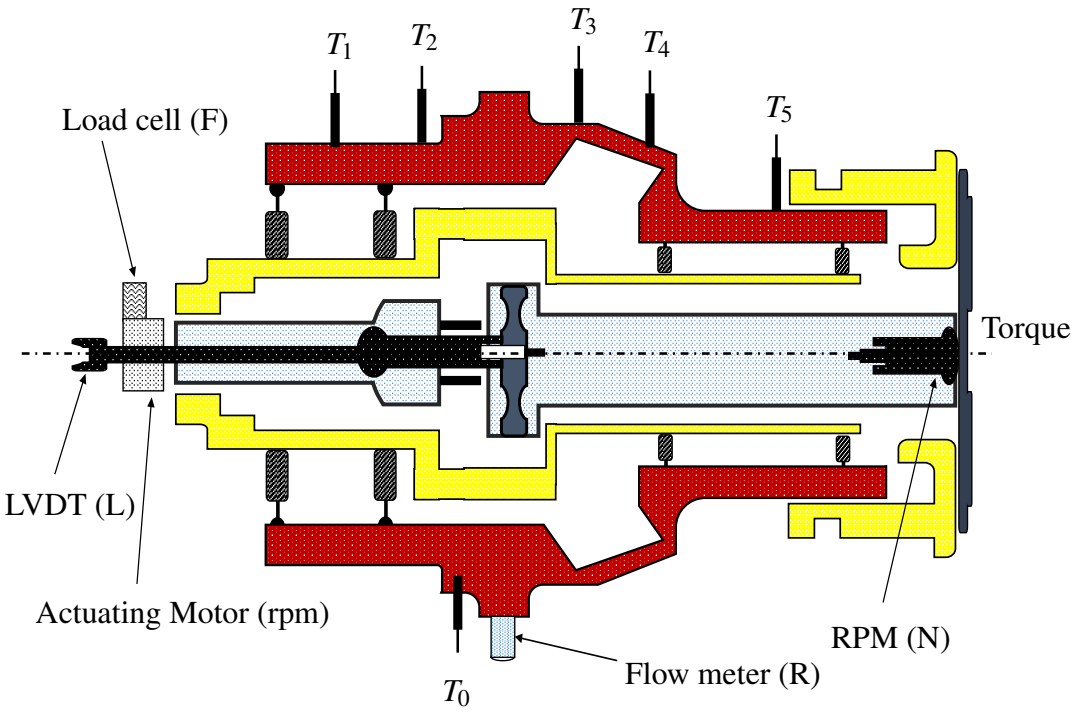

Fig. 2.2 Experimental schematics [2]

during the tests, a rotational speed of 1500 rpm was chosen as it provided the least vibrations and the most smooth operation. A forced lubrication system ensures proper lubrication of the test equipment and also maintains the operating temperature below 60 °C. The measuring instruments / sensors used during the test to record various parameters are given below:

- Torque transducer with a maximum capacity of 5000 Nm and 1% error
- A type HBM load cell with a maximum limit of 20 kN to detect loads as a result of misalignment
- A type HBM load cell with a maximum limit of 10 kN to detect caliberation loads
- A strain gauge mounted on the specimen
- A thermocouple on the specimen
- Temperature sensors on the main bearings

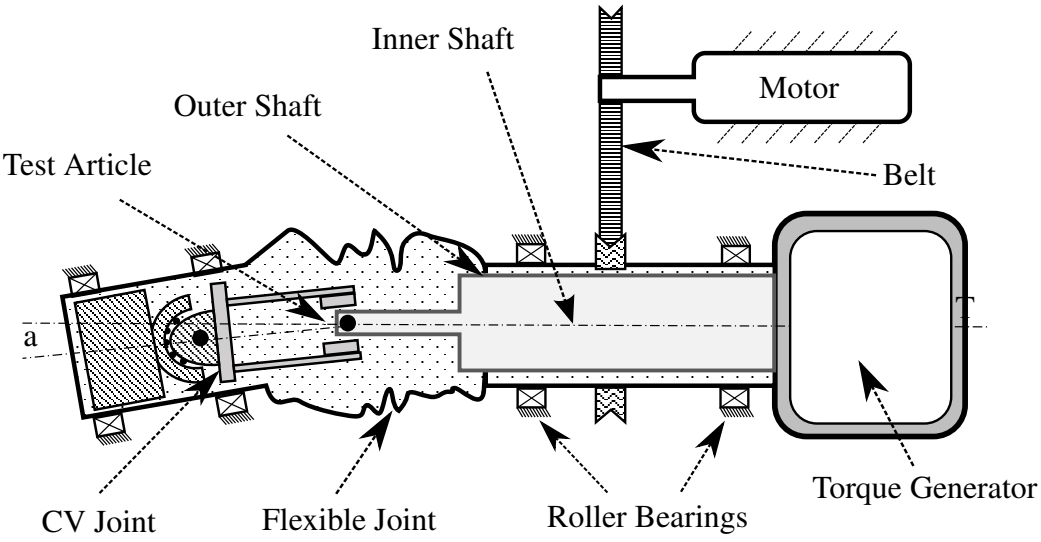

Fig. 2.3 Experimental setup [3]

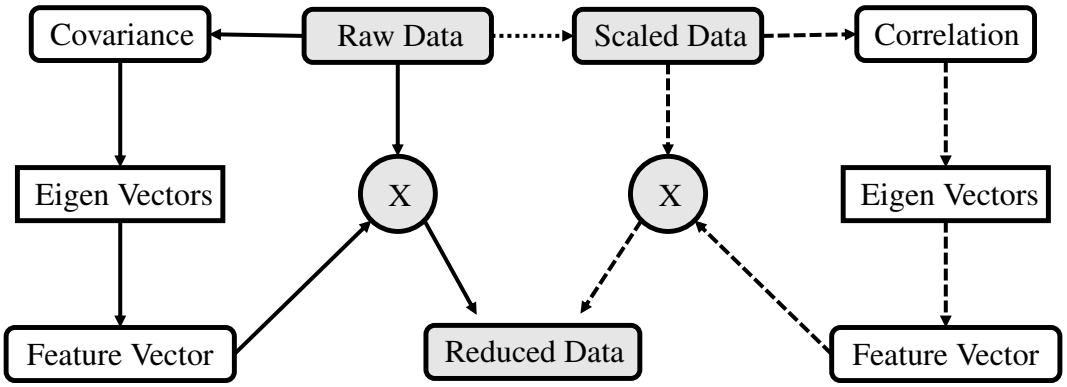

Fig. 2.4 PCA Algorithm

- Two digital flow meters
- An oil debris monitoring system to detect metal particles in the lubricate
- Conditioning modules for all the sensors

The sensor setup has been explained in Figure 2.2 and the schematics of experimental setup has been given in the Figure 2.3. The test spline couplings were made up of nitrogen hardened 42CrMo4. The shaft had crowned teeth profile with a total of 26 teeth, 30 degrees pressure angle, 200mm crowing radius, 1.27mm modulus and 12mm face width. More details of the test setup have been reported in [3]. The

nomenclature to be used throughout this chapter has been given below:

θ = Misalignment angle between shafts ($'$) ***(Independent variable)***

N = Revolutions per minute (RPM) of the driver ***(Independent variable)***

L = Linear Variable Differential Transducer (mm) ***(Independent variable)***

τ = Applied torque (Nm) ***(Independent variable initially)***

T = Average temperature of lubricant (°C) ***(Dependent variable)***

F = Reaction force not related to torque (N) ***(Dependent variable)***

R = oil flow rate (lit/min) ***(Dependent variable)***

V = RPM of actuating motor for misalignment ***(Dependent variable)***

$\bar{x}$ = Mean (Average) of X

σ_x = Standard Deviation of X

σ_{xx}= Variance of X

σ_{xy} = Covariance of X with Y or vice versa

Ψ, Ψ_x = Median, Median of X

Ω_x = Median Absolute Deviation of X

Ω_{xy} = Co-median of X with Y or vice versa

δ = Correlation Median

2.2 Review of PCA

A flow chart for algorithm of PCA has been provided in Figure 2.4. The important terms and steps are briefly explained below.

2.2.1 Covariance

It is a measure of variation of two variables with respect to each other. A non zero value of covariance indicates a possible dependence. A zero covariance guarantees

that there is no LINEAR relationship between the variables. Mathematically:

$$\sigma_{xy} = \sum_{i=1}^{n} \frac{(x_i - \bar{x})(y_i - \bar{y})}{(n-1)} \tag{2.1}$$

Where x and y represent the variables and $\bar{x}$ and $\bar{y}$ their means respectively, n is the total number of observations. The covariance between variables results in a square matrix called covariance matrix. The diagonal of this matrix starting from left top to bottom right represents variance and other elements are symmetric. An example of covariance is provided in the Table 2.1 and of the covariance matrix in Table 2.2.

Table 2.1 Covariance Example [2]

x_i	$x_i - \bar{x}$	y_i	$y_i - \bar{y}$	$a_i b_i$
15	0	23	-4	0
13	-2	27	0	0
12	-3	21	-6	18
17	2	30	4	8
18	3	34	7	21
$\bar{x} = 15$	a_i	$\bar{y} = 27$	b_i	$\sigma_{xy} = 10.8$

Table 2.2 Sample Covariance Matrix [2]

	T	F	L	θ	R	N
T	0.20					
F	0.90	99.0				
L	0.00	-0.03	0.00			
θ	0.01	-0.20	0.00	0.00		
R	0.00	-0.02	0.00	0.00	0.00	
N	1.20	-18.0	0.05	0.32	0.00	35.0

2.2.2 Eigenvalues and Eigenvectors

In a covariance Matrix A with an order $n \times n$, if there exist an X and λ such that:

$$AX = \lambda X \Rightarrow (A - \lambda I)X = 0 \tag{2.2}$$

Then $\lambda = n$ eigenvalues, $X = n \times n$ eigen space and $I = n \times n$ identity matrix

2.2.3 Feature Vector

The eigenvectors with highest eigenvalues which explain the most spread of the data are chosen for the next step and constitute the feature vector. The original data is then multiplied by the feature vector to give rise to reduced data with some loss of information.

2.2.4 Loading Plot

Loading plots are used to find the relationships between feature vector containing the eigenvectors with highest eigenvalues. The eigenvectors with highest eigenvalues are called as Principal Components (PCs). The steps necessary to draw a loading plot are given below:

Steps

- Reduced dataset
- Correlation of every variable with first two PCs
- Assign X axis for correlation with first PC and Y for the second PC
- Using correlation coefficients, every variable is plotted

Interpretation

- If one variable in the same quadrant increases or decreases, the other variables in the same quadrant do the same
- Variable close to each other have comparable statistical importance
- Variables in opposite quadrants behave opposite
- Variables farther from the origin are the most significant and vice versa

2.2.5 Correlation Matrix

A covariance matrix after centering the data around the mean and normalizing by standard deviation is said to be correlation matrix.

2.2.6 Median Based PCA

Median may also be used in PCA instead of mean as the criterion of spread. Median based PCA has been found to be the least sensitive to outliers in the data.

Median

It is the number lying exactly in the middle of a data series. Consider the series 34, 23, 67, 12, 9, 7, 93, 25. Arranging 7, 9, 12, 23, 25, 34, 67, 93. Two numbers appear exactly in the middle so median will be their mean. The median may or may not coincide with Mean or Mode.

$$\Psi_x = \Psi(X) = Median(X) \tag{2.3}$$

Table 2.3 Median Absolute Deviation Example [2]

x_i	Ordered	$\lvert x_i - \tilde{x}\rvert$	Ordered
21	11	10	0
31	16	5	2
16	19	2	2
19	21	0	5
11	23	2	10
41	31	10	10
23	41	20	20
	$\tilde{x} = 21$		Ω_x=5

Table 2.4 Co-Median Example [2]

x_i	$x_i - \tilde{x}$	y_i	$y_i - \tilde{y}$	$a_i b_i$
22	−1	25	−1	1
30	7	27	1	7
16	−7	21	−5	35
19	−4	31	5	-20
11	−12	34	8	-96
39	16	25	−1	-16
24	1	19	−7	-7
$\tilde{x} = 23$	a_i	$\tilde{y} = 26$	b_i	Ω_{xy} = -7

Median Absolute Deviation

It is equivalent to standard deviation and denoted with **MAD**. An example explains it in the Table 2.3 and can be found as:

$$\Omega_x = \Psi|X - \Psi_x| \tag{2.4}$$

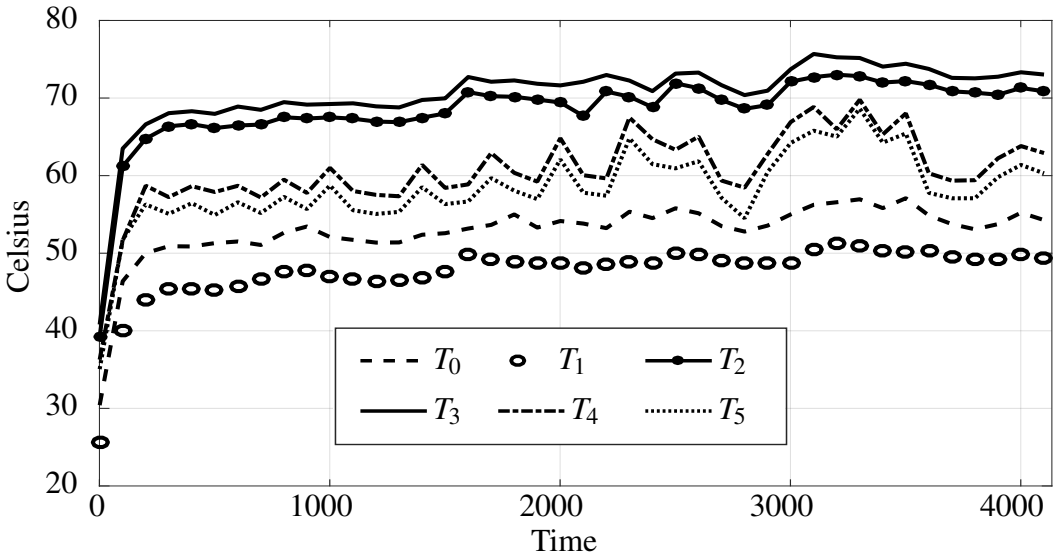

Fig. 2.5 Temperature trends of lubricant at various points (down sampled data) [2]

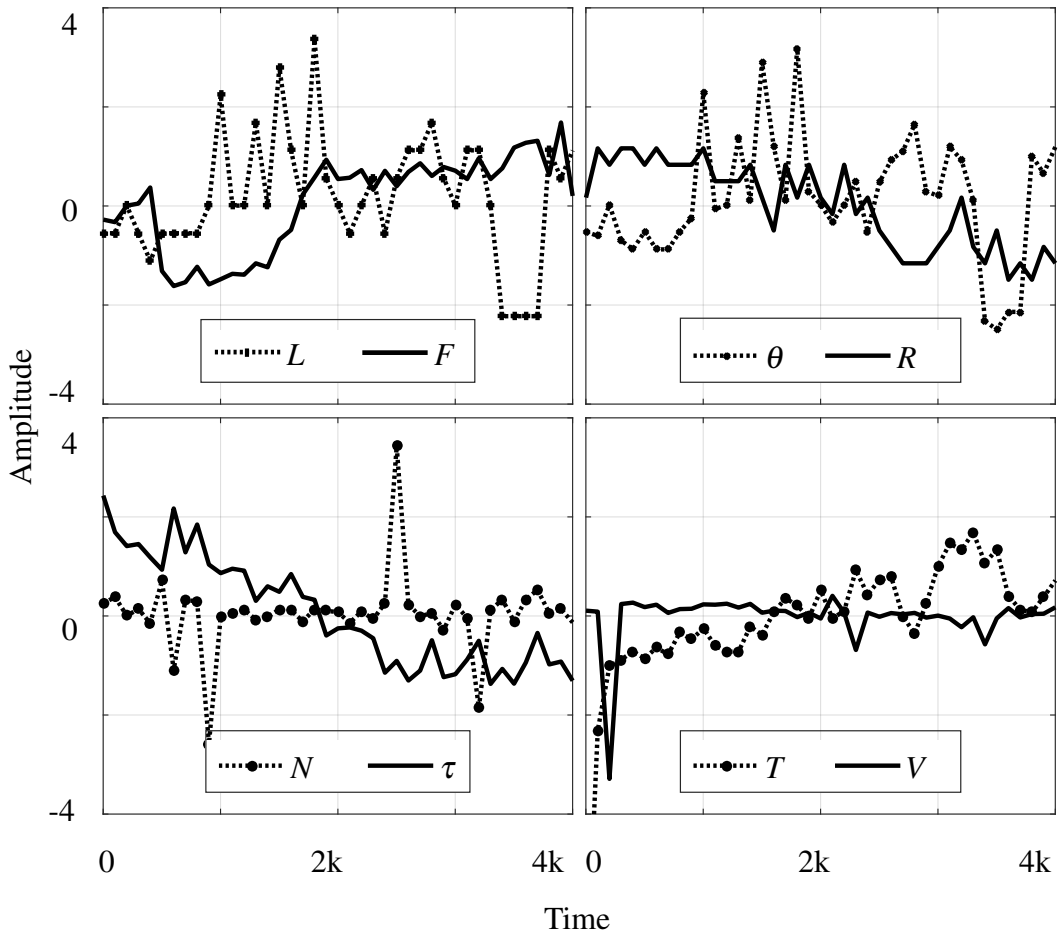

Fig. 2.6 Scaled and down sampled trends of other variables in the experiments [2]

Co-Median

It is equivalent to covariance and denoted with **COM**. An example in the Table 2.4 explains the methodology to find it. Mathematically:

$$\Omega_{xy} = \Psi[(X - \Psi_x)(Y - \Psi_y)] \tag{2.5}$$

2.2.7 Correlation Median

It is equivalent to the correlation coefficient. It can be found using Equation 2.6. The rest of the procedure to evaluate co-median matrix, eigenvalues, eigenvectors and

feature vector is the same as for a covariance matrix.

$$\delta_{xy} = \frac{\Psi[(X - \Psi_x)(Y - \Psi_y)]}{(\Psi|X - \Psi_x| \times \Psi|Y - \Psi_y|)}$$

or

$$\delta_{xy} = \frac{\Omega_{xy}}{(\Omega_x.\Omega_y)} \tag{2.6}$$

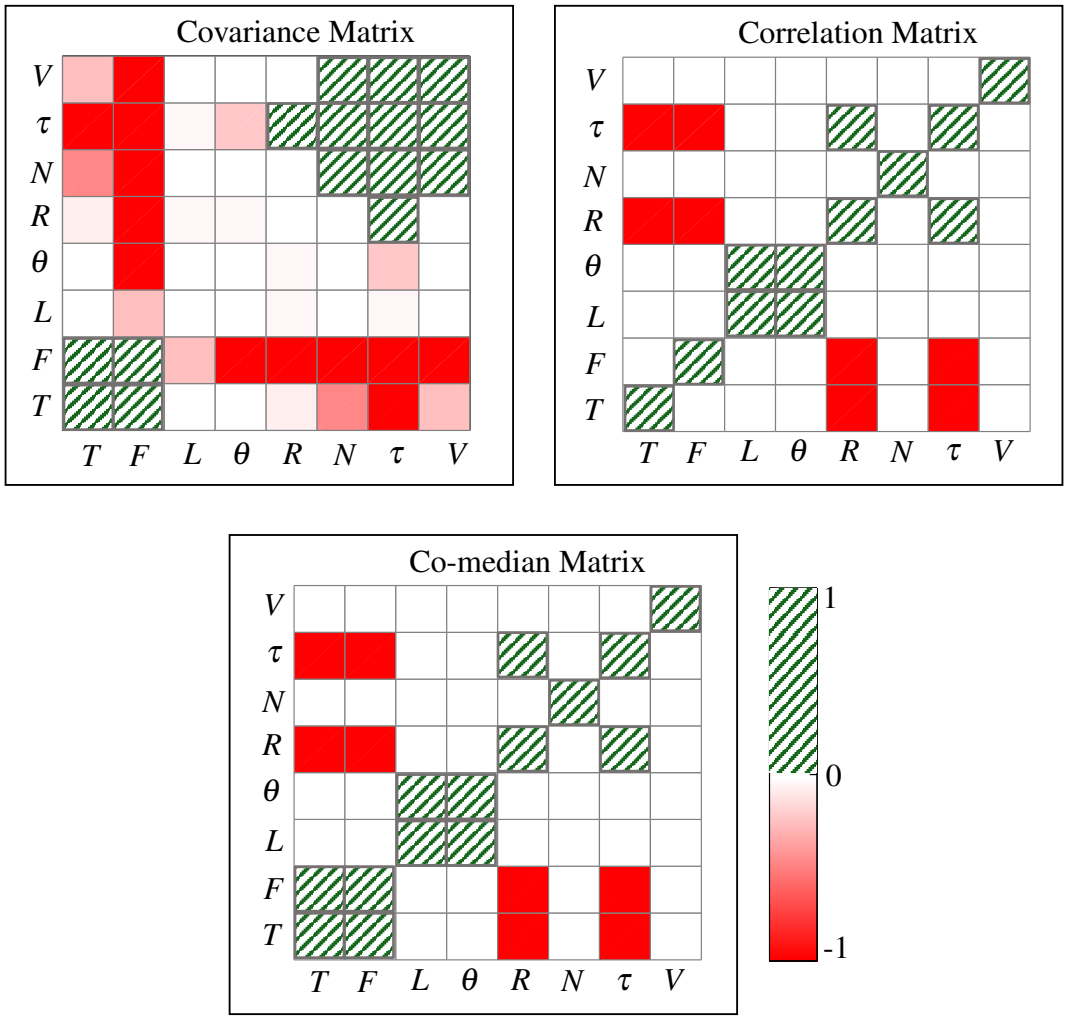

Fig. 2.7 Comparison of Covariance, Correlation and Co-Median Matrices after removal of outliers [2]

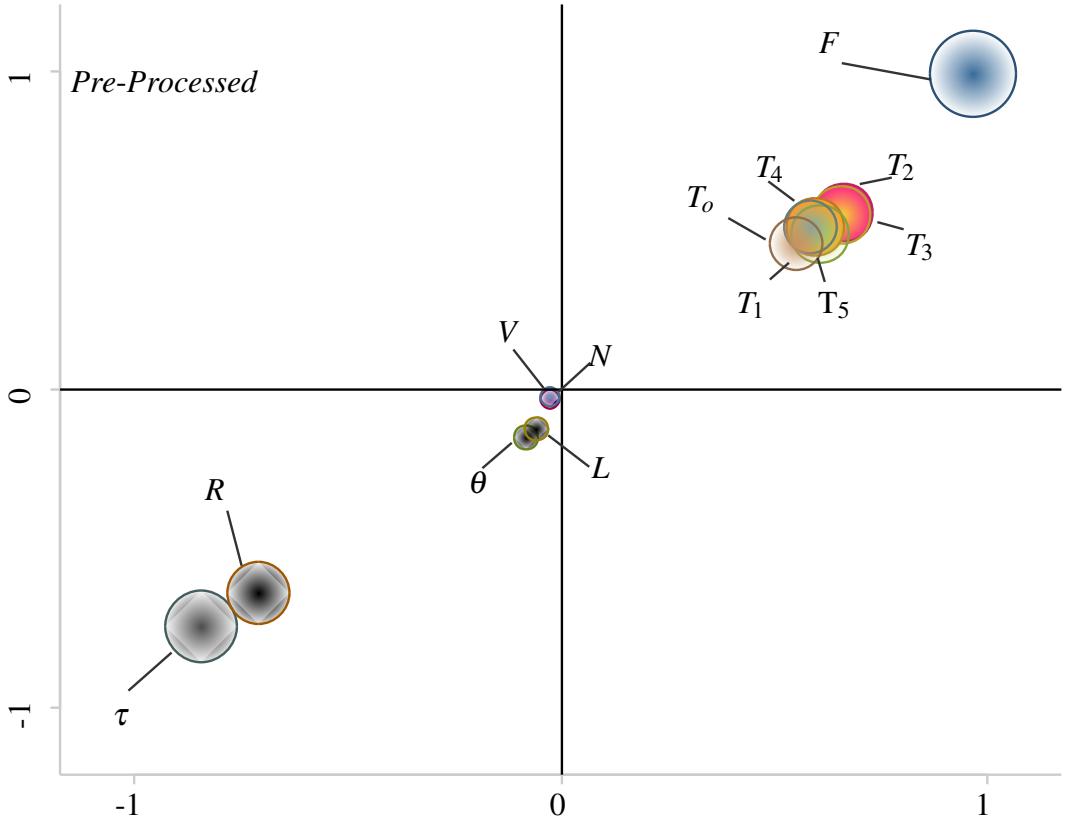

Fig. 2.8 Co-median based loading plots for relations between variables before processing of data [2]

2.3 Results

Temperature readings from sensors have been shown in Figure 2.5, where T_0 is the temperature of lubricating oil at outlet and T_{1-5} are readings of the temperature of lubricating oil at different positions of lubrication circuit. Figure 2.6 shows trends of experimental data. It may be clearly seen that the experimental data made little sense from an outset. Hence, PCA was applied to this experimental. PCA of experimental data without any outliers is carried out. The outliers were filtered out carefully and manually. Figure 2.7 shows Covariance, Correlation and Median Correlation matrices after removal of outliers. These matrices do give some information about the possible dependence of some variables. But these still do not give information about the significance of each variable. The covariance matrix shows a little more complex relationships than expected physically.

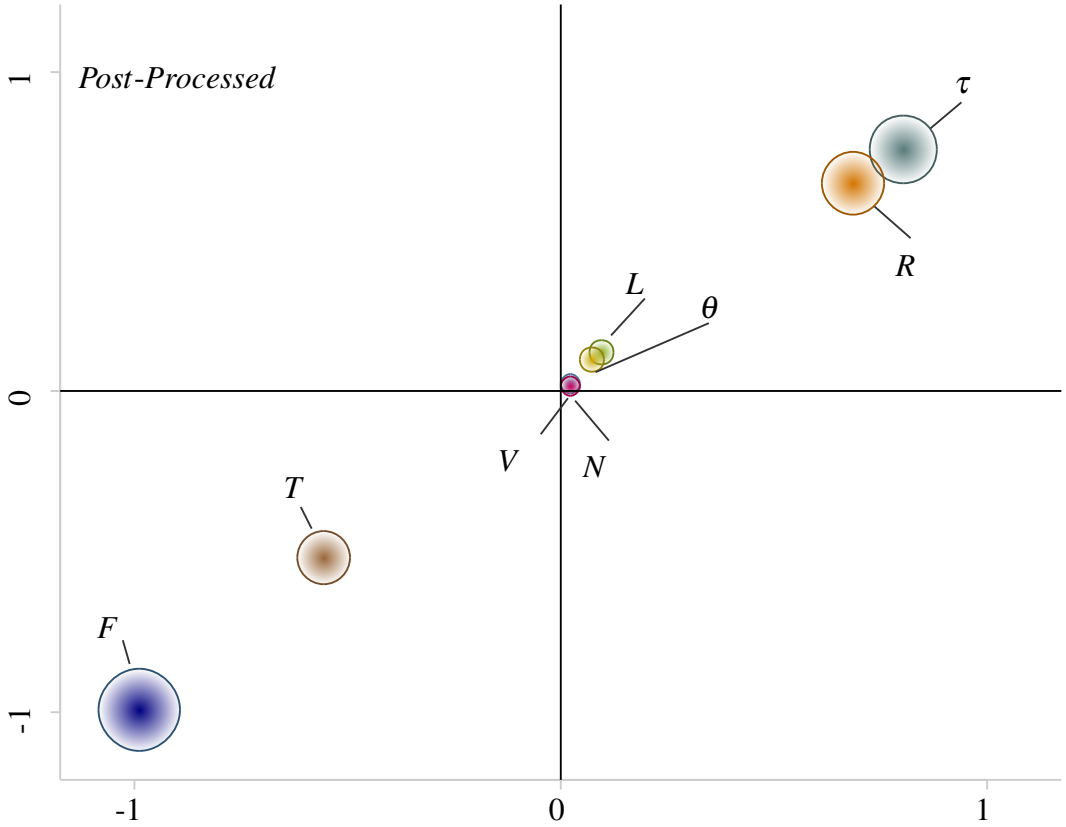

Fig. 2.9 Co-median based loading plots for relations between variables after processing of data [2]

This is because of different units of quantities and covariance matrix is not a very useful choice for such datasets. Co-median matrix appears to have slightly clearer information. Figure 2.10 presents the correlation of principal components evaluated by all three methods using covariance, correlation and comedian matrices. First three sets represent correlations after removal of outliers and the last three sets with 'Out' as subscript represent correlations in the presence of outliers. It can be readily observed that covariance and correlation based PCA fails to identify the significant variables. However, comedian based PCA appears to be less sensitive to the presence of outliers. Hence, statistically the most significant parameters in descending order are - reaction force F, applied torque τ, lubricating oil flow rate R and average of temperature from all sensors T.

It is worth mentioning that correlation is not causation. The absence of correlation does guarantee no linear relationship. But, the occurrence of a correlation does not automatically imply a causal relationship between the parameters of interest.

Therefore, it is highly recommended to use PCA as an initial tool to make an educated guess at the underlying relationships between different experimental variables, but it must be validated physically after observing the actual dynamics of the system under consideration. If non linear relationships are probable, then a more suitable choice would be Kernel PCA (K-PCA), a variant of PCA exclusively used for nonlinear relations. Lastly, loading plots are drawn from the given matrices and their correlation with the respective parameters. The procedure to draw and interpret a correlation plot will be explained later. However, as a quick reference, it is useful to note that the distance between points representing variables on a correlation plot dictates their similar or dissimilar behaviors. Also, the distance of any point from the origin conveys the statistical importance of the relevant parameter.

2.4 Discussions

Table 2.5 A priori and loading plot based information on independent and dependent variables [2]

	A priori information					Loading plot information			
Independent	N	θ	τ	L	Independent	N	θ	V	L
Dependent	V	T	F	R	Dependent	τ	T	F	R

"Various variables are controlled by the means of a proportional-integral-derivative (PID) control. The variables in the feedback loop of by PID controller are the misalignment angle (θ), driving motor rpm (N) and actuator motor rpm (V). LVDT (L) is used as a sensor for misalignment in the PID control. Applied torque, though fixed at a certain value, is not part of PID control. Hence, as the surfaces of spline couplings interact, the effects are reflected in the torque. So reaction force (F) at the driven end of the shaft, average temperature (T), oil flow rate (R) and torque (tau) are the variables and they can give an insight into the phenomenon of fretting during the experiment. A work done by the authors in past [42] has given the complete details about the dynamics of reaction moments in spline couplings for the given test bench under consideration." [2]

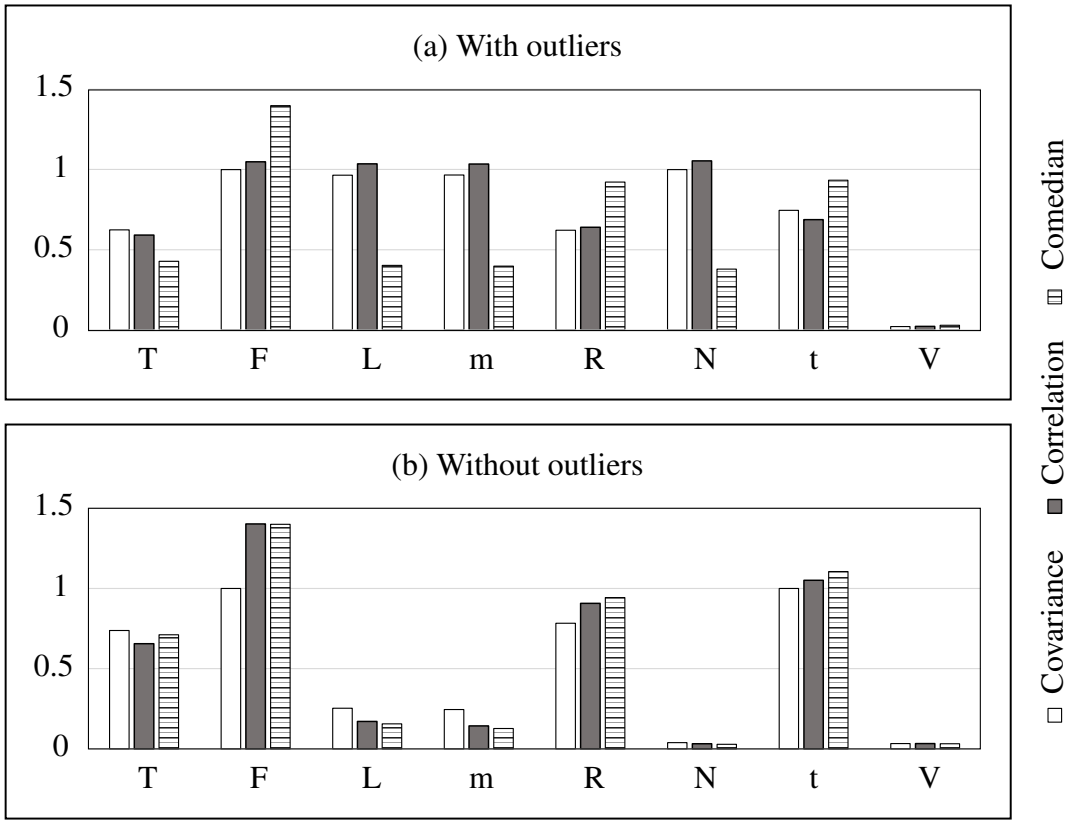

Fig. 2.10 Statistical Importance of Variables [2]

2.4.1 Corroboration With Operating Conditions

"In order to understand, validate and correctly use the PCA it is necessary to corroborate the interpretation of results obtained with the practical operating conditions. Also, it is of paramount importance to validate the experimental procedure statistically which in itself is yet another advantage. The operating conditions / parameters during the experiment were a rotational speed N of 1450 rpm, a misalignment of $10'$, a torque of 1000 Nm, total 10 million cycles, a sampling time of 100 s with lubrication and a total of 4135 readings in real time. These are the independent variables with one condition that they are supposed to be constant throughout the experiment. So out of eight variables being monitored four have been defined to be operating conditions, whereas four variables are dependent on them and should change their values as the cycles progress. Interaction between the hub and shaft of

spline coupling is responsible for variations in the value of applied torque. These conditions are reflected well in the loading plot as explained in the next section." [2]

2.4.2 Loading Plot Interpretation

"Loading plot shows a statistical picture of variables. The variables which appear closer to the origin should be the constant / independent variables or operating conditions, whereas those farthest from it would be the dependent (dynamic) parameters changing their values with each cycle. To summarize the conclusions about dependence and independence of variables based upon a priori knowledge of experimental set up and the information from loading plot, Table 2.5 gives the complete picture." [2]

2.4.3 Relationships Between Variables

"The loading plot is providing much more information about relationships between different variables which have been summarized below;

- Statistically, the most significant variables are the reaction force (F), torque (τ), lubricating oil flow rate (R) and average temperature (T) of the lubricating oil in descending order. Other variables are insignificant.
- Two pairs of variables behave similarly (increase or decrease together) which are:-

  - Lubricating oil flow rate and torque.

  - Reaction force and temperature of lubricating oil.
- If any variables in the current set were to be used for the purpose of characterization of fretting wear under given conditions, they have to be the reaction force and torque or lubricating oil flow rate.
- Relationships between other variables were quite less significant and did not convey much information about their dependence.

A more useful experimental interpretation has finally been shown in Figure 2.8 and Figure 2.9 using the technique of Principal Component Analysis (PCA) and

it could be applied in other similar experimental scenarios as well." [2]. More cases without taking an average temperature using the presented approach have been summarized in the Appendix B.

The primary purposes of the work presented in this chapter were to validate the test bench statistically, corroborate it physically, identify the most significant test parameters, design the future experiments in a more cost effective manner, interpret the variations in different parameters and decipher the underlying relationships among them. It was found that as the test progressed the value of applied torque decreased. It was then physically validated after noting that the torque was being applied in an open loop and after the evolution of wear depth, it tended to reduce. It was a practical design constraint of the experimental setup. Normally, in the field the torque would be in close loop. However, this effect was taken under consideration during interpretation of experiments. As the torque reduced so did the frictional work which resulted in less increases in the temperature and consequently a lower lubricant flow rate as the less heat transfer was required. Misalignment angle as expected played a less significant role as it was in a closed loop control. The observation of changes in the open loop torque lead to more robust and accurate models of fretting wear in the later stages of the research activity. Another interesting statistical observation was the relative insensitivity of co-median based PCA to the occurrence of outliers. The reasons and background for this behavior are beyond the scope of this work. Nevertheless, this has been mentioned to aid future researchers working in the field of statistical interpretation of raw experimental data. An important future addition in this approach could be kernel PCA based upon co-median to cater for not only noisy but also non-linear trends and interdependence of various experimental variables.

Chapter 3

Empirical and Neural Modeling of Fretting Wear

Owing to the complex nature of the phenomenon of fretting wear, based upon the experimental data, empirical and neural network based models were developed to predict fretting wear for characteristic experimental conditions. An effort to develop an empirical model between abrasive wear and operating conditions was made in [43] but it was not focused on spline couplings. Another empirical model for fretting wear of heat exchanger tubes has been presented in [44] but once again, it could not readily be applied to spline couplings. In [45], an evaluation of the suitability of empirical equations for a variety of tribological conditions and materials has been carried out and it concluded that use of empirical relations might be justified in problems involving low wear volume with some loss of accuracy. In [46], empirical wear relations for centrifugal slurry pumps were proposed. Another use of empirical equations for the prediction of fretting corrosion for simplified single electrical contact has been reported in [47].

Very recently, a combined numerical and empirical approach was applied in [48] for prediction of tool wear during machining which could not be readily applied to mechanical components like spline couplings. An empirical prognosis model for cutting tool wear of Hydroshield tunnel boring machine has been proposed in [49] which also signified a good potential of the application of such techniques in the current work. A recent study [50] focusing modeling of complex wear associated with grid-to-rod fretting in light water nuclear reactors proposed a so called multi-

stage engineering wear model which was in essence also an empirical model. Even though, it seems to be quite promising, but it still needs more rigorous experimental validation in the field. Nevertheless, such works indicate the potential of application of empirical models for the phenomenon as complex as fretting albeit for very particular cases. An additional advantage of such studies and models is often an insight into the theoretical formulation of the problem which could help greatly in the development of analytical solutions. For example, in the quoted work as well as during this research, it has been found that fretting wear strongly depends upon geometric considerations too along with tribological conditions of the fretting pair.

Table 3.1 Training experimental data

	Experiments	1	2	3	4	5	6
Input	Torque (Nm)	700	700	1000	1000	1300	1300
	Misalignment ($'$)	0	10	5	10	0	10
Output	Wear (10^{-5} mm^3)	0	6.7	4.3	9.2	0	13
	Clearance (10^{-4} rad)	0	13.6	11	18	0	19.4

Table 3.2 Empirical predictions

	Samples	1	2	3	4	5	6	7	8	9
Input	τ (kNm)	0.7	0.7	0.7	1	1	1	1.3	1.3	1.3
	θ ($'$)	0	5	10	0	5	10	0	5	10
Empirical	W (mm^3)	0	3.2	6.4	0	4.6	9.2	0	6	11.9
	A_c	0	6.3	12.6	0	9	18	0	11.7	23.4

The experimental setup used during tests for this experimental activity has already been explained in Chapter 2. The findings and experiments presented in this section also resulted in a publication [4].

3.1 Empirical Modeling

By curve fitting the experimental results following relations were derived.

$$V = k_1 \tau \theta \tag{3.1}$$

$$A_c = k_2 \tau \theta \tag{3.2}$$

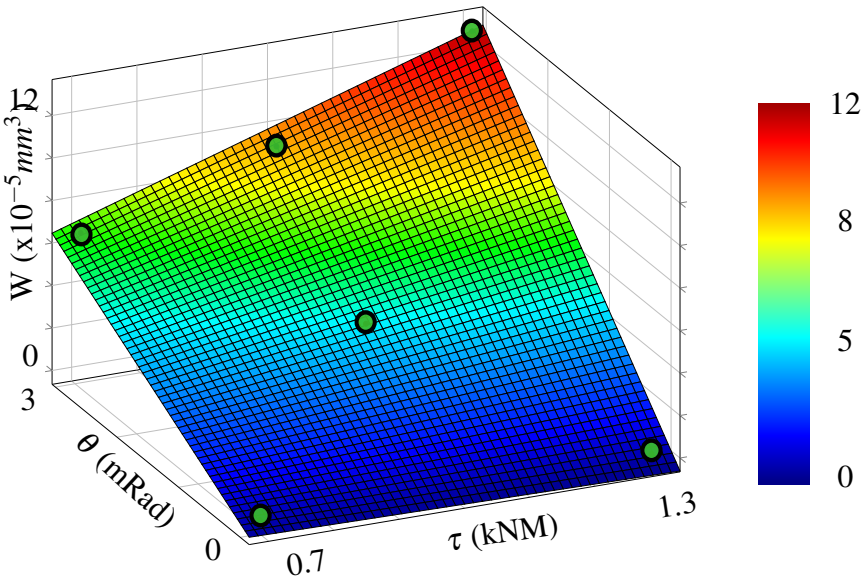

Fig. 3.1 Empirical model of wear [4]

Table 3.3 Neural network predictions

	Samples	1	2	3	4	5	6	7	8	9
Input	τ (kNm)	0.7	0.7	0.7	1	1	1	1.3	1.3	1.3
	θ ($'$)	0	5	10	0	5	10	0	5	10
Neural	W (mm^3)	0	3.4	6.9	0	4.5	9.3	0.5	6.6	12.4
	A_c	0.3	10.4	16.8	0	10.5	18.1	0.1	10.8	19.4

where V is wear volume, τ is torque, θ misalignment angle and A_c the angular clearance. The coefficients k_1 and k_2 have the values 3.158 $\times 10^{-5}$ mm^3/Nm/rad and 6.181 $\times 10^{-4}$ N/m respectively. The fitting of experimental data has been shown in the Figure 3.2. Since, the number of cycles for all experiments were same i.e., 10 millions, hence they have not been incorporated into the empirical modeling. The chosen set of experiments for the purpose of modeling has been provided in the Table 3.1. The empirical relations so obtained could be compared with classical Archard's equation where torque corresponds to the applied force and misalignment to sliding amplitude. The empirical model for wear is a result of curve fitting with 95 percent confidence bounds using bisquare and Levenberg-Maquardt method and the root mean square error (RMSE) for wear is found to be 0.27. The empirical equation for angular clearance has been developed with 95 percent confidence bounds by least absolute residual (LAR) and Levenberg-Maquardt method and the RMSE in

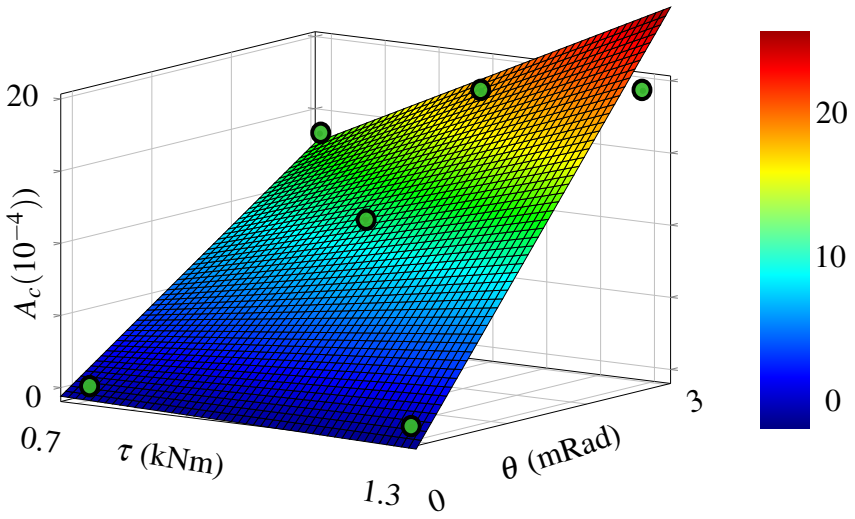

Fig. 3.2 Empirical model of angular clearance [4]

this case turned out to be 0.71. It is clear that the fretting wear volume and angular clearance depend upon the misalignment angle and applied torque. The equation for fretting wear can be compared with Archard's equation for wear [23].

$$W = kPs \tag{3.3}$$

where k is a constant, P is the total normal load and s is the sliding distance. Applied torque actually is responsible for the applied normal load and misalignment angle gives rise to sliding amplitude. If material properties are also considered then wear equation after inclusion of material hardness H becomes:

$$W = \frac{k\tau\theta}{H} \tag{3.4}$$

3.2 Neural Modeling

3.2.1 Neural Network Structure

Neural networks are often used as non-linear approximators. A typical neural network consists of three layers namely; input, middle or hidden and output layers. The first layer takes in inputs, the 2nd layer processes them to give the final output in the third layer. Each layer consists of individual nodes called neurons and each

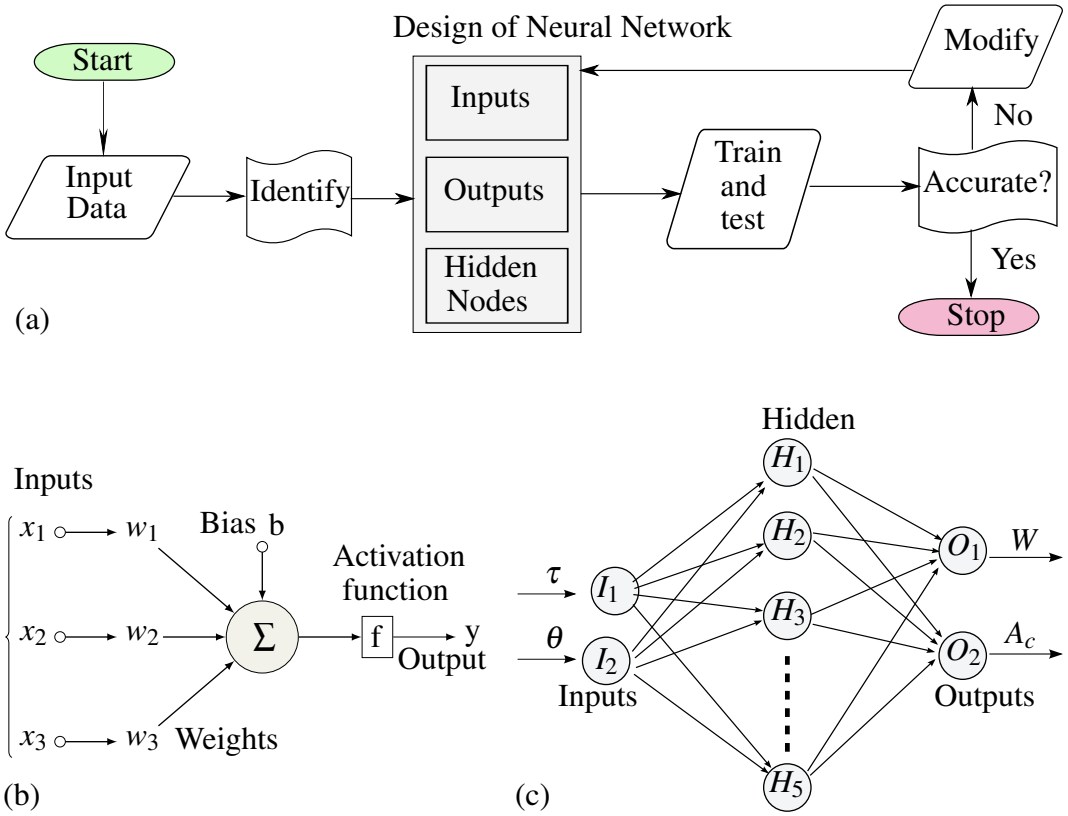

Fig. 3.3 (a) Flow chart of neural network (b) Weights and bias (c) Used neural network [4]

node connected to every node in the preceding or receding layer. Each connection is called as a path and they are assigned random weights in the beginning. A detailed topology of neural network used in this work is provided in the Figure 3.3. In this section, their suitability for prediction of fretting wear in spline couplings has been evaluated.

3.2.2 Neural Network Results

Like empirical modeling, neural network was also trained for angular clearance and fretting wear volume. The performance of empirical and neural models was then compared with experimental data. Both were found to yield reasonable results with neural network outperforming empirical model. The predictions from neural network have been shown in the Table 3.3.

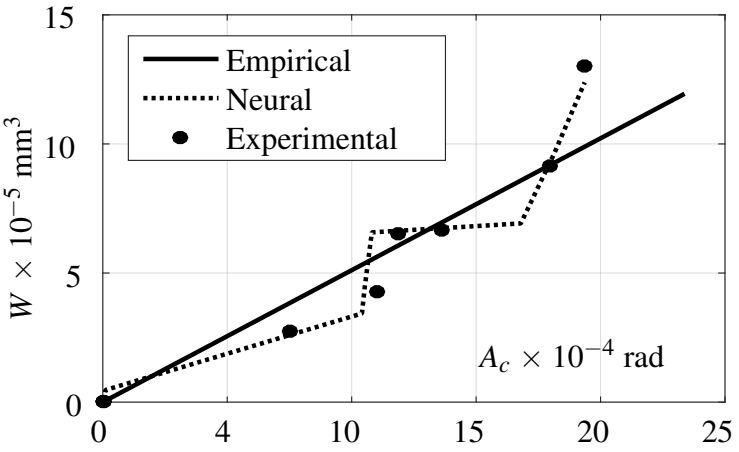

Fig. 3.4 Comparison of Performance [4]

(b)

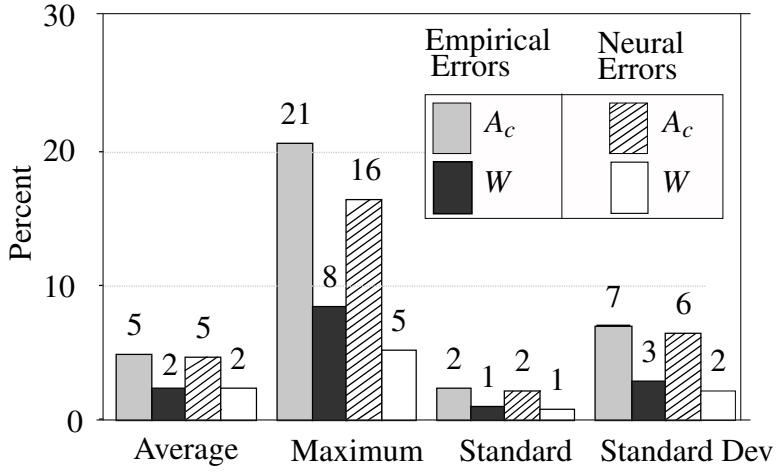

Fig. 3.5 Comparison of Error [4]

3.3 Performance Comparison

Empirical model was relatively poor at capturing the non-linearities and characteristic experimental trends. From the experimental as well as neural network based data, it was observed that an increase in the torque results in an increase in fretting wear in equal proportions. However, in the case of angular clearance, it tends to reduce with every increment in the torque. This observation made sense because an increase in the torque implies an increase in the applied normal load and an increase in the applied load implies an increased contact area for fretting. When the contact area increase, more wear volume might be the result of a reduced depth. Thus, while wear volume is linearly related to applied load, the wear depth is not. The comparison

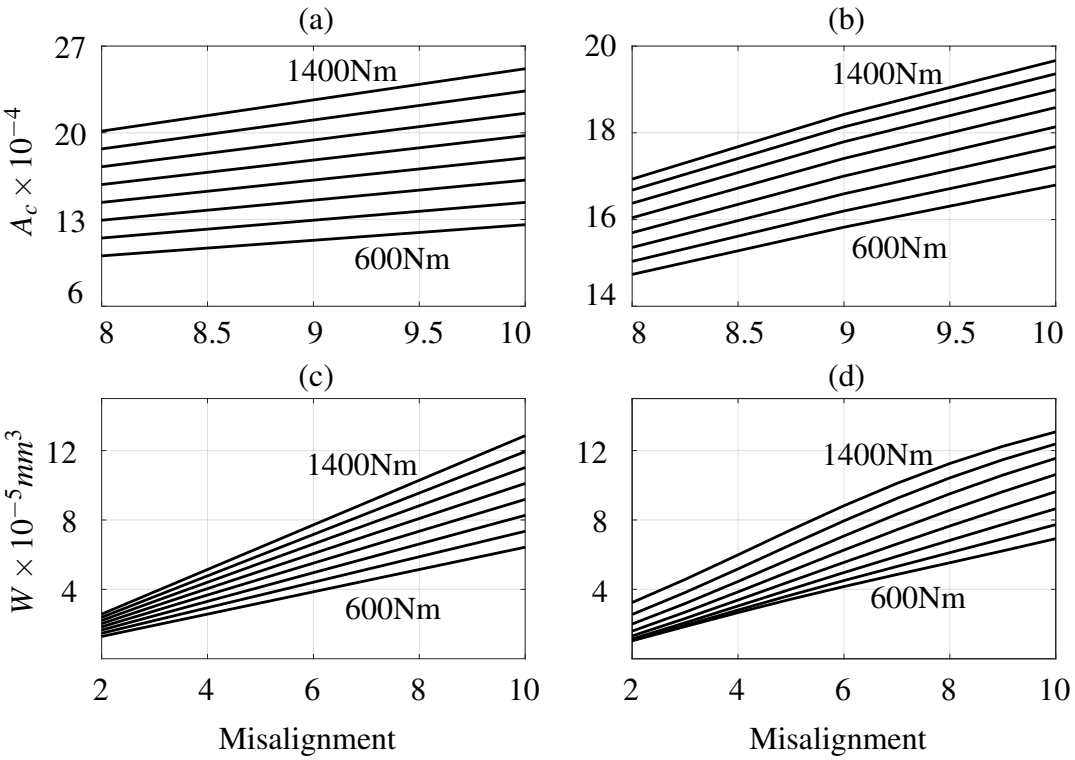

Fig. 3.6 Simulations: (a) and (c) Empirical relations, (b) and (d) Neural networks [4]

of results from empirical and neural networks is detailed in the Figure 3.4 and comparison of errors from both approaches is provided in the Figure 3.5.

3.4 Simulations

Finally, both empirical and neural approaches had been evaluated for simulations of fretting wear and changes in angular clearance. The results are shown in the Figure 3.6. The trends from simulations clearly show that neural networks tend to give more realistic estimates. The reason for more representative trends from neural networks is their capability to model nonlinear phenomenon and it was observed that the relationships between applied misalignment angle and fretting damage under different torques were not strictly linear. Even if they are approximated to be linear, they do not increase or decrease in proportion for different torques which results in slight under-performance of empirical models.

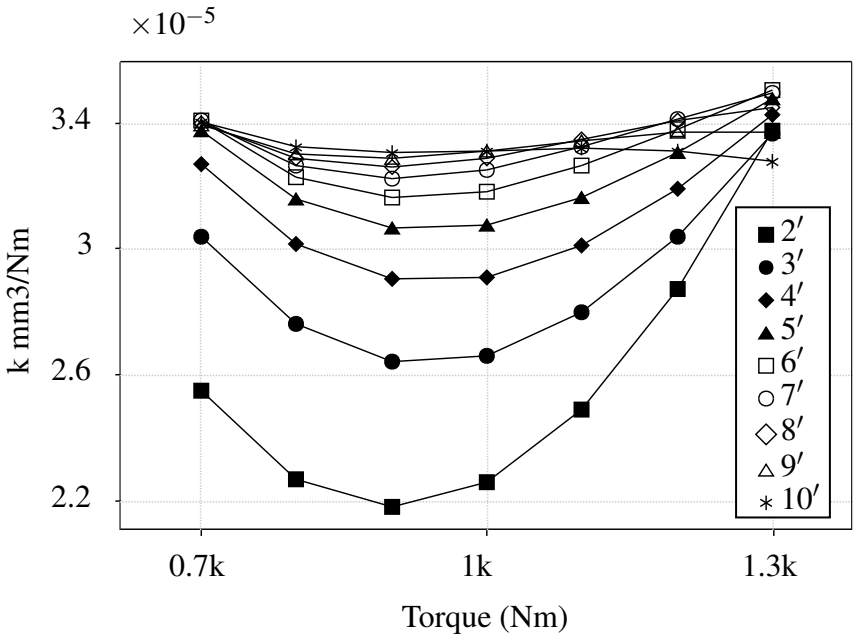

Fig. 3.7 Simulated variations in Archard's wear coefficient by neural network [4]

3.5 Discussions

Simulation trends show that the empirical model provides over-estimated predictions of angular clearance. This trend is not seen in experiments because angular clearance can not go on to increase indefinitely with an increase in torque or misalignment angle. As the wear progresses, the contact area changes and finally a point comes when increments in torques or misalignment angles result in very small changes in wear depth (a direct measure of angular clearance). It also depends heavily on the material properties and geometry of the spline coupling. On the other hand, a neural network was able to capture these intricate details and trends. So, whereas the wear volume tends to increase in direct proportion with torque and misalignmnt, the wear depth does not. It was observed during experiments that the value of Archard's wear coefficient changes with the varied operating conditions. Thus, the same neural network was used to predict the variations in Archard's wear coefficient. The results of these predictions have been shown in the Figure 3.7 and the Figure 3.8. Neural network based simulations present and capture the phenomenon quite effectively. Thus, the potential of neural networks for modelling fretting wear is quite clearly visible.

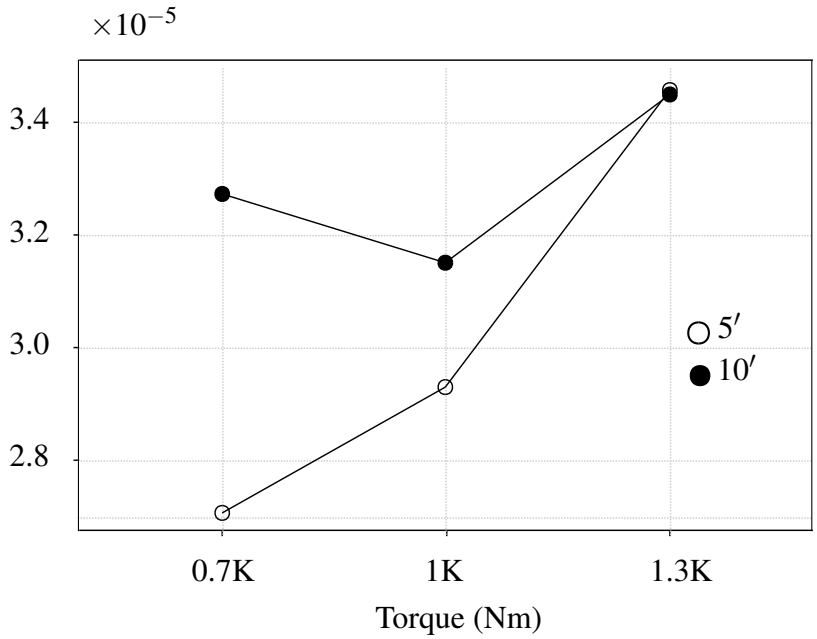

Fig. 3.8 Comparison of variations in Archard's wear coefficient between experimental and neural network based estimates [4]

A limitation of this work is that it is not generally applicable to all spline couplings of different geometries and materials. The trends might be the same, but exact predictions will not be possible. Also, this work did not take into account the effects of surface roughness. This approach can be used only with spline couplings on which sufficient experiments have been performed. So, it still is relevant and applicable in the cases the operation of spline couplings is in the question not their design. From a designer's point of view, this approach is not very promising. But, from a maintenance point of view for fixed design of spline couplings and their materials, this approach can be quite effectively used to model and predict the fretting wear.

3.6 Conclusions

This chapter may be concluded by stating that for an industrial application where not many variations in the design, material or tribological conditions of spline couplings are expected, empirical or neural network based models can be rather useful with the latter being more accurate. However, this approach could not be very useful for the cases where a more general solution is sought thus limiting its application. One

possible avenue of usefulness of such an approach would be modeling of coefficient of friction after providing as input the operating conditions, material properties and experimental outputs. Such a model would increase its accuracy over the period of time as more and more experimental details would be added to it. After necessary training, the developed neural networks could be effectively used to predict fretting wear in a variety of circumstances. In any case, it could be safe to infer that for the case at hand with limited time, few test samples and lack of generality in this approach, it does not hold attraction for wider applications except for very specific cases where experimental data is available. These limitations gave rise to the need for a more robust and relatively easy to follow approach to at least qualitatively assess the fretting damage in spline couplings during operation which is exactly the subject of the next chapter as well.

Chapter 4

Roughness Parameters and Fretting Wear

Roughness parameters significantly affect some very important phenomenon like friction, contact, heat conduction, wear and fretting fatigue [5]. Based on the work presented in this chapter, several findings have been reported in [6]. In [51], the role of surface texture and roughness parameters on friction and the transfer film formation has been reported in the case of Ultra High Molecular Weight Polyethylene pin sliding against steel plates. An optical profilometer was used to characterize the roughness of the textures in it. This work showed that the coefficient of friction depended heavily on the surface texture. A method and criterion to select the most relevant 3D roughness parameter for a surface has been reported in [52] but it was found to be not very useful in the present work because of the complex geometry of spline couplings and the availability of only 2D profilometer. The influence of surface roughness over the contact interface for fretting in dry and boundary lubricated conditions has been reported in [53] for AISI 1034 / AISI 52100. It attempted to provide a method to evaluate the surface finish as a factor in friction and wear damage. The current work differs with this work in the sense that it attempts to correlate the variations in roughness parameters with the fretting damage directly. An account of manufacturing ceramic knee implants by the conditioned roughness and wear of ceramics has been provided in [54] which is quite useful in understanding the significance of roughness and its role on wear. The references [55–57] reported that it is very difficult to achieve perfect alignment in the case of lightweight aero-engine spline couplings. As a result, the teeth end up sliding on each other during the

operation. The sliding gives rise to fretting wear and it heavily depends upon the surface conditions. Keeping in mind the above discussion, it became imperative to explore the relationships between fretting and surface conditions about which not a lot material is available in the literature. Hence, a detailed investigation of roughness parameters of spline shaft teeth before and after the tests was carried out, compared with fretting damage and their correlation with each other was carried out. Isolating the most significant roughness parameters with respect to fretting damage was the final aim of this approach which was successfully accomplished and the results are reported in this chapter.

Table 4.1 Formulae for calculation of various roughness parameters [5]

$R_a = \frac{1}{n}\sum_{1}^{n}\lvert y_i\rvert$	$R_q = \sqrt{\frac{1}{n}\sum_{i=1}^{n} {y_i}^2}$	$R_z = \frac{1}{n}\sum_{i=1}^{n}(p_i - v_i)$
$k = \frac{R_v}{R_t}$	$R_{pm} = \frac{1}{n}\sum_{i=1}^{n} R_{pi}$	$R_{vm} = \frac{1}{n}\sum_{i=1}^{n} R_{vi}$
$R_{ti} = R_{pi} + R_{vi}$	$R_{tm} = \frac{1}{n}\sum_{i=1}^{n} R_{ti}$	R_y = The largest R_{ti}
$R_{sk} = \frac{1}{NR_q^3}\sum_{i=1}^{N} Y_i^3$	$R_{ku} = \frac{1}{NR_q^4}\sum_{i=1}^{N} Y_i^4$	$R_t = R_p + R_v$
$\Delta_q = \sqrt{\frac{1}{n-1}\sum_{i=1}^{N}(\frac{\delta y_i}{\delta x_i} - \theta_m)^2}$ $\theta_m = \frac{1}{n-1}\sum_{i=1}^{n-1}(\frac{y_i - y_{(i-1)}}{x_i - x_{(i-1)}})$	$S_m = \frac{1}{N}\sum_{i=1}^{n} S_i$	$\Delta_a = \frac{1}{n-1}\sum_{i=1}^{n-1}\frac{\delta y_i}{\delta x_i}$

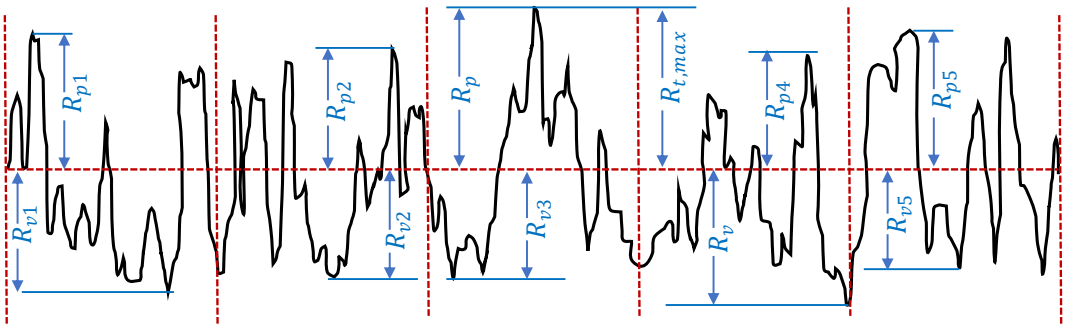

Fig. 4.1 Wear definitions [5]

4.1 Review of Roughness Parameters

The nomenclature of roughness parameters to be used in this work have been first provided in the Nomenclature below. The reference for the review of roughness parameters presented here is [5].

4.1.1 Maximum Height of Peaks (R_p)

It is the maximum height of the profile above the mean line within the assessment length. In figure R_{p3} represents this parameter. But this parameter itself is not found to be significant in this analysis.

4.1.2 Mean Height of Peaks (R_{pm})

It is the mean of the maximum height of peaks (R_p) obtained for each sampling length of the assessment length. The equation for this parameter is given below.

$$R_{pm} = \frac{1}{n}\sum_{1}^{n} R_{pi} \tag{4.1}$$

4.1.3 Mean of Maximum Peak to Valley Height (R_{tm})

It is the mean of all maximum peak to valley heights obtained within the assessment length of the profile. Mathematically,

$$R_{tm} = \frac{1}{n}\sum_{1}^{n} R_{ti} \tag{4.2}$$

From the figure,

$$R_{tm} = R_{t1} + R_{t2} + R_{t3} + R_{t4} + R_{t5} \tag{4.3}$$

Nomenclature

Δa	Mean slope of profile
Δq	Root mean square slope of profile
A_c	Clearance angle between teeth
P_c	Peak count
R_a	Arithmetic average height
R_k	The core roughness depth
R_q	Root mean square roughness
R_y	Largest peak to valley height
R_z	Ten point height
R_{pk}	The reduced peak height
R_{sk}	Skewness
R_{ku}	Kurtosis
S_m	Mean spacing at mean line
t_p	Bearing line length and area curve
k	Profile solidity factor
R_p	Maximum and mean height of peaks
R_{pm}	Mean height of peaks
R_v	Maximum depth of valleys
R_{vm}	Mean depth of valleys
R_t	Maximum height of profile
R_{tm}	Mean of maximum peak to valley height
M_{r_1}	Material ratio (Upper limit of core)
M_{r_2}	Material ratio (Lower limit of core)
W	Fretting wear damage

4.1.4 Arithmetic Average Height (R_a)

It is also known as centre line average (CLA) and is defined as the average absolute deviation of the roughness irregularities from the mean line over one sampling length. This parameter gives a good general description of height variations. However, it is

not sensitive to small changes in the profile. Mathematically:

$$R_a = \frac{1}{n}\sum_{1}^{n}|y_i| \tag{4.4}$$

4.1.5 Profile Solidity Factor (R_k)

It is the ratio between the maximum depth of valleys and the maximum height of the profile. Mathematically,

$$R_k = \frac{R_v}{R_{max}} \tag{4.5}$$

Where R_v is the maximum depth of the profile below the mean line within the assessment length as shown in the figure where R_{v4} represents the R_v parameter.

4.1.6 Mean Slope of the Profile (Δa)

Mechanical properties such as friction, elastic contact, reflectance, fatigue, crack initiation and lubrication affect this parameter. This parameter can be calculated by calculating all slopes between each two successive points of the profile and then calculating an average of these slopes. Mathematically:

$$\Delta a = \frac{1}{n-1}\sum_{i=1}^{n-1}\frac{\delta_{yi}}{\delta_{xi}} \tag{4.6}$$

Summary of equations used to estimate these parameters have been provided in Table 4.1.

4.2 Experimental Setup

The same test bench as explained in earlier chapters had been used for experimental measurements taken during this work. Each of the 26 teeth of spline couplings under test was subjected to profilometer tests before and after the test. The profilometer gave values of various roughness parameters for a total of nine experiments. The test ran for 10 million cycles under varying conditions of applied torque and misalignment angles. In addition to roughness parameters, the angular clearance between the teeth

before and after the test while ensuring that same teeth are in contact both before and after the test. Angular clearance was then used to measure the fretting wear volume lost during the experiments after measuring the dimensions of wear scar. In this way, it was possible to interpret experimental data with respect to angular clearance and fretting wear volumes. The profilometer used during these tests has been shown taking measurements of roughness parameters in the Figure 4.3.

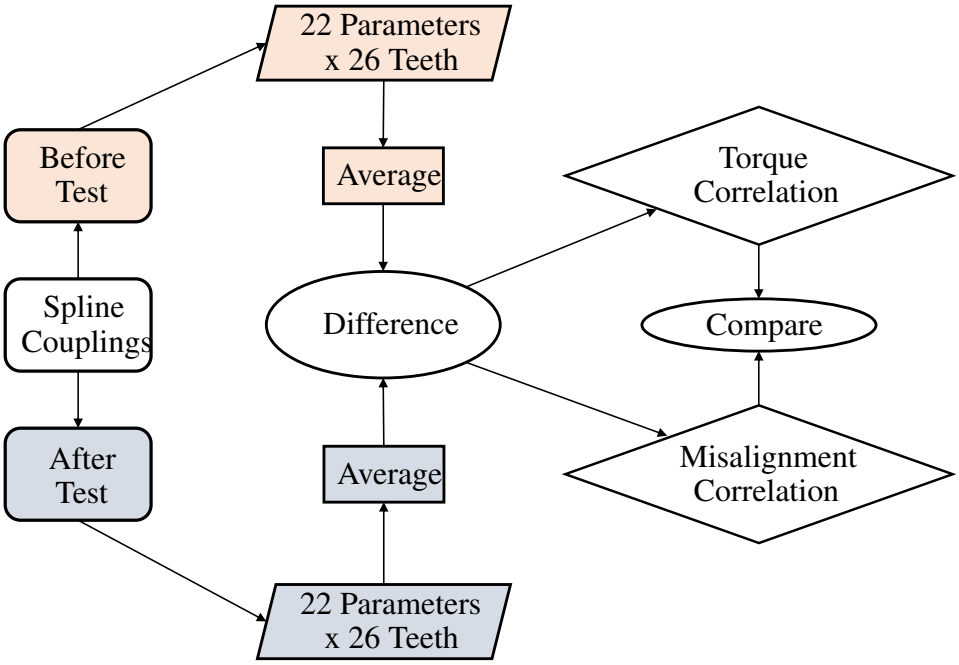

Fig. 4.2 Data analysis

4.3 Data Analysis

After measuring the percentage differences in roughness parameters before and after the experiment, they were plotted against torques and misalignments. There were three different conditions of torques and misalignment angles which gave rise to nine different experiments. The correlation between parameters and torques were found for each of the misalignment angles and the same was done in case of misalignment angles for each of the torques. This resulted in significant reduction in the experimental data and made it easier to interpret and make sense out of data. The algorithm for the analysis of experimental data has been further explained in Figure 4.2.

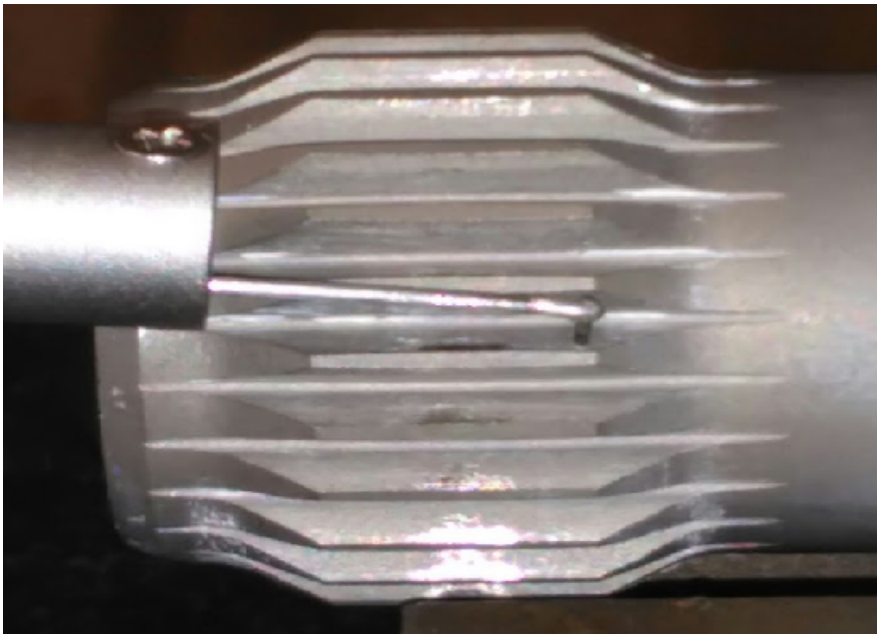

Fig. 4.3 Profilometer taking measurements of roughness parameters

4.4 Results and Discussions

The experimental results have been presented in the Figure 4.4 and Figure 4.5. It appears from the given results that it is still hard to interpret this data and find the underlying relationships between different roughness parameters and operating conditions. However, angular clearance and fretting wear volume can most readily be seen to increase in direct proportion to misalignment angles and torques. All roughness parameters seem to behave slightly differently for different conditions.

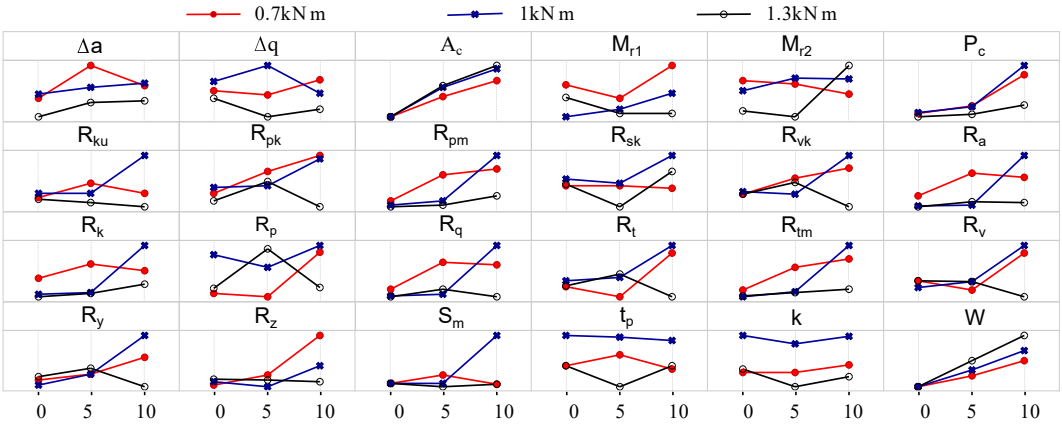

Fig. 4.4 Torque curves versus misalignment angles [6]

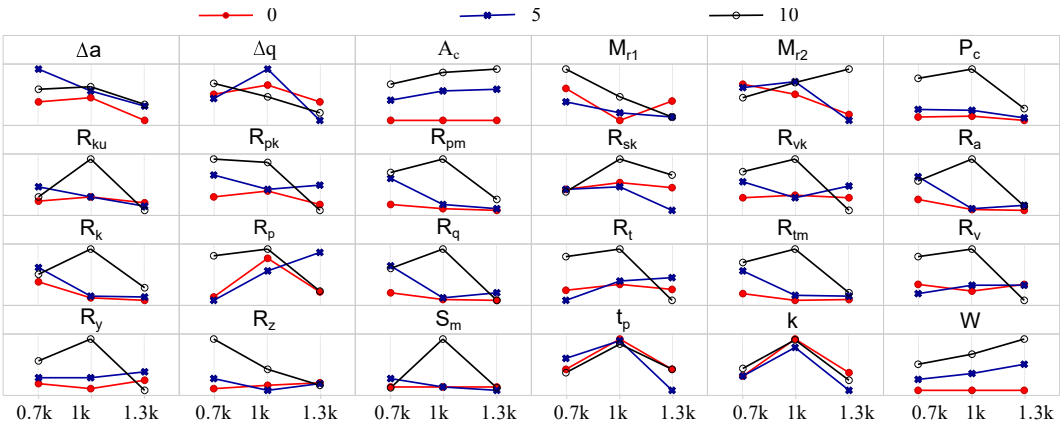

Fig. 4.5 Misalignment curves versus torques [6]

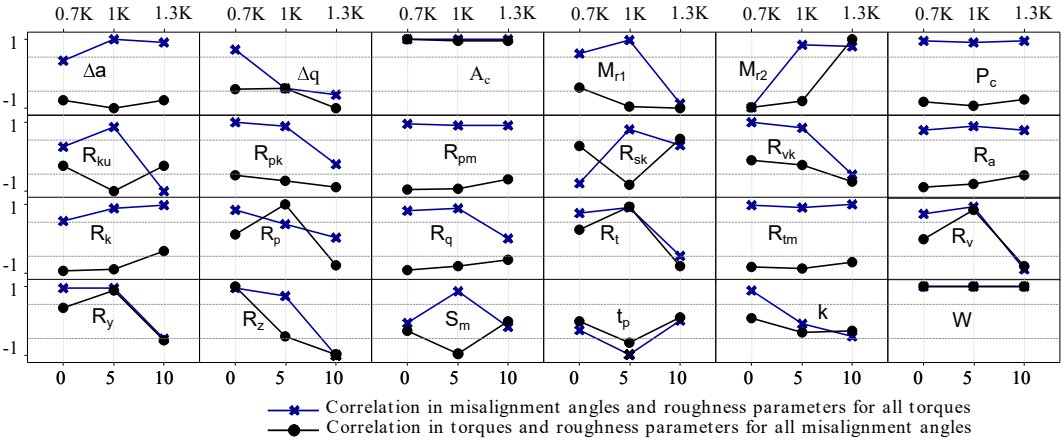

Fig. 4.6 Correlation of roughness parameters with torques and misalignments [6]

4.4.1 Effects of Misalignment

Each of the torques was treated fixed and percentage differences in all the roughness parameters for each of the misalignment angles were plotted. It could be readily observed that only the parameter named peak count P_c could be easily interpreted in terms of changes with respect to misalignment angles and torques.

4.4.2 Effects of Torque

Similarly, in the next step, each of the misalignment angles was treated as constant and the values of percentage changes in the roughness parameters were plotted against corresponding torques. It also gave similar and hard to interpret the results.

4.4.3 Correlation Analysis

Pearson product-moment correlation coefficient [58] has been employed to analyze further. It is used to find the underlying linear relationships between any two parameters of interest. Mathematically:

$$r_{xy} = \frac{\sigma_{xy}}{\sigma_x \sigma_y} \tag{4.7}$$

Where r_{xy} is the correlation coefficient, σ_{xy} is the covariance of x and y, σ_x is the standard deviation of x, σ_y is the standard deviation of y and x, y are the variables of interest. The relation for covariance is provided as:

$$\sigma_{xy} = \sum_{i=1}^{n} \frac{(x_i - \bar{x})(y_i - \bar{y})}{(n-1)} \tag{4.8}$$

Where $\bar{x}$ and $\bar{y}$ are means of x and y respectively, and n is the total number of observations.. The statistical analysis based upon correlation coefficient was carried out. The values of correlation coefficient close to -1 or 1 suggest a strong correlation whereas those close to zero represent a lack of at least a linear relationship thereof. It is pertinent to mention here that correlation should never be confused with causation rather meaningful and physical or experimental validation of the results so obtained is always necessary. It is also important to note that a value of correlation close to zero only confirms the absence of a linear relationship, the non-linear relationships might still be present.

4.4.4 Observations

Thus, it was decided to find correlations of each roughness parameter with misalignment and torques separately as explained earlier. The results of correlations

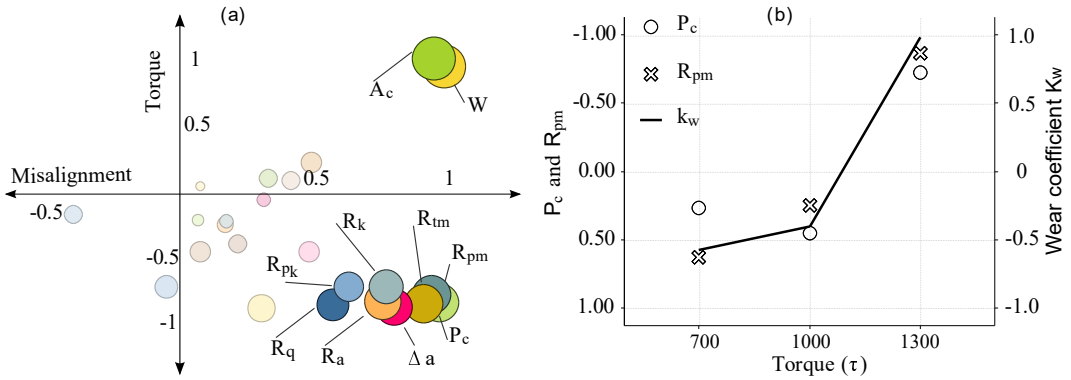

Fig. 4.7 (a) Correlation plot of roughness parameters (b) Archard's wear coefficient and significant parameters [6]

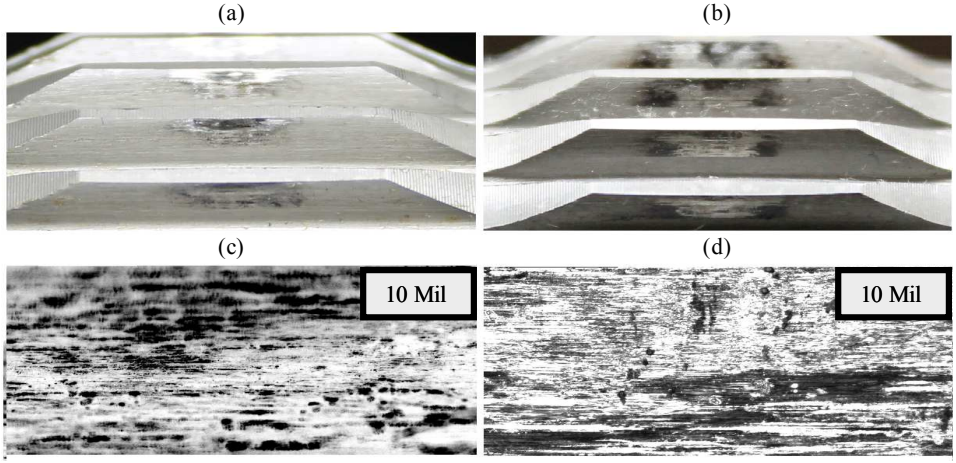

Fig. 4.8 Wear scars (a) 700 Nm and 5′ (b) 700 Nm and 10′ (c) Microscopic view: 700 Nm and 10′ (d) Microscopic view: 1000 Nm and 0′ [6]

with operating conditions has been shown in the Figure 4.6. The observation of the Figure 4.7 reveals the following important observations:

- Very few parameters show a uniform behavior in terms of correlation.
- Even those parameters which show a wide variation do so in a kind of mirroring effect in case of torque and misalignment angles.
- There seems to be a pattern emerging in the way the values of roughness parameters are evolved.
- It is possible to use values of roughness parameters to relate them with the angular clearance of fretting wear volume, which could prove to be a cheap,

robust and effective way for the condition monitoring of spline couplings or other similar mechanical components.

- In the case of angular clearance and fretting wear volume, the initial observation of a uniform and ever increasing behavior with an increase in misalignment angle or torque has been yet again confirmed.

Finally, all the roughness parameters have been plotted on a so called correlation plot and shown in the Figure 4.7 (a). The correlation plot helps visualize the trends and statistical significance more clearly.

4.4.5 Interpretation of Correlation Plot

The variables appearing the farthest from origin represent the most significant parameters statistically, whereas those close to origin represent the least significant ones. As a result, it could be clearly seen that the roughness parameters R_{pm}, P_c and R_{tm} are the most important roughness parameters when it comes to interpreting them with respect to angular clearance A_c and wear volume W. Two of the roughness parameters have been plotted versus changes in normalized wear coefficient K_w and they indeed match with each other, thus confirming that the proposed analysis of roughness parameters may be used for condition monitoring of spline couplings.

This chapter provides few important observations. The roughness parameters may indeed be used as an indicator of safe operational life of spline coupling like mechanical components. Correlation analysis may be used as an effective tool for better interpretation of experimental data in fretting wear experiments. Finally, it also provides the most significant roughness parameters with respect to angular clearance and fretting wear. In future, tools like support vector machines could be used to establish and interpret non-linear relationships too.

4.5 Limitations and Conclusions

One of the limitations of this approach is that even though a correlation has been established in this preliminary work, it does not still confirm existence of a causation. For confirmation of causation more experiments will be required in the future. But

this work does show that there is a high probability of causation between the explored significant roughness parameters because similar trends were observed for a variety of spline couplings under varying operating conditions for different teeth. Another limitation of this approach to assess fretting damage is the fact that it provides only a relative and qualitative measure of fretting damage rather than an accurate estimation. The method presented in the current approach requires the recording of roughness parameters before a spline coupling is put into operation and then repeating the process to find the percentage difference between them after a certain operational period.

One of the advantageous aspects of this work is the fact that different spline couplings put in operation in aero-engines when subjected to the proposed analysis can give very important insight about mechanical and design integrity. It can be used as a maintenance measure for monitoring from an operational point of view. It can also be employed as a measure to compare not only the left over fretting life of different spline couplings,, but also the performance comparison of aero-engines. Over the period of time, when more and more data related to roughness parameters is collected, it would increase the confidence and accuracy in the qualitative estimates of fretting life of spline couplings. This approach, though general is not quantitative, thus it emphasized the need for a more general and preferably an analytical model to predict fretting wear in spline couplings in a more reliable and systematic manner and that is the subject of the next chapter.

Chapter 5

Analytical Modeling of Fretting Wear

This work focused on analytical modeling of fretting wear in gross-slip regime in case of spline couplings. The modeling was based upon the wear energy formulation [24, 26]. Experiments for the purpose of validation of theory were verified to be in the gross-slip regime by the means of extended Mindlin formulation already reported in the subsection 1.4.2. In literature, a finite element simulation and experimental validation of fretting wear has been proposed in [59] for a cylinder on flat configuration. However, it was not suitable for the case at hand, the spline couplings, owing to their complex mechanical configuration. Wear induced by debris formation has been studied under fretting and reciprocating sliding conditions to investigate elastic-plastic shakedown analysis of fretting wear in [60]. Fretting wear behavior of a nuclear fuel rod in the grid-to-rod configuration has been studied experimentally under the primary coolant conditions of a nuclear reactor in [61]. Friction and wear performance of ball bearing sliding against diamond-like carbon coatings has been investigated in [62]. A finite element based method to predict wear in head-stem taper junction of total hip replacements has been proposed in [63] which is automated by a python script linked to Abaqus and the wear patterns have been validated with observations of retrieved prostheses. But in literature there are not many approaches exclusively dedicated to modeling of fretting wear in spline couplings. This chapter tries to bridge that gap.

5.1 Fretting Wear Volume Formulation

The experimental and theoretical considerations have been explained in the Figure 5.1. Let us consider that the pitch radius of the spline coupling is denoted by R_p and the torque acting on the spline coupling by τ. Then, the applied normal force on all the

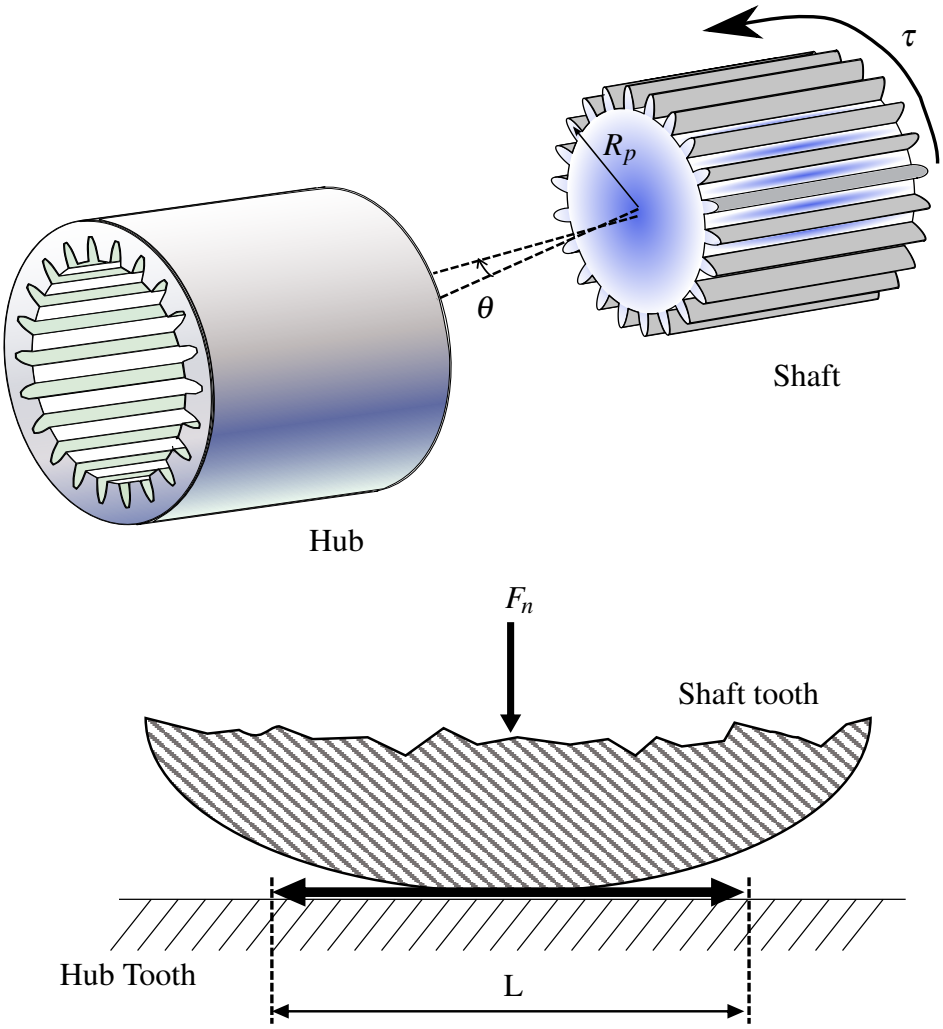

Fig. 5.1 Misalignment and resulting sliding of teeth [1]

teeth (assuming the perfect distribution of load), may be given as:

$$F_n = \frac{\tau}{R_p} \tag{5.1}$$

Let us also consider that there is a misalignment in radians between the hub and the shaft shown with θ in the Figure 5.1 and the total number of teeth is n. Then this

applied force will be distributed among all the teeth in contact and it will act at an angle so the normal force may now be represented as:

$$F_n = \frac{\tau \cos\theta}{nR_p} \tag{5.2}$$

Also, from the study of kinematics of the spline couplings, it has been found that the sliding amplitude as a result of misalignment can be given as:

$$L = R_p\theta \tag{5.3}$$

However, during one revolution, the spline coupling teeth complete two amplitudes of sliding and also it occurs across all the teeth in contact. Therefore, the new expression to represent sliding per revolution may be given as:

$$S = 2nR_p\theta \tag{5.4}$$

Using the above values of F_n and S in the Equation 1.2 and modifying it for N of cycles:

$$V = 2\mu\alpha N\tau\theta\cos\theta \tag{5.5}$$

The above equation clearly shows that the total fretting wear volume is independent of the number of teeth in contact. This makes sense because if the same force is divided over a high number of meshing teeth, it will result in decelerated wear and vice versa.

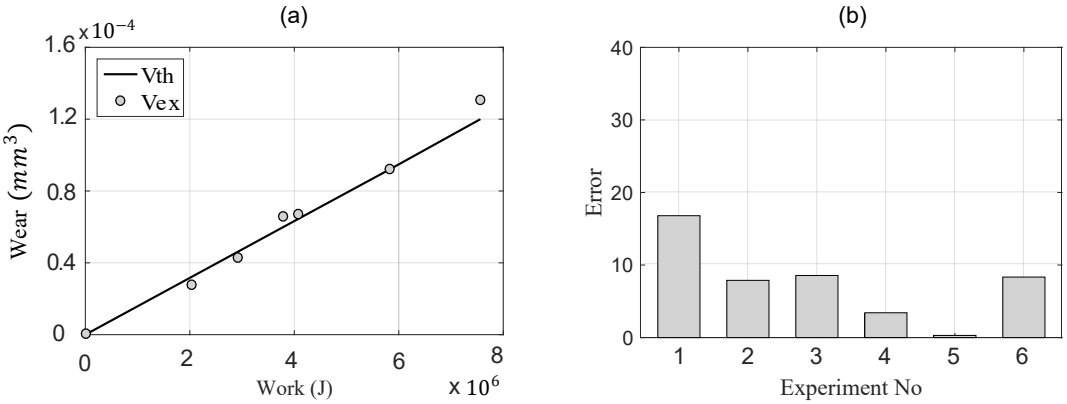

Fig. 5.2 Misalignment and resulting sliding of teeth [1]

5.2 Validation of Wear Volume Formulation

Above theory developed for fretting wear volume has been validated against experimental data obtained from the test bench after several experiments on spline couplings. It was found that the average value of wear energy coefficient α for the given set of tests was 1.58×10^{-19} m^3/J and the value of the coefficient of friction for lubricating conditions was taken to be 0.1. The values of applied torques ranged from 700Nm to 1300Nm and the values of misalignment angle ranged from $0'$ to $10'$. The results of comparison between experimental data and the theoretical predictions have been shown in the Figure 5.2 which are reasonably accurate.

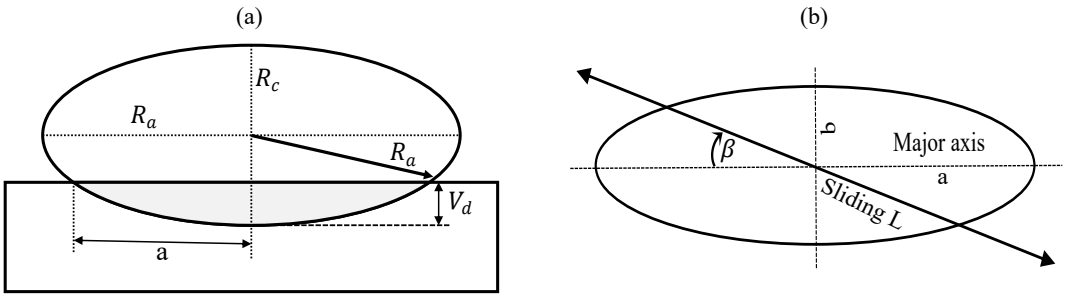

Fig. 5.3 (a) Evolution of wear depth (b) Orientation of sliding [1]

5.3 Fretting Wear Depth Formulation

Even though, the fretting wear volume has been quite accurately modeled in the above section, the designer is always more interested in the evolution of wear depth because that in effect dictates the strength and stiffness of the teeth. Therefore, in this section an analytical methodological approach for the said purpose has been presented. Let us consider an ellipsoid with major and minor radii R_a and R_b respectively sliding over a flat surface. The depth radius of the ellipsoid is denoted with R_c. As it slides, as a result of wear, it loses some of its material and the volume is removed. The situation has been explained in the Figure 5.3. Using the formula for ellipsoidal cap the following relationship may be used to represent the wear volume loss as a function of wear depth V_d.

$$V = \frac{\pi R_a R_b}{3{R_c}^2} V_d^2 (3R_c - V_d) \tag{5.6}$$

Equating the volumes presented in the Equation 1.2 and Equation 5.5:

$$\frac{\pi R_a R_b}{3{R_c}^2} V_d^2 (3R_c - V_d) = \mu \alpha F_n S \tag{5.7}$$

Rearranging the terms to express the relationship in terms of wear depth V_d:

$$3{V_d}^2 R_c - {V_d}^3 = \frac{3\mu\alpha{R_c}^2}{\pi R_a R_b} F_n S \tag{5.8}$$

or

$${V_d}^3 - 3R_c{V_d}^2 + \frac{3\mu\alpha{R_c}^2}{\pi R_a R_b} F_n S = 0 \tag{5.9}$$

The above expression may be used to predict the wear depth volume as a function of number of cycles given the applied torque, misalignment angle, coefficient of friction and wear energy coefficient along with the geometry of sliding ellipsoid. The equation could be expressed in simple terms by treating geometric and tribological properties of the material pair to be constant as:

$${V_d}^3 - 3{V_d}^2 R_c + AN\tau\theta\cos\theta = 0 \tag{5.10}$$

where $A = 6\mu\alpha{R_c}^2/\pi R_a R_b$ is a constant with the same units as the wear energy coefficient. If both pin and flat surface are made up of the same material then their fretting wear volumes would be the same, but the evolution of wear depth on the flat surface will be much slower because the point of contact will continuously keep on changing. Also, the width of wear track will depend upon the contact radii a and b and their orientation of sliding β. The length of wear track will be exactly equal to the sliding amplitude L. Therefore, equating the wear volumes of both surfaces, denoting the wear depth of sliding pin with V_{d1}, wear depth of stationary surface with V_{d2} and using geometric considerations:

$$\frac{\pi R_a R_b}{3{R_c}^2} V_{d1}^2 (3R_c - V_{d1}) = L V_{d2} \frac{2ab}{\sqrt{a^2 \sin\beta^2 + b^2 \cos\beta^2}} \tag{5.11}$$

where the contact radii a and b may also be represented in terms of wear depth on the pin as:

$$a = \frac{R_a}{R_c}\sqrt{2R_c V_{d1} - {V_{d1}}^2} \tag{5.12}$$

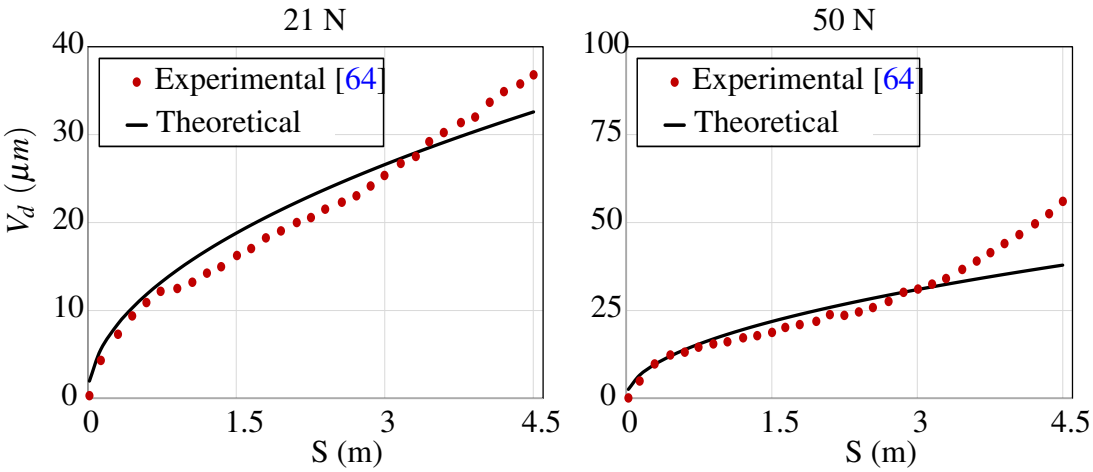

Fig. 5.4 Wear depth: Experimental validation

and

$$b = \frac{R_b}{R_c}\sqrt{2R_cV_{d1} - {V_{d1}}^2} \tag{5.13}$$

Putting the values of a and b and simplifying:

$$\frac{\pi}{3}V_{d1}^2(3R_c - V_{d1}) = 2LV_{d2}\sqrt{\frac{2R_cV_{d1} - {V_{d1}}^2}{{R_a}^2\sin\beta^2 + {R_b}^2\cos\beta^2}} \tag{5.14}$$

Finally:

$$V_{d2} = \frac{\pi V_{d1}^2(3R_c - V_{d1})}{6L}\sqrt{\frac{{R_a}^2\sin\beta^2 + {R_b}^2\cos\beta^2}{2R_cV_{d1} - {V_{d1}}^2}} \tag{5.15}$$

The above relationship shows that the evolution of wear track geometry on the flat surface depends upon the angle of sliding, principal radii of the slider and the evolution of wear depth on the sliding surface.

5.4 Validation of Wear Depth Formulation

For the purpose of validation, the equation for fretting wear depth evolution has been translated for a simple case of ellipsoidal pin-on-disk apparatus as:

$${V_d}^3 - 3{V_d}^2R_c + 3\mu\alpha F_nS\frac{{R_c}^2}{\pi R_aR_b} = 0 \tag{5.16}$$

The theory developed here was then validated against a past experimental work [64] in which real time recording of wear depth took place as the test progressed. The experimental specifications used during simulations were a radius of 5 mm of the spherical pin, a sliding distance of 4.5 m, wear coefficient $k = \mu\alpha$ as 1.76×10^{-13} Pa^{-1} for 21 N and 10^{-13} Pa^{-1} for 50 N. The slight difference in experimental and theoretical trends could be attributed to changes in the value of the coefficient of friction as reported in the reference [64] as well. As may be observed from the Figure 5.4, the theoretical predictions match quite well with the experimentally recorded values of wear depth as the sliding distance increases. Also, the theory was originally developed for a general ellipsoidal shape of pin but it has been validated for a spherical pin on the disk case too. Hence, the theory developed may be trusted for prediction of wear in case of mechanical components like spline couplings which have different radii of curvature.

Table 5.1 Comparison of simulated wear with experiments [1]

τ Nm	θ $'$	V_w (theory) $mm^3 \times 10^{-5}$	V_w (experimental) $mm^3 \times 10^{-5}$	Error Percent
700	5	2.75	2.76	0.19
700	10	6.75	6.66	1.36
1000	5	4.25	4.26	0.21
1000	10	9.27	9.17	1.09
1300	5	6.52	6.54	0.20
1300	10	13.0	13.0	0.29

5.5 Application to Spline Couplings

Finally, the theory was applied to the case at hand, spline couplings. During the experiments, it was observed that the applied torque was operating in open loop. It meant that as the wear progressed, the applied torque reduced. Thus, it necessitated the use of modified values of applied torque during the test. As a result, empirical relations were derived for estimation of force or torque during the test which has been provided below:

$$F_n' = F_n - p_1 V_d^3 + p_2 V_d^2 - p_3 V_d \tag{5.17}$$

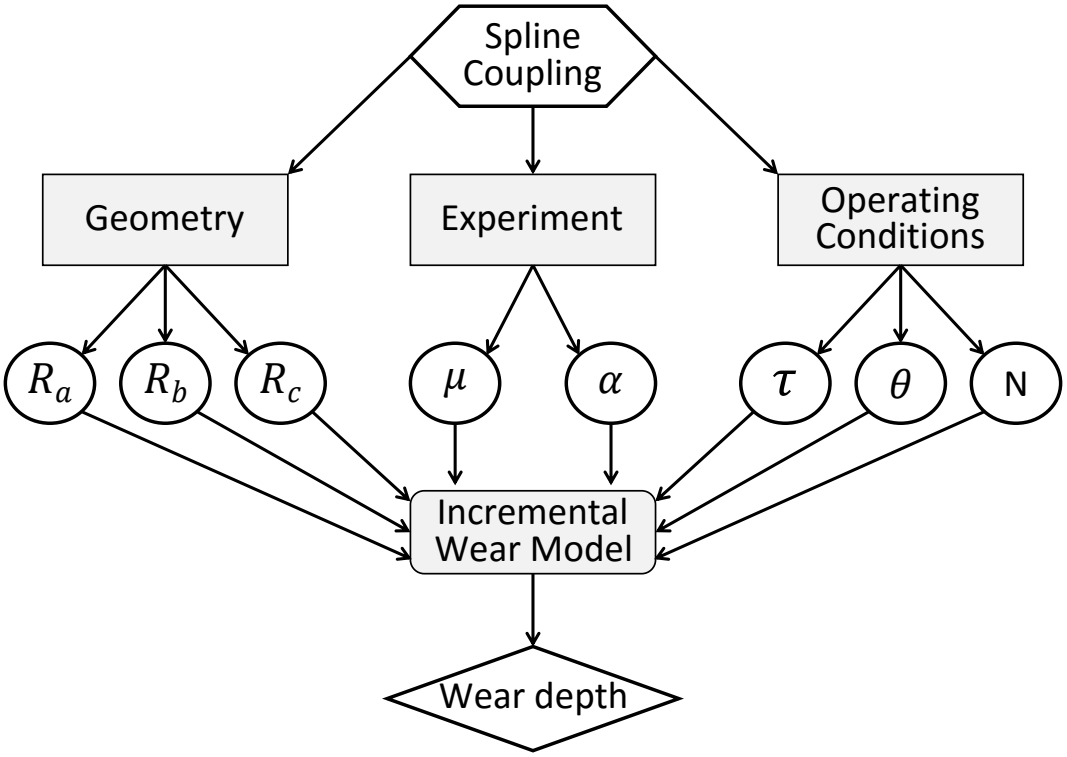

Fig. 5.5 Algorithm for using the theory of incremental wear formulation [1]

where F_n' was the force at each iteration of wear, $p_1 = 3.386 \times 10^{22}\ N/m^3$, $p_2 = 1.444 \times 10^{16}\ N/m^2$ and $p_3 = 2.101 \times 10^9\ N/m$. Similarly, the coefficient of friction was observed to vary during the tests which has been empirically related to applied and test conditions as follows:

$$\mu = A\theta + B \tag{5.18}$$

The values of coefficients A and B can be calculated as:

$$A = u_1\tau^2 + u_2\tau + u_3$$

$$B = v_1\tau^2 + v_2$$

Where $u_1 = 4.254 \times 10^{-9}\ min^{-1}(Nm)^{-2}$, $u_2 = -1.488 \times 10^{-5}\ min^{-1}\ (Nm)^{-1}$, $u_3 = 0.0121\ min^{-1}$, $v_1 = 3.668 \times 10^{-8}\ (Nm)^{-2}$ and $v_2 = 0.05325$. In the above expression θ is taken in minutes. After applying above relations and experimental conditions of spline couplings, the summary of results and their comparison with experimental values has been provided in the Table 5.1. The reason for more accurate results presented in the Table 5.1 as compared to those in experimental validation of the-

ory given in the Figure 5.4 is that force and coefficient of friction of have been experimentally fitted in the former. But even without those empirical relations, the approach has already been shown to provide predictions with reasonable accuracy. In the real scenario, the force or torque will be provided in the closed loop, thus there would not be a need to fit applied torques or normal forces with evolution of wear depth. Similarly, if there are not many changes in the applied and surface conditions, relationships for the evolution of coefficient of friction might not be required either. It will also be useful to summarize the methodology of the whole process in a clear sequence of events shown in the Figure 5.5.

The work presented in this chapter provides a methodological framework for the prediction of fretting wear in mechanical components like spline couplings. It is also applicable to other similar scenarios. So this approach can be quite useful in the modeling of fretting wear in a variety of scenarios using a single formulation which makes this approach quite attractive and promising for future applications. And the same approach was used to formulate and extend it in certain other applications as will be shown in the next chapter.

Chapter 6

Wear Endurance Work

6.1 Introduction

Classically, there are Wohler SN curves [65] available for predicting the fatigue life of different materials in terms of the applied stress and number of cycles which the material can withstand in a cyclic loading condition. Ideally, we would like to have similar curves for different materials or geometries in case of fretting wear, but not many such data or formulations are currently available. A very promising and interesting closely matching approach was proposed in the [66] which presented a term "critical energy density" with special focus on the durability of coatings. It was defined as: "The amount of energy which needs to be delivered to contact area in order to perforate the coating". Here we present a new concept to estimate the life of a spline coupling in terms of its coating life. It is assumed that the material will be considered to be more prone to failures only after its coating has been completely removed from the contact area.

However, in the case of sliding Hertzian contacts, it posed certain challenges. The first challenge was the presence of a varying contact area which results in different stress after each fretting cycle and thus changes in the wear depth rate. The second challenge was that it did not strictly depend upon tribological properties alone, but rather also on the geometry of the components. Therefore a new concept named **"Wear Endurance Work" (WEW)** has been proposed which may be defined as: **"It is the amount of work per unit volume (of the component with coating) required to completely perforate the coating"**. This Wear Endurance Work w_e

has then been related analytically to several tribological and geometric properties of the components to make a prediction of their safe operational life. Basically, this approach gives rise to critical energy per unit volume instead of a critical number of cycles in the case of SN Wohler curves. However, once the critical energy is known, it is quite direct to find number of cycles given the applied load and sliding amplitude thus making the approach pretty general and more widely applicable.

In the forthcoming sections, a detailed and step by step explanation of the extended derivation based upon the formulation presented in chapter 5 will be provided. The preliminary results will also be provided. The potential of the proposed technique will be discussed in detail and its usefulness along with applicability will be elaborated.

6.2 Formulation of WEW

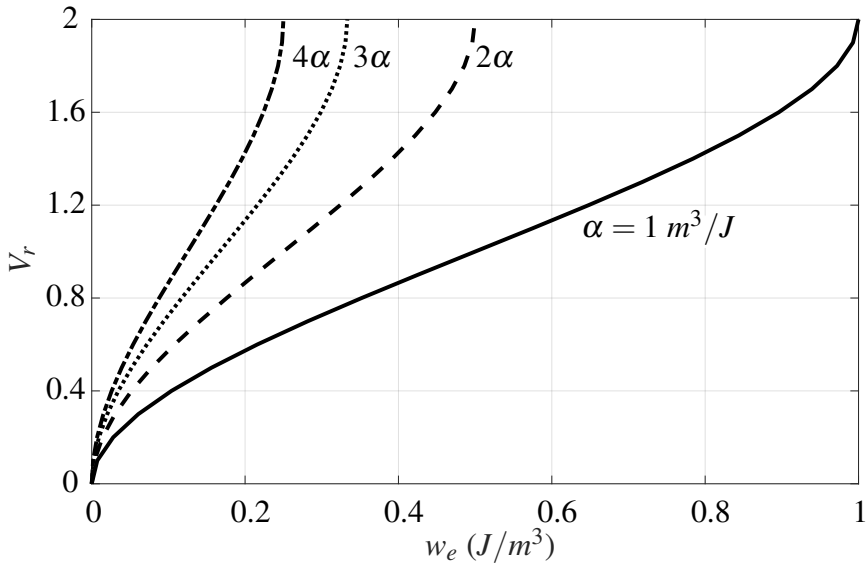

Fig. 6.1 Wear endurance work versus thickness ratio for a general case

We will begin by considering an ellipsoid with radii of curvature as R_a, R_b and R_c. The Equation 5.9 may be rewritten after treating $W = \mu F_n S$ to be the frictional work as:

$$V_d{}^3 - 3R_c V_d{}^2 + \frac{3\alpha R_c{}^2}{\pi R_a R_b} W = 0 \tag{6.1}$$

Dividing the above equation by ${R_c}^3$ and taking $V_d/R_c = V_r$ as the wear depth ratio, $V_e = 4\pi R_a R_b R_c/3$ as the volume of the ellipsoid:

$$ {V_r}^3 - 3{V_r}^2 + \frac{4\alpha W}{V_e} = 0 \tag{6.2} $$

or

$$ {V_r}^3 - 3{V_r}^2 + 4\alpha w_e = 0 \tag{6.3} $$

where $w_e = W/V_e$, the wear endurance work done per unit volume of the ellipsoid. The above equation may be rewritten as:

$$ w_e = \frac{3{V_r}^2 - {V_r}^3}{4\alpha} \tag{6.4} $$

Now any value of V_r could be chosen as the 'critical value' of wear depth to R_c ratio depending upon the particular application and design requirements. The maximum value of V_r could be 2 if whole ellipsoid were worn. Hence, using the range from 0 to 2 and by treating α to be 1, a very good insight of the 'Wear Endurance Work' could be obtained as shown in the Figure 6.1.

6.3 WEW Formulation for Thickness

Let us now consider that the ellipsoid has been provided with a protective layer of coating with thickness t as shown in the Figure 6.2. This will result in new radii of curvature as follows:

$$ R'_a = R_a + t, R'_b = R_b + t, R'_b = R_c + t $$

Using the formulae for wear depth developed in the previous chapter:

$$ {V_d}^3 - 3R'_c{V_d}^2 + \frac{3\mu\alpha{R'_c}^2}{\pi R'_a R'_b} F_n S = 0 \tag{6.5} $$

or

$$ {V_d}^3 - 3(Rc + t){V_d}^2 + \frac{3\mu\alpha(R_c + t)^2}{\pi(R_a + t)(R_b + t)} F_n S = 0 \tag{6.6} $$

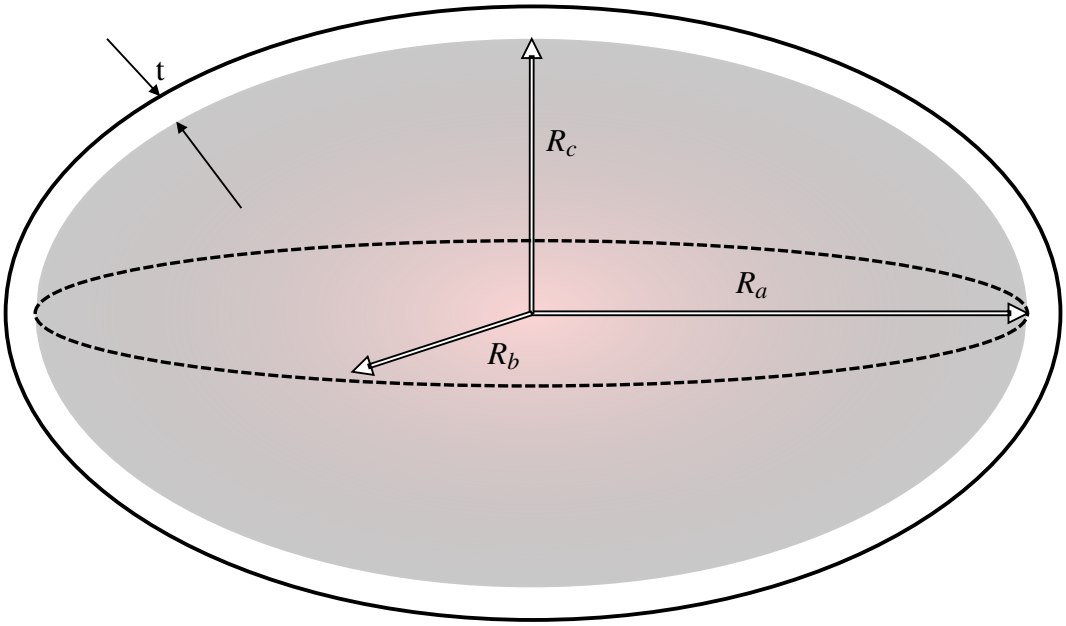

Fig. 6.2 An ellipsoid with protective thickness

Rearranging and assuming $t/R_a = T_a$, $t/R_b = T_b$ and $t/R_c = T_c$:

$$V_d{}^3 - 3Rc(1+T_c)V_d{}^2 + \frac{3\mu\alpha R_c{}^2(1+T_c)^2}{\pi R_a R_b(1+T_a)(1+T_b)}F_nS = 0 \tag{6.7}$$

Dividing the above equation by $R_c{}^3$ and taking $V_d/R_c = V_r$:

$$V_r{}^3 - 3(1+T_c)V_r{}^2 + \frac{3\mu\alpha(1+T_c)^2}{\pi R_a R_b R_c(1+T_a)(1+T_b)}F_nS = 0 \tag{6.8}$$

or

$$V_r{}^3 - 3(1+T_c)V_r{}^2 + \frac{4\mu\alpha(1+T_c)^2}{V_e(1+T_a)(1+T_b)}F_nS = 0 \tag{6.9}$$

Where $V_e = 4\pi R_a R_b R_c/3$ is the volume of an ellipsoid on which coating of thickness t has been added. Also the terms $\mu F_n S$ represents the frictional work done W. Therefore:

$$V_r{}^3 - 3(1+T_c)V_r{}^2 + \frac{4\alpha(1+T_c)^2}{V_e(1+T_a)(1+T_b)}W = 0 \tag{6.10}$$

The term W/V_e represents the proposed parameter WEW the frictional work done per unit volume of the ellipsoid denoted by w_e. Hence:

$$V_r{}^3 - 3(1+T_c)V_r{}^2 + \frac{4\alpha(1+T_c)^2}{(1+T_a)(1+T_b)}w_e = 0 \tag{6.11}$$

Hence wear endurance work is given as:

$$w_e = \frac{V_r{}^2(3+3T_c - Vr)(1+T_a)(1+T_b)}{4\alpha(1+T_c)^2} \tag{6.12}$$

The substrate of coating is reached when $V_r = T_c$. Therefore:

$$w_e = \frac{T_c{}^2(3+2T_c)(1+T_a)(1+T_b)}{4\alpha(1+T_c)^2} \tag{6.13}$$

6.4 WEW for an Ellipsoid With Coating

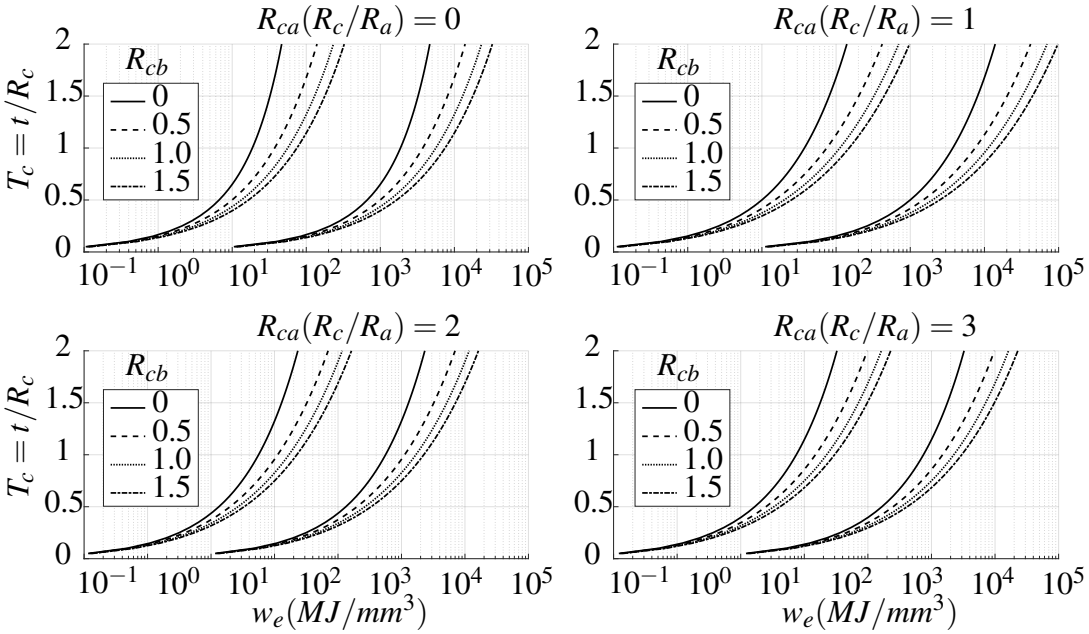

Fig. 6.3 Wear endurance work per unit volume: Left hand set of trends are a result of higher wear energy coefficient and vice versa

In the same manner, different scenarios for an ellipsoid instead of a sphere may be realized after necessary modifications in representation of mathematical model

become possible. For the said purpose, the Equation 6.13 may be rewritten after considering $R_{ca} = R_c/R_a$ and $R_{cb} = R_c/R_b$ as:

$$w_e = \frac{{T_c}^2(3+2T_c)(1+T_cR_{ca})(1+T_cR_{cb})}{4\alpha(1+T_c)^2} \tag{6.14}$$

The results of this transformation have been summarized in Figure 6.3. The four trends at the left hand side represent higher wear energy coefficient whereas those on the right hand side represent lower values of wear energy coefficient. The most useful characteristic of the WEW is the capability to introduce any criterion as the critical value of wear cycles. It could be the thickness of coating, plain wear depth evolution up to a certain value without any coating, combination with some factor of safety and so on. Thus, this approach is a compact and comprehensive representation of geometric and tribological properties of various combinations of materials.

6.5 WEW for a Sphere With Coating

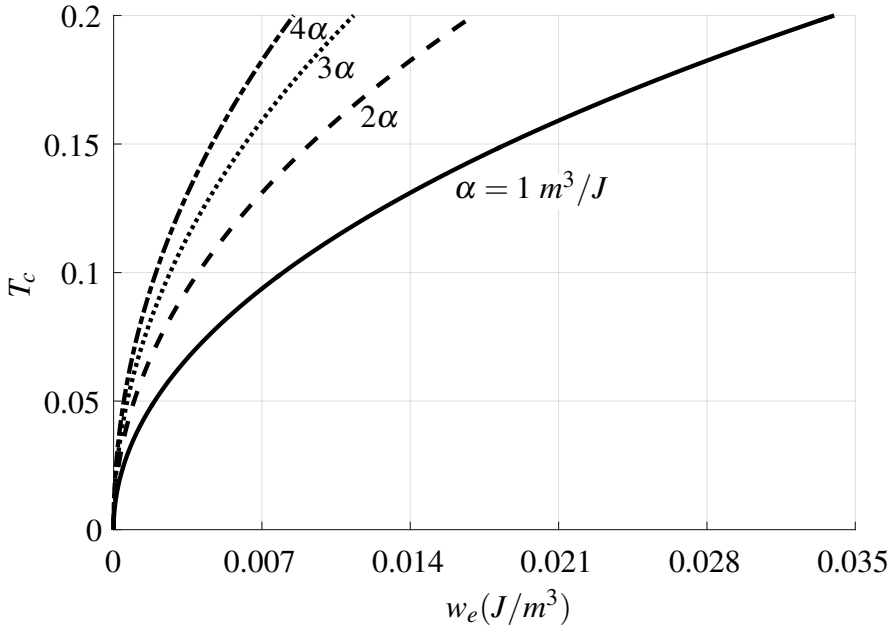

Fig. 6.4 Sphere: Wear endurance work versus coating thickness ratio $T_c = t/R_c$

Now, it may be clearly seen from the above equation that wear endurance work depends upon wear energy coefficient and the ratios of thickness with the radii of principal curvature of the ellipsoid on which protective coating is to be added.

Let us consider that the ellipsoid under-consideration is a special case in which $R_a = R_b = R_c$ thus making it a sphere in effect. Then, the expression for WEW will be reduced to:

$$w_e = \frac{{T_c}^2(3+2T_c)}{4\alpha} \tag{6.15}$$

Finally the Figure 6.4 shows the relationship between thickness ratio and wear endurance work for several wear energy coefficients. This confirms the suitability of the proposed approach with regards to wear endurance of coating unless the substrate is reached for any spherical shaped component in the sliding Hertzian contact configuration. This can be of great help for designers in the design stage of mechanical components like spline couplings. Representing the wear endurance work in such forms also makes it possible to readily compare performance of various materials with different tribological properties represented by wear energy coefficient α. Also, since the wear work per unit volume instead of number of cycles to reach substrate has been been presented, this allows to take into account different combinations of coefficients of friction, applied normal forces and sliding displacements. As a result, it becomes readily possible to compare different designs and materials in a straightforward manner.

This chapter provided a novel concept called "Wear Endurance Work" which provides a unified framework for comparison and analysis of experiments conducted under various geometrical, tribological and material pair conditions. The approach has a potential to be used as a benchmark / standard for comparison and decision making during the design process. ***If the sliding amplitude is assumed to be L, it is quite straightforward to find total number of cycles N for any given coefficient of friction and geometry for a range of applied forces as:*** $N = w_e V_e/(\mu F_n L)$***. Then, a plot between applied force and corresponding number of cycles will be analogous to classic Wohler SN curves but for Wear instead of fatigue***.

Currently, work is underway to refine and validate this approach even further for more design and tribological scenarios. During the validation of various fretting wear scenarios, it was observed that frequency also plays an important role in the process. This is why a preliminary study on the effects of frequency has also been carried out which has been presented in the next chapter. An inclusion of frequency effects into the analytical model would make this approach even more general and will form an important part of the future work.

Chapter 7

Frequency Dependence of Fretting

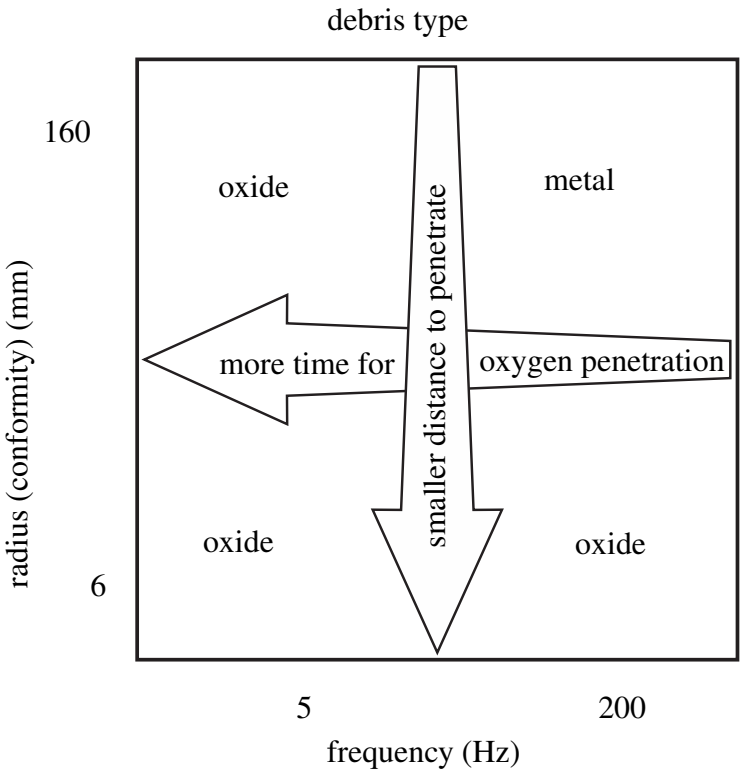

Fig. 7.1 Phenomenological fretting debris map [7]

It makes sense to consider that frequency might be a significant factor in fretting. The rationale for this consideration is the fact that fretting is itself a result of cyclic loading with small sliding amplitudes. Under higher frequencies, the material could be considered to have less time to stabilize itself from the effects of thermal and

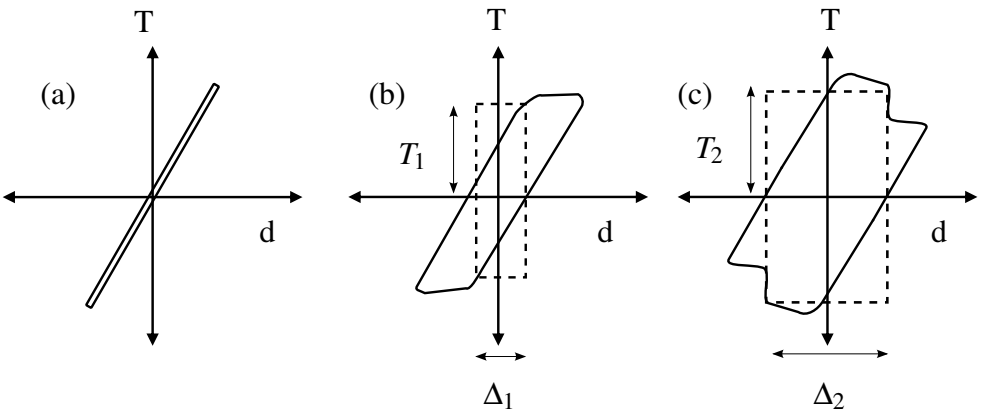

Fig. 7.2 Fretting loops and wear regimes. T represents the friction force. Δ_1 is the amplitude for the incipient partial slip. Δ_2 is the amplitude for the incipient gross slip. T_1 and T_2 are corresponding amplitudes of frictional force respectively: (a) Stick (b) Stick-slip (c) Gross-slip [8]

mechanical loading which might in turn affect the fretting life of the component. And indeed, this aspect has been addressed by some past works. For example, a preliminary study of the effects of frequency on fretting was conducted in [67]. The important observational conclusions of this work were that fretting fatigue is accelerated under high frequency in partial slip conditions and fretting wear is accelerated under high frequency in gross-slip conditions. They considered the frequency range of 10 to 20000 Hertz and for two materials, namely; low carbon steel and austenitic stainless steel. In this work, the experimental setup ensured rectilinear reciprocating motion, whereas the current work focused on investigation of frequency effects when the sliding was fretting but followed an arc instead of a straight linear pattern. Another constraint of the current work was no provision of high frequency in the test setup. Hence, it would require more detailed experimentation to make reliable conclusions.

A recent study [7] concluded that actually frequency in conjunction with contact geometry influences the fretting wear. They observed that frequency dictates the time the nascent metal surfaces (produced as a result of fretting wear) gets to interact with oxygen, which in turn controls the oxidation of the surface and significantly influences the fretting life of the component. The work concluded by presenting a so called phenomenological debris type fretting map which identified the type of debris as a function of contact geometry (conformity) and fretting frequency. The map is shown in the Figure 7.1. In the reference [68], a piezoelectric fretting device

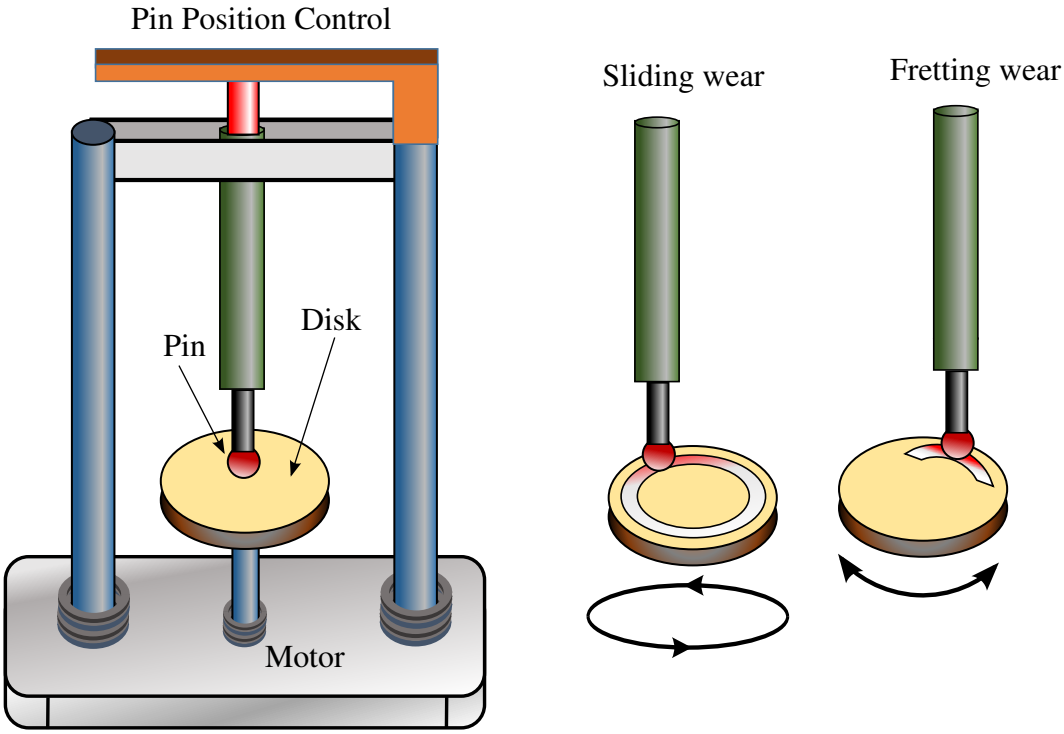

Fig. 7.3 Schematic of the test bench and modification for fretting wear

has been proposed to study the influence of frequency on fretting release and release rates using a high accuracy radiotracer technique. The authors also note quite rightly, that the literature on the relationship between fretting frequency and fretting wear has been rare.

The results presented in this chapter are very preliminary. They lack experimental and theoretical rigor. However, they have been included because they have significant potential for better understanding of fretting as will be explained later. This chapter could in effect be considered for further extension in future work. In addition to theoretical method of Mindlin's theory, different fretting regimes may also be identified by experimental means. For that purpose, fretting maps are recorded and plotted from experiments. The changes in frictional force with respect to sliding position are plotted for a complete fretting loop. The shape and area enclosed by the loop provide information about the regime. A typical classification of wear regimes based upon the characteristic fretting loops has been provided in the Figure 7.2.

Based upon the experience and observations, it was postulated that the frequency should affect the fretting behavior of the materials under consideration. There were

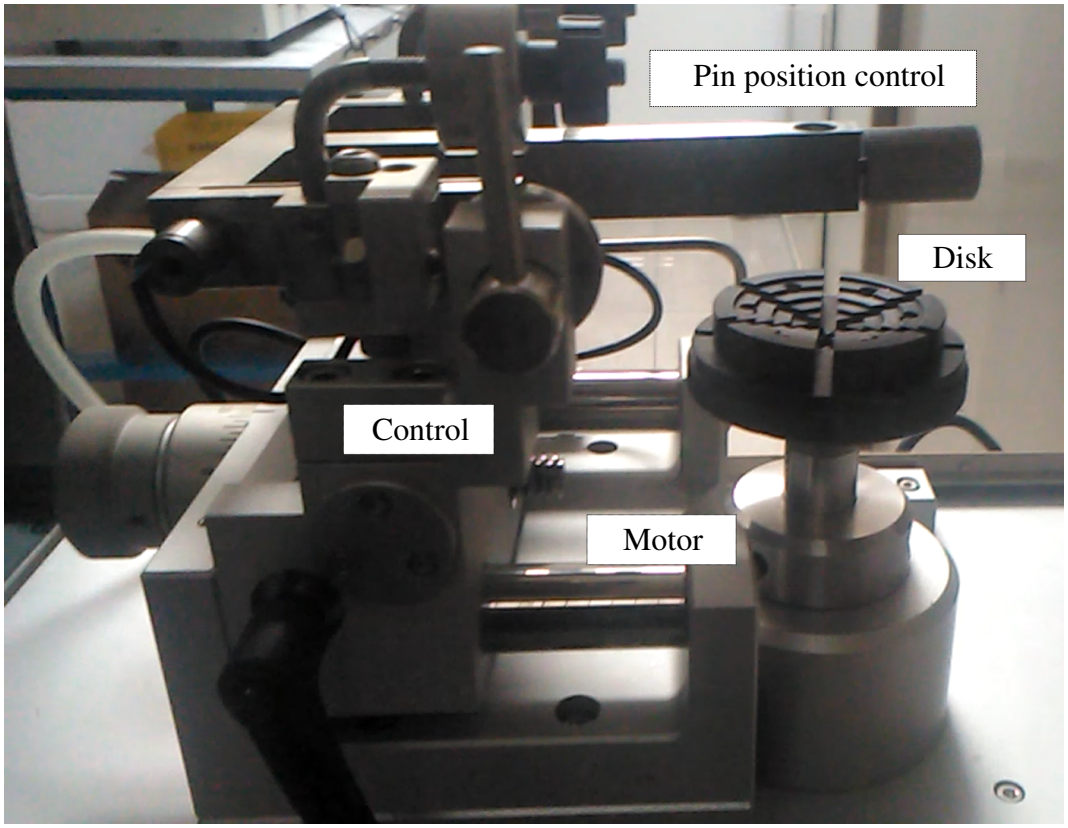

Fig. 7.4 Wear test bench used in the experiments

two factors responsible for this postulate. One, whenever the disk rotates, it increases the temperature of the contacting surfaces. Two, the rotation of disk also results in a strain on the contact area. If fretting oscillations are applied at a certain frequency, the frequency is expected to affect the way temperature and strain is induced in the contacting surfaces which in turn will affect the tribological and material properties of the fretting pair. With this aim in mind, this preliminary study started to investigate the influence of frequency on fretting.

7.1 Experimental Setup

A conventional and standard pin-on-disk bench has been utilized in this work to study the effects of frequency over fretting. Classically, such a test bench is used for sliding wear tests. However, during the present work, it was slightly modified in an effort to replicate fretting conditions as closely as possible. The proposed

Table 7.1 Experimental conditions for fretting-frequency tests

Time (mins)	Frequency (Hz)	Fretting Amplitude (mm)	Normal Force (N)
5	6	100	40
5	6	150	40
5	10	100	40
5	10	150	40
10	6	100	40
10	6	150	40
10	10	100	40
10	10	150	40
15	6	100	40
15	6	150	40
15	10	100	40
15	10	150	40

modification in the working has been explained in the Figure 7.3. By moving the pin using the position control mechanism, different velocities may be realized for the same rotational frequency. The pin stays fixed, but the disk is rotated by the driving motor. Conventionally, this setup is used for tests on sliding wear in which the disk makes complete revolutions at the specified speed. However, this standard operation has been modified in the current test. Both cases of sliding wear as well as fretting wear after modification have been shown. In case of fretting wear configuration, the disk rotates in opposite directions followed by each other. This helps in producing fretting like conditions. But, the test bench was capable of a maximum frequency of 10 Hz in the case of fretting conditions. This severely limited the testing range. Nevertheless, it still provided some interesting results with regard to dependence of frequency on fretting. Both pin and disk were made up of steel. The size, geometry and material of contacting surfaces were not changed in any of the experiments. The force was also kept constant which was 40N and provided by the means of a dead weight. Only variables in the experiment were frequency, test duration and sliding amplitude. The position of pin with respect to disk, coefficient of friction, normal force, frictional force and the total siding displacement were recorded in real time to compare the results later on. The full details of experimental conditions have been provided in the Table 7.1.

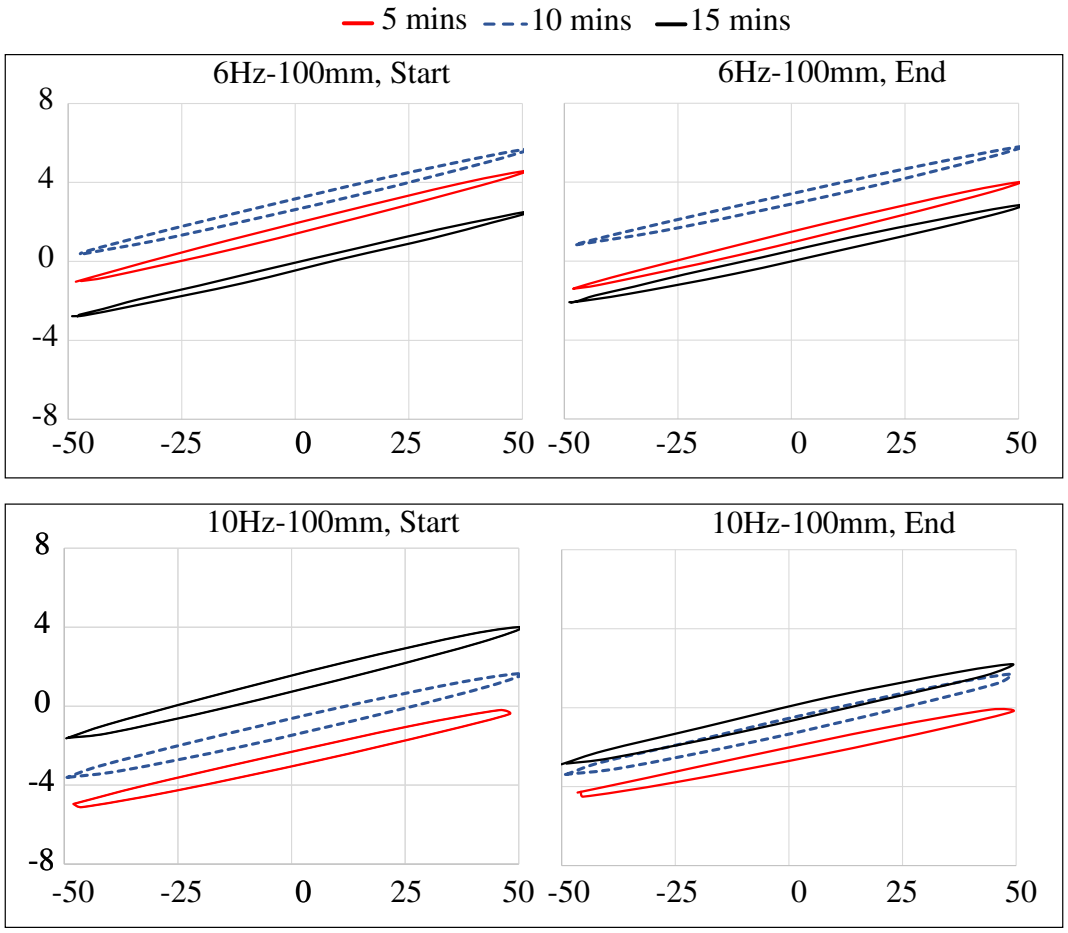

Fig. 7.5 Comparison of effects of frequency and time: X-axis represents the position (mm) and Y-axis shows the frictional force (N)

7.2 Results and Discussions

For comparison purposes, fretting loops from the first and the last minute were plotted from the time durations of 5 minutes, 10 minutes and 15 minutes. The reason for this particular selection was to take into account effects owing to increase in temperature if any. The tests were conducted at room temperature and exposed to the room environment. There was no lubricant or temperature control mechanism in place. It was decided to study the fretting loops at the beginning and the end of an experiment to study the effects of fretting amplitude and frequency on fretting loops or in other words the frictional force. The Figure 7.5 shows the fretting loops for the fretting amplitude of 100mm. The variations in fretting loops could be observed in the following cases:

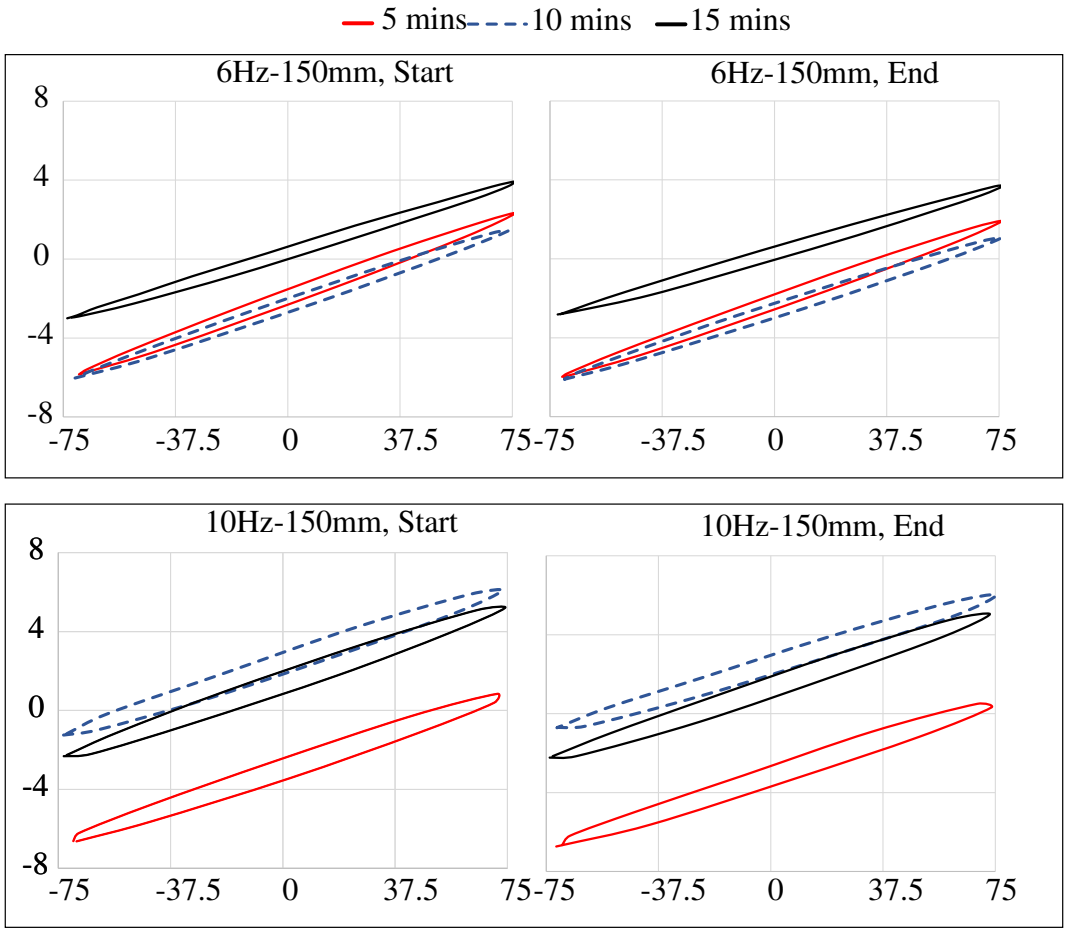

Fig. 7.6 Comparison of the effects of frequency and time: X-axis represents the position (mm) and Y-axis shows the frictional force (N)

- 6 Hertz, 100 mm for the test of duration at 15 minutes shown with black loop in upper two figures of Figure 7.5.
- There were small variations in other two cases as well, but were not so significant
- 10 Hertz, 100 mm, a significant variation could be observed for the test of 15 minutes in lower two figures of the Figure 7.5.
- There was a variation in the test of 5 minutes as well, but surprisingly there was none for 10 minutes.

Similar observations were made on the experimental data where fretting amplitude was 150mm as shown in the Figure 7.6. In this case, there were no significant

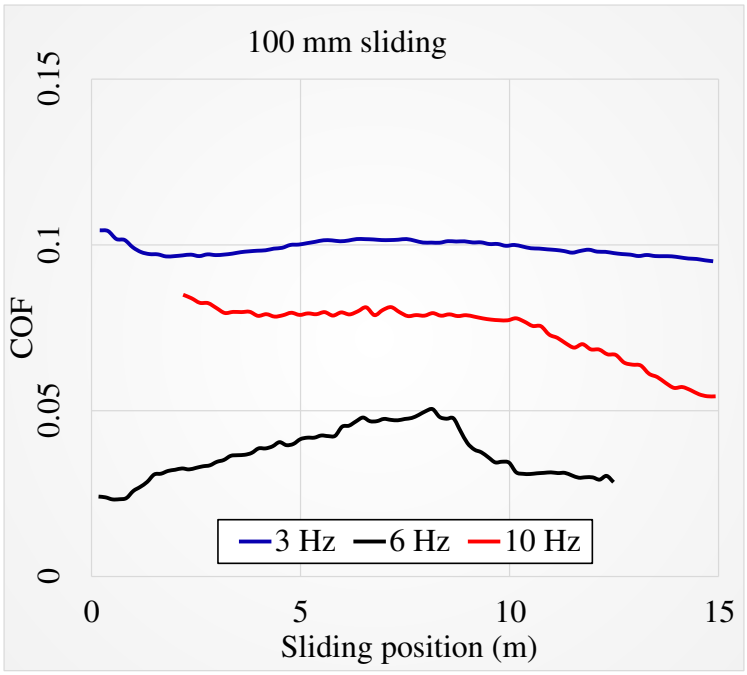

Fig. 7.7 Comparison of the effects of frequency and time: X-axis represents the position (mm) and Y-axis shows the frictional force (N)

variations observed except for the test of 10 minutes duration shown in blue dotted line which was not very pronounced either. From the above observations, it may be seen that when the fretting amplitude is higher for the same frequency, the material pair gets more time to stabilize itself both thermally as well as mechanically which results in almost uniform fretting or tribological behavior regardless of the length of the test for the given duration. On the other hand, when fretting amplitude is less and frequency is higher, it produces more significant variations in fretting loops. The physical reasons for changes in the mean value of friction force are as follows (It is worth noting that the test bench was not primarily designed for fretting tests):

- Across various tests, the higher applied frequencies gave little time to material to stabilize itself thermally and vice versa
- During the same test, the elliptical shape of fretting loops signifies that it is in the mixed stick-slip regime and the coefficient of friction changes its values because the sliding surface first comes at rest thus static coefficient of friction comes at play whereas once it gets in to motion, the dynamic coefficient of friction becomes significant [69]

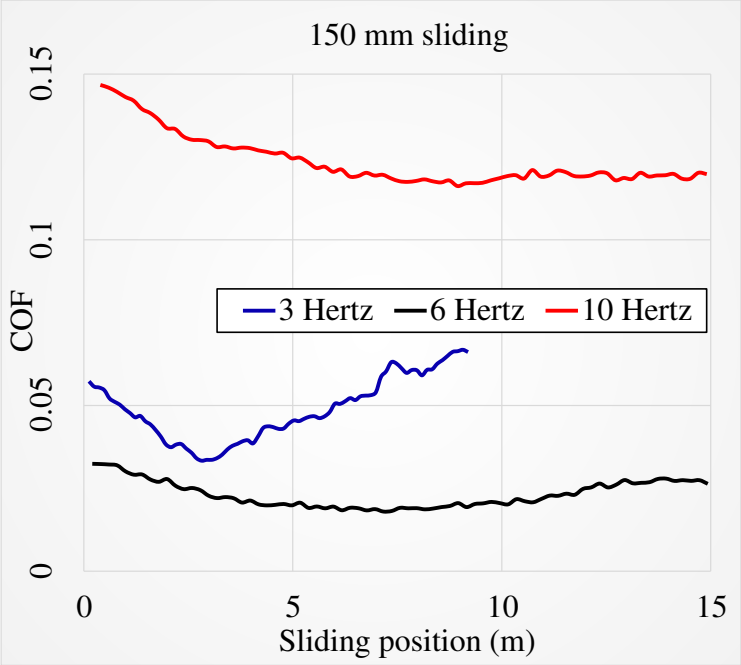

Fig. 7.8 Comparison of the effects of frequency and time: X-axis represents the position (mm) and Y-axis shows the frictional force (N)

For the sake of completeness, the variations in the coefficient of friction as the tests progressed under various operating conditions, have also been provided in the Figure 7.7 and Figure 7.8 for a sliding of 100 and 150 mm respectively. As may be seen that for 100mm sliding amplitude:

- The coefficient of friction for an applied frequency of 3 Hertz almost stays constant.
- It increases and then decreases for a fretting frequency of 6 Hertz.
- It continues to decrease for a fretting frequency of 10 Hertz.

Similarly, observing the figure for fretting amplitude of 150mm, following observations may be drawn.

- The coefficient of friction first decreases and then increases for fretting frequency of 3 Hertz.
- The coefficient of friction almost stays constant for fretting frequency of 6 Hertz.

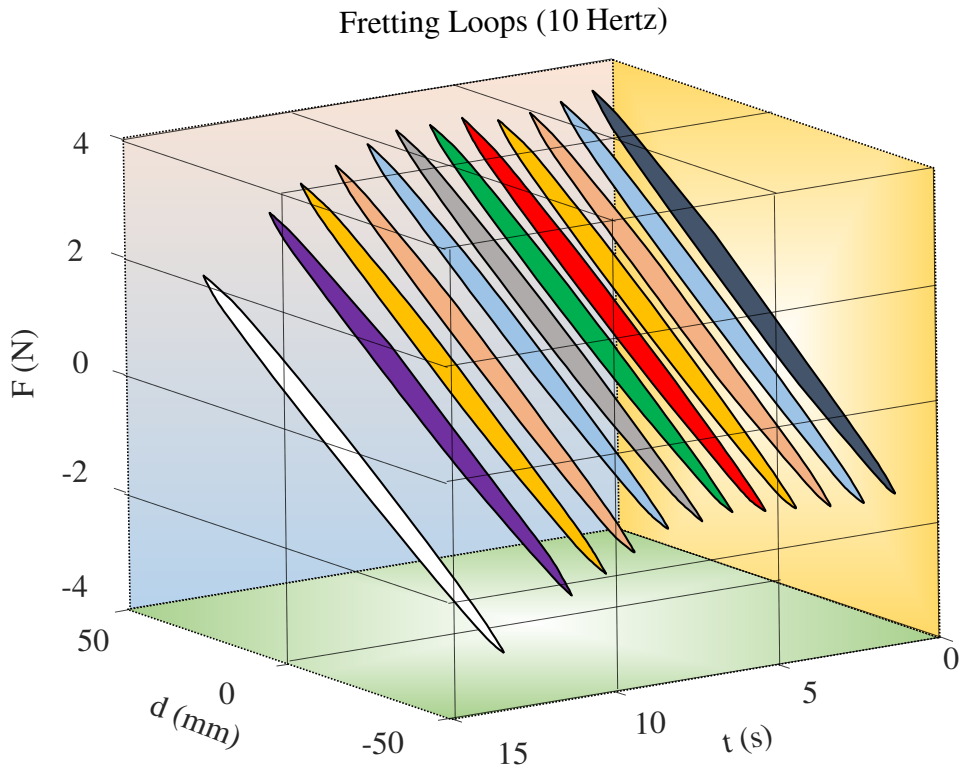

Fig. 7.9 Variations in fretting loop for the frequency of 10 Hertz and sliding amplitude of 100mm

- On the other hand, the coefficient of friction continues to decrease for fretting frequency of 10 Hertz and fretting amplitude of 150mm.

A very important observation at least apparently is the fact that even though applied conditions remained the same with the same material pair, the values of the coefficient of friction varied widely for different sets of experiments. This might be due to the fact that despite the same material, there may be variations in the materials, surfaces, temperature, humidity and random observation errors. Thus, the apparent discrepancy in the values of the coefficient of friction in the same tribological pair of materials is not as important as the evolution of coefficient of friction as the test progresses.

These observations merit a detailed experimental study of fretting wear performance of different materials under different wide ranging frequencies and their correlation with intrinsic material properties along with geometric and thermal properties. It makes sense to do these experiments because spline couplings also operate on varying frequencies, resulting in various applied fretting frequencies and different

fretting amplitudes as a result of variations in the misalignment angles. Also, such an experiment will enable to analyze all the work done in this thesis in a compact, tractable and unified framework for example statistical analysis, roughness parameters, material properties, tribological properties, fretting amplitudes, frequencies, thermal trends and modeling of fretting wear for onward and even more robust application on spline couplings.

Chapter 8

Conclusion

8.1 Conclusions

The safe operation of an important aero-engine mechanical component namely crowned spline coupling has been studied with respect to fretting wear. At present, there are not many models available to predict fretting wear of a crowned spline coupling in a systematic and methodological manner. The significant contributions of this work are the following: A framework for statistical validation of fretting wear tests has been developed but it is quite general. An extension in Mindlin's theory has been proposed to identify wear regimes in case of elliptical contacts thus making sure that the corresponding modeling techniques can be applied confidently. For the cases in industrial applications, where no significant design or operating variations are involved, it has been shown that empirical and neural network based modeling for spline couplings will provide reasonable results with latter being more accurate. Then, an in situ experimental technique has been investigated using roughness parameters. The advantage of this approach lies in the fact that by simply using a profilometer to record values of roughness parameters before a coupling is put in to operation, it becomes possible to monitor fretting damage at least qualitatively during various stages of operation by repeating the procedure. This has applications in maintenance and monitoring of spline couplings as it provides a cheap and effective method to qualify spline couplings. However, the empirical or neural network based modeling approaches are less general in nature. Hence, an analytical approach was devised to predict fretting wear and its evolution in a methodological manner. It

was successfully tested and validated on several experimental data thus proving its usefulness. Then, a novel concept of Wear Endurance Work (WEW) was proposed to compare and quantify the fretting wear life of spline couplings for any geometry and friction of coefficient combinations. The biggest advantage of this concept is that it can help the designers in robust and reliable spline coupling design and also gives them an opportunity to compare different design and tribological conditions in a compact fashion. This approach could also provide Wohler like curves to estimate life of a spline coupling but in terms of work per unit volume thus readily incorporating varying combinations of geometry and tribo-couples. And finally, a set of preliminary tests on the relationship between frequency and fretting were was performed which proved that there is some dependence of frequency over fretting but it requires more rigorous experimental investigation on more specific test benches.

It has been found that it is possible to model incremental fretting wear in case of spline couplings. The developed formulation is specific enough to cater for spline couplings and general enough to apply to a variety of other wear problems in various mechanical components involving sliding Hertzian contact. A software routine had been developed in order to assist the designers in quick and reliable design of spline couplings. However, the user interface or source code has not been included in the thesis owing to proprietary constraints.

8.2 Limitations and Future work

The current work was focused on fretting wear for a particular case of wear: gross slip regime. However, in the case of stick-slip regime, fretting fatigue also becomes a significant factor and then a competition between fretting wear and fatigue in conjunction with each other is established. As a part of future work, it will be very useful to unify formulation of fretting wear and / or fretting fatigue for both cases of gross slip and stick-slip regimes. Additionally, some initial tests on classical wear bench have been performed to analyze effects of frequency on fretting wear. A more detailed study in this direction and incorporation of frequency as a factor in the mathematical models of fretting wear could give rise to even more accurate and widely applicable models. However, the experiments on frequency-fretting relation in this work were not very reliable owing to modification in a classical wear test machine. Nevertheless, they did point at the potential of study in this regard.

Publications

Journal Articles

– Experimental characterization of roughness parameters for fretting wear in spline couplings. **Meccanica**, October 2016

DOI: 10.1007/s11012-016-0535-7

– A Methodological Approach For Incremental Fretting Wear Formulation, September 2016, **Tribology Letters**, Volume 64-2

DOI: 10.1007/s11249-016-0760-1

– Characterization of Fretting Wear Experiments on Spline Couplings by Principal Component Analysis, **Proceedings of the Institution of Mechanical Engineers, Part J: Journal of Engineering Tribology**, December 2016

DOI: 10.1177/1350650116682162

– Prediction of fretting wear in aero-engine spline couplings made of 42CrMo4, **Proceedings of the Institution of Mechanical Engineers, Part C: Journal of Mechanical Engineering Science**, September 2016

DOI: 10.1177/0954406216669177

– Principal Component Analysis for Characterization of Fretting wear Experiments on Spline Couplings, 2015, **Procedia Engineering**, Volume 109, 73–79.

DOI: 10.1016/j.proeng.2015.06.209

References

[1] Francesca Cura, Waqar Qureshi, and Andrea Mura. A Methodological Approach for Incremental Fretting Wear Formulation. *Tribology Letters*, 64(2):20, nov 2016.

[2] Waqar Qureshi, Francesca Cura, and Andrea Mura. Characterization of fretting wear experiments on spline couplings by principal component analysis. *Proceedings of the Institution of Mechanical Engineers, Part J: Journal of Engineering Tribology*, dec 2016.

[3] Vincenzo Cuffaro, Francesca Curà, and Andrea Mura. Test Rig for Spline Couplings Working in Misaligned Conditions. *Journal of Tribology*, 136(1):011104, nov 2013.

[4] W. Qureshi, F. Cura, and A. Mura. Prediction of fretting wear in aero-engine spline couplings made of 42CrMo4. *Proceedings of the Institution of Mechanical Engineers, Part C: Journal of Mechanical Engineering Science*, sep 2016.

[5] E.S. Gadelmawla, M.M. Koura, T.M.A. Maksoud, I.M. Elewa, and H.H. Soliman. Roughness parameters. *Journal of Materials Processing Technology*, 123(1):133–145, apr 2002.

[6] Waqar Qureshi, Francesca Cura, and Andrea Mura. Experimental characterization of roughness parameters for fretting wear in spline couplings. *Meccanica*, oct 2016.

[7] A. R. Warmuth, P. H. Shipway, and W. Sun. Fretting wear mapping: the influence of contact geometry and frequency on debris formation and ejection for a steel-on-steel pair. *Proceedings of the Royal Society A: Mathematical, Physical and Engineering Sciences*, 471(2178):20140291–20140291, may 2015.

[8] Olof Vingsbo and Staffan Söderberg. On fretting maps. *Wear*, 126(2):131–147, sep 1988.

[9] H. W. Brown. A Reliable Spline Coupling. *Journal of Engineering for Industry*, 101(4):421–426, 1979.

[10] Adrien Barrot, Manuel Paredes, and Marc Sartor. An Assistance Tool for Spline Coupling Design. In *Advances in Integrated Design and Manufacturing in Mechanical Engineering*, pages 329–342. Springer-Verlag, Berlin/Heidelberg, 2005.

[11] Vincenzo Cuffaro. *Prediction Method for the Surface Damage in Splined Couplings*. PhD thesis, Politecnico di Torino, 2013.

[12] D. W Dudley. How to design involute splines. *Product Engineering*, pages 75–80, 1957.

[13] D. W. Lee, X. Banquy, and J. N. Israelachvili. Stick-slip friction and wear of articular joints. *Proceedings of the National Academy of Sciences*, 110(7):E567–E574, feb 2013.

[14] I. G. Goryacheva, P. T. Rajeev, and T. N. Farris. Wear in Partial Slip Contact. *Journal of Tribology*, 123(4):848, 2001.

[15] F. Alwahdi, F.J. Franklin, and A. Kapoor. The effect of partial slip on the wear rate of rails. *Wear*, 258(7-8):1031–1037, mar 2005.

[16] M. Eriten, A.A. Polycarpou, and L.A. Bergman. Physics-based modeling for partial slip behavior of spherical contacts. *International Journal of Solids and Structures*, 47(18-19):2554–2567, sep 2010.

[17] K. L. Johnson. Surface Interaction between Elastically Loaded Bodies under Tangential Forces. *Proceedings of the Royal Society A: Mathematical, Physical and Engineering Sciences*, 230(1183):531–548, jul 1955.

[18] A.R. Wayson. A study of fretting on steel. *Wear*, 7(5):435–450, sep 1964.

[19] A. V. Dimaki, A. I. Dmitriev, N. Menga, A. Papangelo, M. Ciavarella, and V. L. Popov. Fast High-Resolution Simulation of the Gross Slip Wear of Axially Symmetric Contacts. *Tribology Transactions*, 59(1):189–194, jan 2016.

[20] C.H. Hager, J.H. Sanders, and S. Sharma. Characterization of mixed and gross slip fretting wear regimes in Ti6Al4V interfaces at room temperature. *Wear*, 257(1-2):167–180, jul 2004.

[21] L. Gallego and D. Nelias. Modeling of Fretting Wear Under Gross Slip and Partial Slip Conditions. *Journal of Tribology*, 129(3):528, 2007.

[22] J. F. Archard. Contact and Rubbing of Flat Surfaces. *Journal of Applied Physics*, 24(8):981, 1953.

[23] J. F. Archard and W. Hirst. The Wear of Metals under Unlubricated Conditions. *Proceedings of the Royal Society A: Mathematical, Physical and Engineering Sciences*, 236(1206):397–410, aug 1956.

[24] Xiangjun Qiu and M. E. Plesha. A Theory for Dry Wear Based on Energy. *Journal of Tribology*, 113(3):442, 1991.

[25] C.M. Rodkiewicz and Y. Wang. A dry wear model based on energy considerations. *Tribology International*, 27(3):145–151, jun 1994.

[26] S. Fouvry, T. Liskiewicz, Ph. Kapsa, S. Hannel, and E. Sauger. An energy description of wear mechanisms and its applications to oscillating sliding contacts. *Wear*, 255(1-6):287–298, aug 2003.

[27] A. Ramalho and J.C. Miranda. The relationship between wear and dissipated energy in sliding systems. *Wear*, 260(4-5):361–367, feb 2006.

[28] Jamil Abdo. Materials Sliding Wear Model Based on Energy Dissipation. *Mechanics of Advanced Materials and Structures*, 22(4):298–304, apr 2015.

[29] J. Sequard-Base, C. Lenauer, V. Lazarev, K. Gavrilov, A. Doikin, and G. Vorlaufer. A modified energy-based model for describing wear processes applied to an internal combustion engine. *International Journal of Computational Methods and Experimental Measurements*, 3(2):150–164, jun 2015.

[30] Von Herrn Heinrich Hertz. lieber die Berührung fester elastischer Körper . *Journal f. d. reine u. angewandte Mathematik 92*, pages 156–171, 1881.

[31] Heinrich Hertz. Ueber die Berührung fester elastischer Körper. *Journal fur die Reine und Angewandte Mathematik*, 1882(92):156–171, 1882.

[32] R. D. Mindlin. Compliance of Elastic Bodies in Contact. In *The Collected Papers of Raymond D. Mindlin Volume I*, pages 197–206. Springer New York, New York, NY, 1989.

[33] Izhak Etsion. Revisiting the Cattaneo Mindlin Concept of Interfacial Slip in Tangentially Loaded Compliant Bodies. *Journal of Tribology*, 132(2):020801, 2010.

[34] Waqar Qureshi, Francesca Curá, and Andrea Mura. Principal Component Analysis for Characterization of Fretting wear Experiments on Spline Couplings. *Procedia Engineering*, 109:73–79, 2015.

[35] Karl Pearson. LIII. On lines and planes of closest fit to systems of points in space. *The London, Edinburgh, and Dublin Philosophical Magazine and Journal of Science*, 2(11):559–572, 1901.

[36] F Mosteller and JW Tukey. *Data analysis and regression: a second course in statistics.* Addison-Wesley Educational Publishers Inc, 1977.

[37] Svante Wold, Kim Esbensen, and Paul Geladi. Principal component analysis. *Chemometrics and Intelligent Laboratory Systems*, 2:37–52, 1987.

[38] Michael Falk. A Note on the Comedian for Elliptical Distributions. *Journal of Multivariate Analysis*, 67(2):306–317, 1998.

[39] Bernhard Schölkopf, Alexander Smola, and Klaus-Robert Müller. Nonlinear Component Analysis as a Kernel Eigenvalue Problem. *Neural Computation*, 10:1299–1319, 1998.

[40] J P Wu, X P Yan, Z M Jin, J L Tipper, C Q Yuan, and X C Zhou. Application of principal component analysis and a fuzzy C-means clustering algorithm to wear debris morphology classification. *Proceedings of the Institution of Mechanical Engineers, Part J: Journal of Engineering Tribology*, 223(7):1059–1066, nov 2009.

[41] R Roshan, M Priest, A Neville, A Morina, X Xia, C P Warrens, and M J Payne. Subscale tribofilm tribological modelling in boundary lubrication using multivariate analysis. *Proceedings of the Institution of Mechanical Engineers, Part J: Journal of Engineering Tribology*, 225(2):58–71, 2011.

[42] Francesca Curà and Andrea Mura. Experimental and theoretical investigation about reaction moments in misaligned splined couplings. *Mechanical Systems and Signal Processing*, 45(2):504–512, apr 2014.

[43] G.K. Nathan and W.J.D. Jones. The empirical relationship between abrasive wear and the applied conditions. *Wear*, 9(4):300–309, jul 1966.

[44] R. D. Blevins. Fretting Wear of Heat Exchanger Tubes Part II: Models. *Journal of Engineering for Power*, 101(4):630–633, 1979.

[45] M Kalin and J Vižintin. Use of equations for wear volume determination in fretting experiments. *Wear*, 237(1):39–48, jan 2000.

[46] Craig I Walker and Greg C Bodkin. Empirical wear relationships for centrifugal slurry pumps. *Wear*, 242(1-2):140–146, jul 2000.

[47] Young Woo Park and Kang Yong Lee. Development of empirical equations for fretting-corrosion failure-time of tin-plated contacts. *Wear*, 265(5-6):756–762, aug 2008.

[48] Keyvan Hosseinkhani and E. Ng. A Combined Empirical and Numerical Approach for Tool Wear Prediction in Machining. *Procedia CIRP*, 31:304–309, 2015.

[49] F. Köppl, K. Thuro, and M. Thewes. Suggestion of an empirical prognosis model for cutting tool wear of Hydroshield TBM. *Tunnelling and Underground Space Technology*, 49:287–294, jun 2015.

[50] P. J. Blau, J. Qu, and R. Lu. Modeling of Complex Wear Behavior Associated with Grid-to-Rod Fretting in Light Water Nuclear Reactors. *JOM*, 68(11):2938–2943, nov 2016.

[51] P.L. Menezes and S.V. Kailas. Role of surface texture and roughness parameters on friction and transfer film formation when UHMWPE sliding against steel. *Biosurface and Biotribology*, 2(1):1–10, mar 2016.

[52] R. Deltombe, K. J. Kubiak, and M. Bigerelle. How to select the most relevant 3D roughness parameters of a surface. *Scanning*, 36(1):150–160, jan 2014.

[53] K.J. Kubiak and T.G. Mathia. Influence of roughness on contact interface in fretting under dry and boundary lubricated sliding regimes. *Wear*, 267(1-4):315–321, jun 2009.

[54] Anke Turger, Jens Köhler, Berend Denkena, Tomas A Correa, Christoph Becher, and Christof Hurschler. Manufacturing conditioned roughness and wear of biomedical oxide ceramics for all-ceramic knee implants. *BioMedical Engineering OnLine*, 12(1):84, 2013.

[55] W. D. Weatherford, M. L. Valtierra, and P. M. Ku. Mechanisms of Wear in Misaligned Splines. *Journal of Lubrication Technology*, 90(1):42–48, 1968.

[56] P. M. Ku and M. L. Valtierra. Spline Wear-Effects of Design and Lubrication. *Journal of Engineering for Industry*, 97(4):1257–1263, 1975.

[57] S Medina and A V Olver. An analysis of misaligned spline couplings. *Proceedings of the Institution of Mechanical Engineers, Part J: Journal of Engineering Tribology*, 216(5):269–278, jan 2002.

[58] K. Pearson. Mathematical Contributions to the Theory of Evolution. III. Regression, Heredity, and Panmixia. *Philosophical Transactions of the Royal Society A: Mathematical, Physical and Engineering Sciences*, 187:253–318, jan 1896.

[59] I.R McColl, J Ding, and S.B Leen. Finite element simulation and experimental validation of fretting wear. *Wear*, 256(11-12):1114–1127, jun 2004.

[60] S. Fouvry, Ph. Kapsa, and L. Vincent. An elastic–plastic shakedown analysis of fretting wear. *Wear*, 247(1):41–54, jan 2001.

[61] Young-Ho Lee and Hyung-Kyu Kim. Fretting wear behavior of a nuclear fuel rod under a simulated primary coolant condition. *Wear*, 301(1-2):569–574, apr 2013.

[62] Shenjiang Wu, Hiroyuki Kousaka, Satyananda Kar, Dangjuan Li, and Junhong Su. Friction and wear performance of bearing ball sliding against diamond-like carbon coatings. *Materials Research Express*, 4(1), jan 2017.

[63] Russell English, Ariyan Ashkanfar, and Glynn Rothwell. A computational approach to fretting wear prediction at the head–stem taper junction of total hip replacements. *Wear*, 338-339:210–220, sep 2015.

[64] Priit Põdra and Sören Andersson. Simulating sliding wear with finite element method. *Tribology International*, 32(2):71–81, feb 1999.

[65] Walter Schütz. A history of fatigue. *Engineering Fracture Mechanics*, 54(2):263–300, may 1996.

[66] T. Liskiewicz, S. Fouvry, and B. Wendler. Development of a Wöhler-like approach to quantify the Ti(CxNy) coatings durability under oscillating sliding conditions. *Wear*, 259(7-12):835–841, jul 2005.

[67] Staffan Söderberg, U. Bryggman, and Tim McCullough. Frequency effects in fretting wear. *Wear*, 110(1):19–34, jul 1986.

[68] Petra Schaaff, Matteo Dalmiglio, and Uwe Holzwarth. Frequency effect in fretting wear of Co-28Cr-6Mo versus Ti-6Al-4V implant alloys. *Journal of Biomedical Materials Research Part B: Applied Biomaterials*, 77B(1):79–88, apr 2006.

[69] A. Krichen, M. Kharrat, and A. Chateauminois. Effects of Frequency on the Fretting Conditions in a Contact Between PMMA and a Rigid Counterface. *Journal of Tribology*, 120(4):729, 1998.

Appendix A

Source code for Hertzian Formulation

The MATLAB source code for the solution of Hertzian elliptical contact in the case of spline couplings has been provided below for a quick reference and to help other researchers working on the similar components. The code is compatible with MATLAB 2016b version.

```
%Code for calculating hertz contact and stress
close all;
clear all;

%Geometric properties
R11 = 0.2;     %Radii of curvature of first body
R12 = 0.008;
R21 = 1000;    %Radii of curvature of second body
R22 = 1000;    %Positive if convex, negative if concave

%Geometric features of non conforming shapes 1,2
R = 1/R11 + 1/R12 + 1/R21 + 1/R22;  %Equivalent principal curvature
Re = 1/R;
R1 = 1/R11 - 1/R12;
R2 = 1/R21 - 1/R22;
```

```
s_ang = 0;              %Angle between surfaces in degrees

%An auxilary angle
omg = acos(sqrt(R1^2 + R2^2 + 2*R1*R2*cos(2*s_ang*pi/180)) / R);
omg = round(omg * 180/pi);

%Material properties
E1 = 210*10^9;
E2 = 210*10^9;  %Modulus of elasticity
G1 = 80*10^9;
G2 = 80*10^9;   %Shear modulus / Modulus of rigidity

v1 = 0.27;
v2 = 0.27;      %Poisson's ratio

%Material features
t1 = 4*(1-v1^2)/E1;
t2 = 4*(1-v2^2)/E2;

E = (1-v1^2)/E1 + (1-v2^2)/E2;
Ee = 1/E;

rp = 16.51*10^(-3);     %Coupling pitch radius
n = 26;                 %Number of teeth

%Governing integrals in the range of 0 to pi/2
syms x k
hk = symfun(1/sqrt(1-(1-k^2)*sin(x)^2), [x]);               %k=b/a, ratio betweem
ik = symfun(cos(x)^2/(sqrt(1-(1-k^2)*sin(x)^2))^3, [x]);
jk = symfun(cos(x)^2/(sqrt(1-(1-1/k^2)*sin(x)^2))^3, [x]);

%Solution of integrals by Boole's rule
BN = 10;    %Number of divisions for Boole's Rule
HK =  symfun(Boole(hk, 0, pi/2,BN),[k]);
IK =  symfun(Boole(ik, 0, pi/2,BN),[k]);
```

```
JK =  symfun(Boole(jk, 0, pi/2,BN),[k]);

%Solution of transcendental equation
if (omg>=0) && (omg<=5)     %These if statements give good initial guesses for fi
ig = 0.04;
end
if (omg>5) && (omg<=73)
ig = 0.56;
end
if (omg>73)
ig = 0.85;
end
omg1 = omg*pi/180;
f = @(k) k^3/tan(omg1/2)^2 - eval(JK)/eval(IK);
k1 = fzero(f,ig);
HK2 = eval(HK(k1));
IK2 = eval(IK(k1));
JK2 = eval(JK(k1));
f1 = (2*IK2/(pi*sin(omg1/2)^2))^(1/3);
g1 = (2*JK2/(pi*cos(omg1/2)^2))^(1/3);

u=0;
for thet = 4:5:9
for p1 = 600:300:1200
u=u+1;
F(u,:) = p1 * cos(thet*pi/(180*60)) / (rp*n);  %Applied torque
mis(u,:) = thet;
end
end

%Radii of contact
A = f1*((3* F*(t1+t2))/(8*R)).^(1/3);
B = g1*((3*F*(t1+t2))/(8*R)).^(1/3);

%Deformations in the bodies
```

```
D1 = 3 * F * t1 * HK2 ./ (8*pi*A);
D2 = D1 * t2/t1;
D = D1 + D2;

%Area of contact
Q = A .* B * pi;

%Maximum pressure
Pmax = 3 * F ./ (2*Q);

t=-pi:0.01:pi;

W = 0;
subplot(2,1,1);
hold
plotStyle = {'b','k','r','b','k','r'}
for i = 1: 1: u
W = W+1;
H(i,:) = plot(A(i,:)*cos(t)*10^3,B(i,:)*sin(t)*100, plotStyle{i});
xlabel('Major axis radius (a) um');
ylabel('Minor axis radius (b) um');
legendInfo{i} = [num2str(round(F(i,:)*rp*n/cos(thet*pi/(180*60)))) ' Nm']
%s1 = num2str (round(F(i,:)*rp*n/cos(thet*pi/(180*60))));
%s1 = strcat(s1, ' Nm');
%legend (s1);
end
for i = 1: 1: 3
legendInfo1{i} = legendInfo{i};
end
legend(legendInfo1)
subplot(2,1,2);
scatter(Pmax/10^9,D*10^6, 'filled');
xlabel('Maximum Hertzian Pressure (GPa)');
ylabel('Deformation (um)');
```

```
figure
hold
syms a b
W=0;
A = A*1000;
B = B*1000;
for i = 1: 1: u/2
W = W+1;
subplot(1,3,W)
f = @(x,y) Pmax(i,:)/10^9  *  (1 -x.^2/A(i,:)^2 - y.^2/B(i,:)^2).^0.5;
fsurf(f,[-A(i,:) A(i,:) -B(i,:) B(i,:)],'MeshDensity',5)
%ezsurf(Pmax(i,:)/10^9 *(1 - a^2/A(i,:)^2 - b^2/B(i,:)^2)^0.5clos, [-A(i,:), A(i,
s1 = num2str (round(F(i,:)*rp*n/cos(thet*pi/(180*60))));
s1 = strcat(s1, ' Nm');
title(s1)
colormap jet
set(gca,'xlim',[-max(A) max(A)],'ylim',[-max(B) max(B)])
end
```

Appendix B

PCA of different cases

Matlab source code

The matlab source code for PCA analysis of fretting wear tests may be downloaded from the following link. The files section also contains a sample data file. Though, designed for fretting wear experiments initially, the same routine may be used to interpret experimental data from any other field as well.

https://sourceforge.net/projects/pca-for-fretting-wear-test/

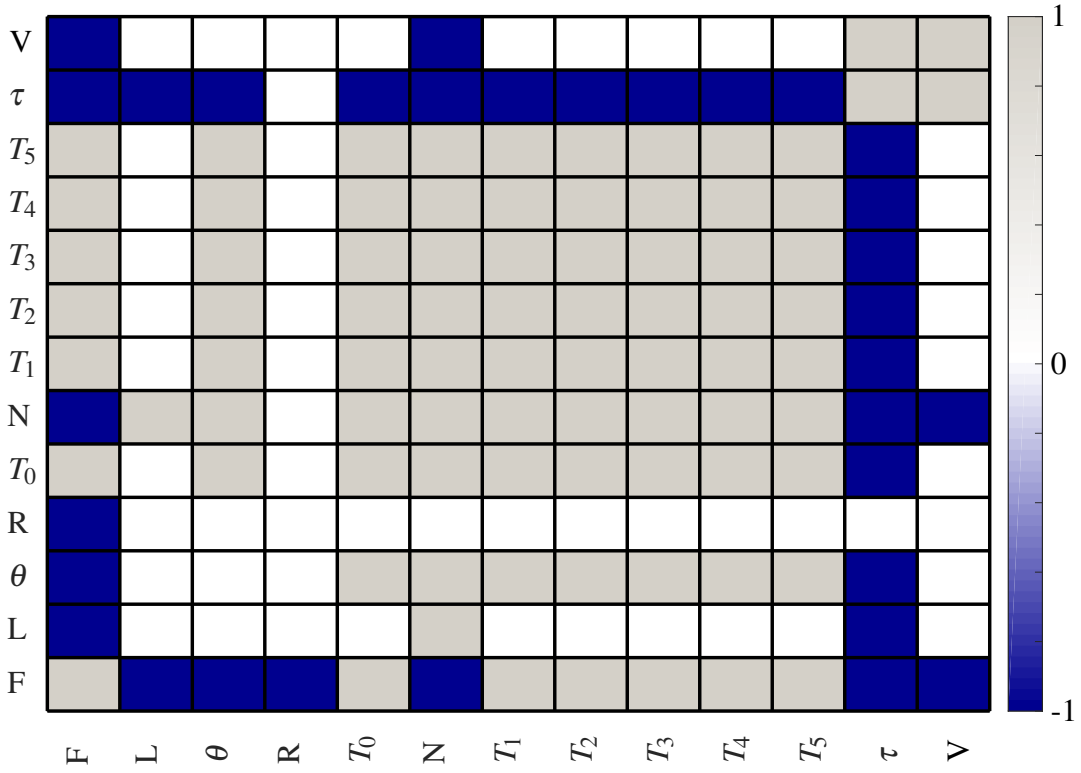

Fig. B.1 Covariance matrix for all the 13 variables of the test bench

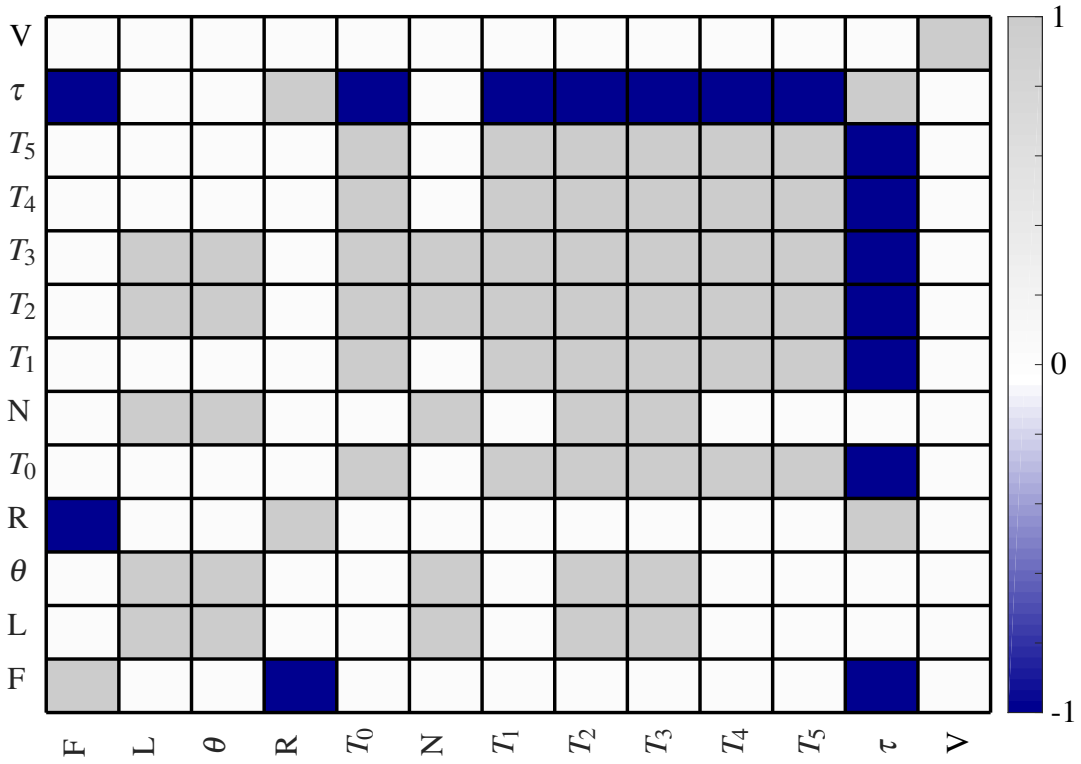

Fig. B.2 Correlation matrix for all the 13 variables of the test bench

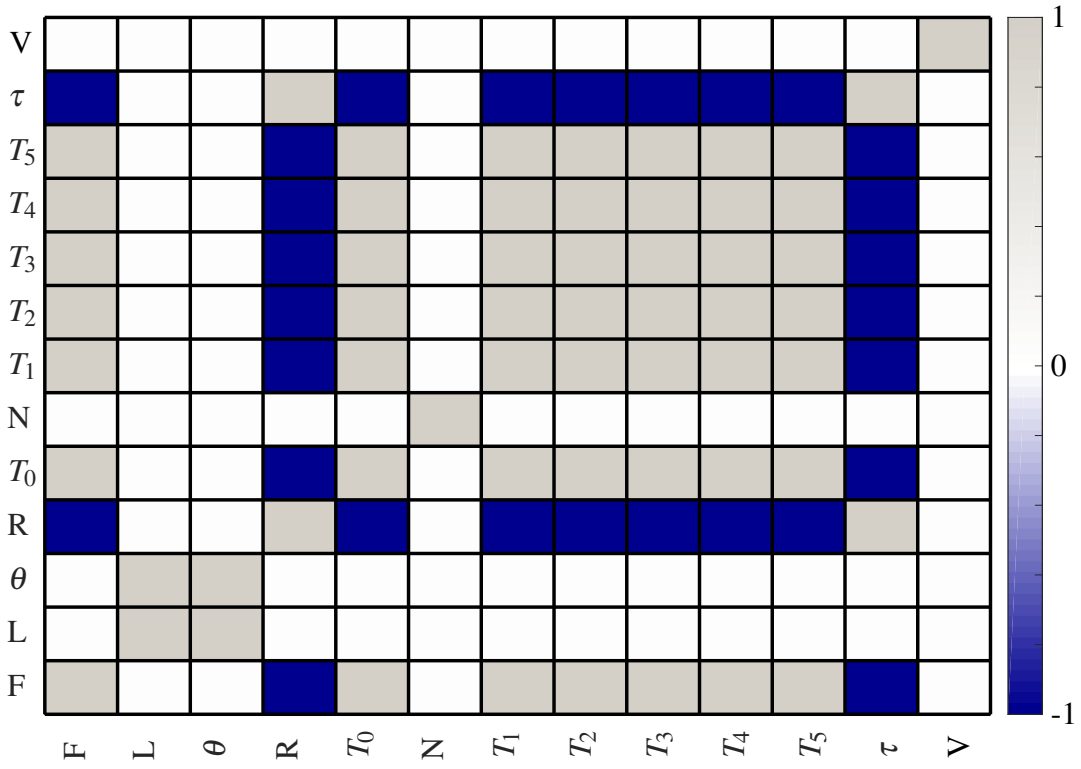

Fig. B.3 Comedian matrix for all the 13 variables of the test bench

Appendix C

Spline Coupling Specifications

The chemical composition of 42CrMo4 has been shown in the figure below. And the geometric parameters of spline couplings have been shown next.

C	Si	Mn	P	S	Cr	Ni
≤	≤	≤	≤	≤		
0.46-0.52	0.40	0.50-0.80	0.025	0.035	0.90-1.20	
Mo	Al	Cu	Nb	Ti	V	Ce
0.15-0.30		≤ 0.30				
N	Co	Pb	B	Other		

SCANALATO INTERNO
INTERNAL SPLINE Y

CLASSE (SEC. SPEC."F") (INF.)
CLASS (PER SPEC. / (REF.)..... 5

CENTRAGGIO SUI FIANCHI
SIDE FIT

TIPO DI SCANALATO
SPLINE TYPE..... *FILLET ROOT*

NUMERO DI DENTI
NUMBER OF TEETH..... 26

PASSO DIAMETRALE
DIAMETRAL PITCH..... 20/30

MODULO
MODULE..... 1.27

ANGOLO DI PRESSIONE
PRESSURE ANGLE..... 30°

DIAMETRO PRIMITIVO MY
PITCH DIA..... 33.020

DIAMETRO DI BASE
BASE DIA..... 28.5963

DIAMETRO ESTERNO
MAJOR DIA..... 35.281+ 35.789

DIAMETRO INIZIO EVOLVENTE
FORM DIA..... 34.874 MIN.

DIAMETRO INTERNO LY
MINOR DIA..... 31.318+ 31.445

FONDO DENTE A PIENO RACCORDO DI RAGGIO MIN.
FULL FILLET ROOT WITH MIN RADIUS..... 0.279

AMPIEZZA CIRCOLARE VANO
CIRCULAR SPACE WIDTH
- MIN EFFICACE *MIN EFFECTIVE*..... 1.994
- MAX REALE *MAX ACTUAL*..... 2.068

LARGHEZZA DI FASCIA TY
FACE WIDTH..... VED. DIS. *SEE DWG.*

QUOTA TRA 2 RULLINI
MEASUREMENT UNDER 2 PINS..... 28.914+ 28.983

DIAMETRO RULLINO
PIN DIA..... 2.5

SCANALATO ESTERNO X
EXTERNAL SPLINE

CENTRAGGIO SUI FIANCHI
SIDE FIT

NUMERO DI DENTI *NUMBER OF TEETH*		26
PASSO DIAMETRALE *DIAMETRAL PITCH*		20/30
ANGOLO DI PRESSIONE *PRESSURE ANGLE*		30°
DIAMETRO PRIMITIVO *PITCH DIA*	Mx	33.020
DIAMETRO DI BASE *BASE DIA*		28.5963
DIAMETRO ESTERNO *OUTSIDE DIA*	Nx	34.595–34.722
DIAMETRO INIZIO EVOLVENTE *FORM DIA*		31.166
DIAMETRO INTERNO *ROOT DIA*		29.972–30.480
FONDO DENTE A PIENO RACCORDO DI RAGGIO MIN *FULL FILLET ROOT WITH MIN RADIUS*		0.305
MAX EFFICACE *MAX EFFECTIVE*		1.960
SPESSORE CIRCOLARE DENTE *CIRCULAR TOOTH THICKNESS*		
MIN REALE *MIN ACTUAL*		1.886
LARGHEZZA DI FASCIA *FACE WIDTH*		VED. DISEGNO *SEE DWG*
QUOTA TRA 2 RULLINI *DIMENSION OVER 2 PINS*		36.806 – 36.858
DIAMETRO RULLINO *PIN DIA*		2.5